This is to certify that the

dissertation entitled

MAGNETOCONDUCTIVITY OF TWO-DIMENSIONAL ELECTRON SYSTEMS

presented by

Frank Oliver Kuehnel

has been accepted towards fulfillment
of the requirements for

Ph.D degree in Physics

M. Dykman
Major professor

Date 12/08/00

Abstract

Magnetoconductivity of two-dimensional electron systems

By

Frank Oliver Kuehnel

The conductivity $\sigma_{xx}(\omega)$ of a low-density nondegenerate 2D electron gas is investigated under conditions where $\hbar\omega_c \gg k_BT \gg \hbar\gamma$ (ω_c is the cyclotron frequency and $\hbar\gamma$ is the disorder-induced width of the Landau level). Such conditions have been met for electrons on helium surface, and can also be achieved in ultra high quality heterostructures. Because of the random potential of defects, single-electron states of the lowest Landau level form a band of a width $\hbar\gamma \ll \hbar\omega_c$. Almost all of these states are localized. Therefore, for $\hbar\omega_c \gg k_BT \gg \hbar\gamma$, the static single-electron conductivity $\sigma_{xx}(0)$ may be expected to be equal to zero. Since for $\omega \gg \gamma$ the conductivity should decay, on the whole $\sigma_{xx}(\omega)$ has a peak at a finite frequency.

From scaling arguments, we show that in the single-electron approximation $\sigma_{xx}(\omega) \propto \omega^{\mu}$ for $\omega \to 0$, with the exponent μ in the range from 0.21 to 0.22, whereas the frequency dependence of the cyclotron resonance absorption peak is non-critical. The far tails of the conductivity peaks are obtained using the method of optimal

fluctuation and are shown to be Gaussian.

In order to investigate the shape of the low frequency peak and cyclotron resonace absorption peak, we use the method of moments (MOM). In MOM, the low-frequency conductivity is restored from its 14 spectral moments, whereas the cyclotron resonance absorption is restored from the calculated 10 spectral moments using the continuous fraction expansion. In combination with the analytical asymptotics, both expansions converge rapidly with increasing number of included moments, and give numerically accurate results throughout the region of interest.

The effect of electron-electron interaction (EEI) on the low frequency conductivity is also investigated. EEI makes the static conductivity finite. For a low-density system, the effect can be described using the notion of a fluctuational field $E_{\rm fl}$ which drives an electron because of electron density fluctuations. Due to this field, spatial diffusion of electrons in a (comparatively strong) random potential of defects gives rise to energy diffusion of each individual electron, with a diffusion coefficient $D_\epsilon = \gamma e^2 \langle E_{\rm fl}^2 \rangle \hbar / m\omega_{\rm c}$. In combination with the known power-law asymptotic of the single-electron conductivity $\sigma_{\rm se}(\omega)$ for $\omega \to 0$, this allows us to find the static many-electron conductivity $\sigma_{\rm me}$.

Acknowledgments

My foremost grateful thanks belong to Prof. Mark I. Dykman whose superbness as a teacher is not excelled by any other person who I know. He is also a person of great humor and I'm very thankful for all the cheerful hours with him.

Substantial gratitude belongs to Leonid P. Pryadko with brilliant ideas and his focused determinism.

In delightful seminars with Tatjana Sharpee, Alex Zhukov and Vadim Smelyanskiy new ideas were bred, jokes were made and despite the troublesome intricacies of physics, life seemed so enjoyable; many thanks belong to them.

To be thanked for their assistance and discussions are Prof. Micheal Thorpe, Prof. Stuart Tessmer, the secretaries Janet King and Debbie Simmons. Of course I have to name a lot more people in the whole department.

For the quality of life, pastime distractions are a necessity. Branislav Blagojevic, Pavel Nadolsky, Brittany Biondo, Robert Lattin, Bernd Kauerauf, Olliver Gaertzen, Martin Fehndrich and Andreas Drecker have to be named.

And whom I have to be eternally grateful is my beloved girl. Without Friederike I couldn't have done the work, I couldn't have spent any more days without her, this is to say thank you that you were here!

Table of Contents

List of Tables

List of Figures

Chapter 1

Introduction

One of the most interesting problems in physics of low-dimensional systems is the effect of the electron-electron interaction (EEI) on electron transport. In some cases the EEI is the strongest interaction which leads to a change of the energy spectrum, as in the fractional quantum Hall effect (QHE). In other cases the EEI can be in some sense weaker than the disorder potential. But even then its effect is extremely important, as it gives rise to electron energy relaxation and dephasing. In its turn, dephasing partly suppresses localization effects arising from the interaction of electrons with a static disorder potential.

On the other hand, the problem of the single-electron localization in a disorder potential is of highest interest itself, the integer quantum Hall effect being an example where essentially all states except those at the Landau level band centers are localized. The simplest model which contains the essential physics of the QHE is the localization of electrons in the lowest Landau level by a random potential of defects. Much effort had been spent to understand the structure of electron states and even exact results

for the density of states had been obtained [5]. However, the transport dynamics of such a model remained largely unsolved and more heuristic arguments were used to interpret the experimental evidence of a localization-delocalization transition [6].

It is only humble to state that the intricate interplay between the localization properties of a static disorder potential and the delocalization through EEI are of uttermost importance in understanding the rich physics of low-dimensional electron systems.

Much work on the EEI refers to high-density systems, where the EEI is in some sense a perturbation. The role of the EEI should be even more important for low-density systems, as indicated by the recent remarkable results on transport and metal-insulator transitions in low-density two-dimensional electron system (2DES) in semiconductors and semiconductor heterostructures [7].

A well-understood effect in low-density systems is Wigner crystallization. It occurs provided the ratio of the characteristic Coulomb energy of the EEI $e^2(\pi n)^{1/2}$ (n is the electron density) to the electron kinetic energy $E_{\rm kin}$

$$\Gamma = e^2(\pi n)^{1/2}/E_{\rm kin} \tag{1.1}$$

exceeds certain critical value Γ_W. In Eq. (1.1), $E_{\rm kin}$ is equal to the biggest of the Fermi energy ϵ_F and k_BT. For $\Gamma > \Gamma_W$, static disorder pins the Wigner crystal, leading to thermally activated static conductivity.

The critical value Γ_W is numerically large. For low temperatures ($E_{\rm kin} = \epsilon_F \gg k_BT$), in which case $\Gamma_W \approx 37$ [8], whereas for a nondegenerate 2DES ($\epsilon_F \ll k_BT$)

$\Gamma_W \approx 130$ [9]. For $\Gamma_W > \Gamma \gg 1$, a 2DES is still strongly correlated. It forms an electron liquid, which in contrast to the crystalline phase, displays self-diffusion, at least for a nondegenerate 2DES, as seen in various numerical simulations [4, 10, 11]. Understanding transport of such a liquid is a challenging problem, in particular because it is hard to find elementary excitations in contrast to the much better understood Fermi liquid. The problem of transport in a correlated electron liquid had been formulated in an early work by Dykman and Khazan [12], the results clearly demonstrate that transport in such a system is dominated by many-electron effects.

In this present thesis the conductivity $\sigma_{xx}(\omega)$ of a nondegenerate 2D electron liquid in a quantizing magnetic field B transverse to the electron layer will be considered. In the limit where the force from the random potential is stronger than that from other electrons, the static conductivity in quantizing magnetic fields was described [13, 14, 15] in terms of the single-electron theory based on the self-consistent Born approximation (SCBA) [16]. This theory does not take into account the interference effects that lead to electron localization in the random potential of scatterers. Such a description appears to contradict the phenomenology of the integer QHE, where all but a finite number of single-particle states in the random potential are *localized* [17].

We will develop a consistent approach to the analysis of the conductivity which will take into account, in a non-perturbative way, both the effects of the electron-electron interaction and the effect of electron localization in a static disorder potential. The new physics emerges from the interplay of strong electron correlations and strong disorder. This interplay has not been explored. It leads to new effects, which are readily accessible to experimental observation. Their analysis requires new techniques, which

combine the ideas from very different areas of modern theoretical physics.

After having reviewed aspects of the QHE in chapter 2 and having briefly surveyed the many-electron effects in a nondegenerate 2D electron liquid in chapter 3, the calculation of the single-electron magnetoconductivty of a high temperature (nondegenerate) 2D electron system will be presented. The calculations will go beyond the standard perturbation approach and the numerical exact magnetoconductivity will be obtained in chapter 4 (low-frequency conductivity) and in chapter 5 (cyclotron resonance absorption). Many-electron effects strongly affect the low-frequency conductivity, and will be discussed in chapter 6, whereupon a suggestion for a new experiment and the conclusion are given in chapter 7 and 8 respectively. A compilation of more intricate calculations can be found in the appendices.

Chapter 2

Single-electron magnetotransport, Quantum Hall effect

The Quantum Hall effect (QHE) was discovered on about the hundredth anniversary of Hall's original work, and the finding was announced in 1980 by von Klitzing, Dorda and Pepper [18]. Klaus von Klitzing was awarded the 1985 Nobel prize in physics for this discovery. In brief, it is found that under certain conditions in an effectively two-dimensional system of electrons subjected to a strong magnetic field, the conductivity tensor takes the form

$$\sigma = \begin{pmatrix} 0 & -ie^2/h \\ ie^2/h & 0 \end{pmatrix} \quad . \tag{2.1}$$

Here h is Planck's constant, $-e$ is the electron charge and $i > 0$ is an integer. In other words, the current density $\mathbf{j}$ is directed precisely perpendicular to the electric

field **E** according to

$$j_\alpha = \sum_\beta \sigma_{\alpha\beta} E_\beta \tag{2.2}$$

and it has the quantized magnitude $j/E = \sigma_{xy} = ie^2/h$. The diagonal conductivity vanishes to any measurable accuracy. At the same time its longitudinal resistance ρ_{xx} also vanishes according to

$$\rho_{xx} = \frac{\sigma_{xx}}{\sigma_{xx}^2 + \sigma_{xy}^2}, \quad \rho_{xy} = \frac{\sigma_{xy}}{\sigma_{xx}^2 + \sigma_{xy}^2}, \tag{2.3}$$

rendering the system as completely dissipation-less. In fact the conductivities are not the fundamental quantities. The Hall and longitudional resistance, $R_H = V_H/I = \rho_{xy}$ and $R_L = V_L/I = \rho_{xx}$ are directly measured in the experiment. The finiteness of the off-diagonal conductivity σ_{xy} which is given by a combination of fundamental constants leads to the peculiar situation where the longitudinal resistivity and conductivity vanishes at the same time.

Astonishingly, the measured Hall resistance

$$R_H = h/e^2 \approx 25812.807572 \pm 0.000095\Omega \tag{2.4}$$

is independent of the geometry, material, and persists over a broad range of physical parameters like magnetic field, temperature and electron density. With its reproducible precision of at least 3.7 parts in 10^9 (3.7ppb) the QHE is practically applied as an Ohm standard [19] and may be used as another way to measure the QED

fine-structure constant $\alpha = \mu_0 c/2R_H$, where the permeability of vacuum μ_0 is by definition exactly $4\pi \times 10^{-7}\mathrm{Hm}^{-1}$ and the speed of light c has been defined to be exactly $299792458\mathrm{ms}^{-1}$.

In the following sections the physical aspects of such a system will be outlined. Firstly, a physical realization of a two-dimensional electron system will be presented and simple conclusions will be drawn from this model. Secondly, in subsequent sections the focus shifts to more intricate details and implications.

2.1 Experimental evidence

The notion of a two-dimensional system (2D) is briefly illustrated in Fig. 2.1. A confining potential $V(z)$ introduces a discrete spectrum with a large but finite energy separation. In the independent electron approximation, and assuming translational invariance along the interface, the electron states are of the form $\psi(x,y)Z_n(z)$ where Z_n satisfies a Schrödinger equation

$$\left[-\frac{\hbar^2}{2m}\frac{\partial^2}{\partial z^2} + V(z)\right] Z_n(z) = E_n Z_n(z). \tag{2.5}$$

The ground state energy gap $\Delta E = E_1 - E_0$ typically exceeds the thermal energy $k_B T$ by an order of magnitude, and thus renders thermal transition to excited states as irrelevant. The electron system is trapped in the ground state $Z_0(z)$, thus any dynamical evolution in the z-direction is frozen.

Hall measurements on 2D systems are performed in the standard Hall bar ge-

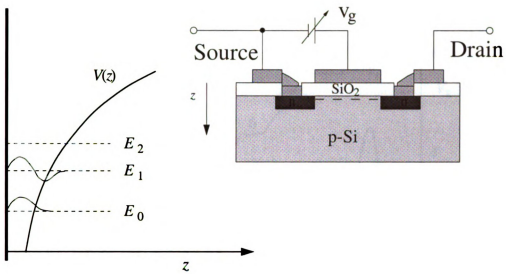

Figure 2.1: The confining potential $V(z)$ with a high, effectively infinite barrier at the interface representing the large band gap of the insulator. The gap $\Delta E = E_1 - E_0$ can be several meV large, for semiconductors (SiO_2-inversion layer) typically 20meV (200 K), much greater than the temperature at which the QHE is observed. A typical realization of a two-dimensional (2D) electron system is formed within the 25Å thick inversion layer (dashed line) of the MOSFET structure (right).

ometry. The electrons are confined in the plane with the Hall bar shape, a strong magnetic field B penetrates this plane transverse to it. The inset of Fig. 2.2 illustrates the Hall bar geometry. Measurements were conducted with a constant source-drain current of 25.5μA, the voltage drops V_H and V_x were recorded as a function of the magnetic field. At certain values of B the longitudinal resistance $R_x = V_x/I$ vanishes. The plateau values of $R_H = V_H/I$ coincide with the region of vanishing R_x.

Attempting to interpret the quantum Hall transport, a single-electron picture is often used. In the simplest case the electron dispersion is determined by a single parabolic band with an effective electron mass m. Starting with the single electron

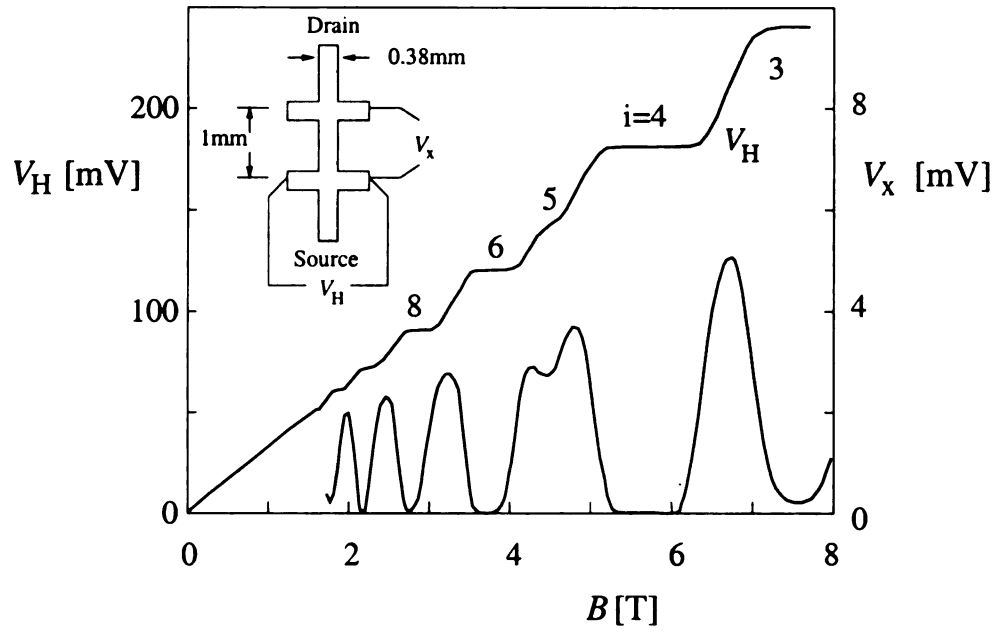

Figure 2.2: Chart recordings of V_H and V_x vs. magnetic field for a GaAs-AlGaAs heterostructure cooled to 1.2K. The source-drain current is 25.5μA and electron density $n_e = 5.6 \times 10^{11}\text{cm}^{-2}$, Cage *et al.* [2].

Hamiltonian

$$H_0 = \frac{1}{2m}(-i\hbar\nabla + e\mathbf{A})^2 = \frac{\mathbf{p}^2}{2m}, \tag{2.6}$$

where $-e$ is the electron charge and $\mathbf{A}$ is the vector potential for the magnetic field, $\mathbf{B} = \nabla \times \mathbf{A}$. Here, it is assumed that $\mathbf{B}$ points along the positive z axis, $\mathbf{B} = (0, 0, B)$, $B = |\mathbf{B}|$. The cyclotron frequency is defined as $\omega_c = eB/m$.

In strong magnetic fields at low temperatures $kT \ll \hbar\omega_c$ it is also fair to assume that all electron spins are aligned with the magnetic field. The Zeeman splitting, $H_S = g^*\mu_B/2\ \hat{\sigma}\mathbf{B}$ depends on the effective Landé factor g^* of the carriers, $\mu_B = e\hbar/2m$ is the Bohr magneton and $\hat{\sigma}$ the Pauli matrix operator. In general g^* depends on the

spin-orbit coupling and on exchange effects. For electrons in the vacuum $g^* = 2$, thus the Zeeman splitting equals the cyclotron resonance gap $\hbar\omega_c$. For electrons on a liquid helium surface, it is safe to neglect electron spin effects.

As will be derived later, the energy spectrum of the Hamiltonian (2.6) is discrete, $E_m = \hbar\omega_c(m + 1/2)$, $m = 0, 1, \ldots$. The density of states (DOS) for this ideal system consists of a sum of δ-functions located at the energy values E_m,

$$\rho(E) = \frac{eB}{h} \sum_m \delta(E - E_m). \tag{2.7}$$

This idealized picture of a 2D system with given translational gauge symmetry is rather contrived and does not capture the essential physics to interpret transport experiments. In "real" 2D systems such as electrons on a liquid helium surface (to be discussed in the next chapter) or electrons confined in a semiconductor inversion layer the electrons are influenced by a random scattering potential which may come from impurities, interface roughness etc. Scattering of electrons is the source of a finite broadening of the energy spectrum, see Fig. 2.3.

A more realistic model will explicitly include the effects of a static disorder potential

$$H = H_0 + V(\mathbf{r}). \tag{2.8}$$

The role of the disorder potential $V(\mathbf{r})$ is essential in the case of the QHE. That the effects of a disorder potential on electrons in a strong magnetic field is not perturba-

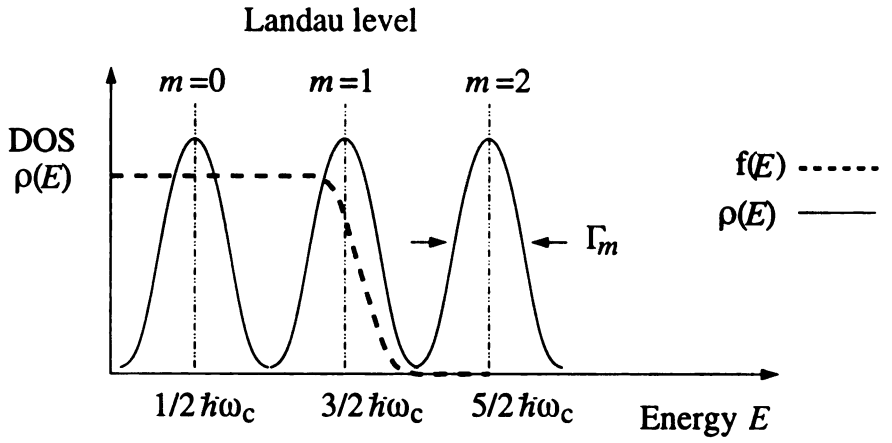

Figure 2.3: The density of state of a 2DES with scattering (solid line). Each degenerate Landau level (dash-dotted lines) $m = 0, 1, \ldots$ of the free electron Hamiltonian (2.6) will be broadened by a Γ_m. Superimposed is the Fermi-Dirac distribution (fat dashed line). Spin splitting is not considered.

tionally small, can be seen from a simple argument. Electrons in a strong magnetic field do not have a finite group velocity. Therefore any perturbation techniques based on the premises of weak interaction between electron and scatterer will fail to describe the basic phenomenon of the QHE, namely the localization of states.

The concept of localized states in disordered systems was pioneered by Anderson [20]. He showed that if a quantum-mechanical system is sufficiently disordered, states have a finite probability of returning to a given site in the long-time limit. This absence of diffusion implies that these states are localized in a finite region of space. The transmission probability decays exponentially on a length scale, which is called the localization length. For localized states the static conductivity vanishes at zero temperature which would deliver a reasonable explanation for the vanishing longitudinal resistance regions at the QH plateaus in Fig. 2.2. The current then is due to edge states where the conduction is dissipation-less.

Usually an explanation of the QHE is based on gauge arguments, a first insight came from Laughlin [21] and consecutively, a more complete line of arguments is due to Halperin [22]. Indeed, the first idea is that the QHE is basically a bulk effect. There is no evidence whatsoever that changes in size, shape and connectivity or edge conditions of a sample lead to any changes in the basic QHE results.

Following the key ideas in [22], extended states do only exist at the exact energy values of the Landau levels (critical energy) of the unperturbed system (2.6). These extended states constitute the channels of conduction through which electrons are transferred dissipation-less $\rho_{xx} = 0$ whenever the Fermi level is far from those critical energies. In combination with the gauge argument [21, 22] the conductivity tensor obtains its form as in (2.1), the longitudinal conductivity σ_{xx} vanishes and the Hall conductivity σ_{xy} is locked onto the plateau value ie^2/h. The electron interaction with a disorder potential is the cause for the finite broadening of the density of states. However from the experimental point of view, all of those new states have to be localized, such that they will not contribute to the conductivity.

To summarize the findings, gauge arguments make the QHE theoretically a precise effect which only depends on fundamental constants and therefore one should obtain remarkably accurate measurement data. It is even more stunning that the localization properties of a two-dimensional electron system stemming from an arbitrary randomness of a disorder does indeed support the 0.0037ppm reproducible exactness of a macroscopic quantum phenomenon, the Quantum Hall effect, instead of wiping it out.

In the following sections a more detailed investigation of the nature of free electron

states, the influence of the disorder potential and the phenomenon of localization will be given.

2.2 Electrons in lowest Landau level

2.2.1 Free electron Hamiltonian in magnetic field

The Hamiltonian (2.6) is of a simple quadratic form. Techniques for solving the harmonic oscillator fully apply and the kinetic energy creation and annihilation operators $d^\dagger, d$ are defined

$$d^\dagger = d_x + id_y,\ d = d_x - id_y, \quad \mathbf{d} = \frac{-i\hbar\nabla + e\mathbf{A}}{\sqrt{2m\omega_c\hbar}}. \tag{2.9}$$

In terms of those operators, (2.6) has the simple form

$$H_0 = \hbar\omega_c \left(d^\dagger d + \frac{1}{2} \right), \quad [d, d^\dagger] = 1. \tag{2.10}$$

The "Landau level quantum number" operator $d^\dagger d$ commutes with H_0, i. e.the Landau level n_L is a good quantum number for wavefunctions of the free electron Hamiltonian in a magnetic field of which the energy spectrum is equidistantly spaced by $\Delta E = \hbar\omega_c$. The set of operators (2.9) is not a full description for the original Hamiltonian H_0, since the representation algebra of a two-dimensional electron system (2DES) has four operators, $\partial_x, \partial_y, x, y$. The magnetic translation creation and annihilation operators

$c^\dagger, c$ are the remaining ones,

$$c^\dagger = e^{i\phi}(c_x - ic_y), \quad c = e^{-i\phi}(c_x + ic_y), \quad \mathbf{c} = \frac{-i\hbar\nabla + e\mathbf{A} - e\mathbf{B}\times\mathbf{r}}{\sqrt{2m\omega_c\hbar}}. \tag{2.11}$$

This set of operators satisfies the commutation relation

$$[c, c^\dagger] = 1, \quad [c, d^\dagger] = 0.$$

Each Landau level n_L is infinitely degenerate. As can be shown, the degeneracy stems from the translational gauge invariance of a 2DES subject to a homogeneous magnetic field, see Appendix A.

Wavefunctions in symmetric gauge

In the symmetric gauge, $\mathbf{A} = B(-y/2, x/2, 0)$, the operator $\mathbf{c}$ is

$$c_x = \frac{-i\hbar\partial_x + eA_x + eBy}{\sqrt{2m\omega_c\hbar}}, \quad c_y = \frac{-i\hbar\partial_y + eA_y - eBx}{\sqrt{2m\omega_c\hbar}},$$

which can be associated with the center of cyclotron orbit motion $\mathbf{R} = (X, Y)$,

$$\mathbf{R} = \mathbf{r} - e\frac{\mathbf{p}\times\mathbf{B}}{m^2\omega_c^2}, \qquad \begin{array}{rcl} X = -l\sqrt{2}c_y & = & x/2 + il^2\partial_y \\ Y = \quad l\sqrt{2}c_x & = & y/2 - il^2\partial_x \end{array}, \tag{2.12}$$

where the commutation relation $[X, Y] = il^2$ holds, $l = \sqrt{\hbar/eB}$ being the magnetic length. As conjugate operators the orbit center coordinates (X, Y) obey the uncertainty principle $\langle\Delta X\rangle\langle\Delta Y\rangle \geq l^2/2$.

It is noted that all eigenstates in the lowest Landau level (LLL) of (2.6) are generated by

$$|0;m\rangle = \frac{1}{\sqrt{m!}}(c^\dagger)^m|0;0\rangle, \quad 0 = c|0;0\rangle, \quad m \geq 0\,. \tag{2.13}$$

In order to obtain the real space representation $\phi_m(\mathbf{r}) = \langle \mathbf{r}|m\rangle$, the operators c, $c^\dagger$ have to acquire such a representation too,

$$c = \frac{1}{l\sqrt{2}}\left(\frac{\bar{z}}{2} + 2l^2\frac{\partial}{\partial z}\right),\ c^\dagger = \frac{1}{l\sqrt{2}}\left(\frac{z}{2} - 2l^2\frac{\partial}{\partial \bar{z}}\right). \tag{2.14}$$

Here we have chosen $e^{i\phi} = i$, such that $z = x - iy$ and with the rules

$$\partial_x = \frac{1}{2}(\partial_z + \partial_{\bar{z}}), \quad \partial_y = \frac{i}{2}(-\partial_z + \partial_{\bar{z}}).$$

From (2.13), (2.14) it is readily seen, that

$$\left(\frac{\bar{z}}{2} + 2l^2\frac{\partial}{\partial z}\right)\phi_0 = 0 \ \Rightarrow \quad \phi_0 = \frac{e^{-|z|^2/4l^2}}{\sqrt{2\pi}l} \tag{2.15}$$

is the normalized ground state $\phi_0 = \langle \mathbf{r}|0\rangle$. Similarly, this result is also obtained by applying the Landau level operators,

$$d^\dagger = \frac{i}{l\sqrt{2}}\left(\frac{\bar{z}}{2} - 2l^2\frac{\partial}{\partial z}\right),\ d = \frac{-i}{l\sqrt{2}}\left(\frac{z}{2} + 2l^2\frac{\partial}{\partial \bar{z}}\right). \tag{2.16}$$

All the remaining states $|n_L;m\rangle$ are generated by repeated application of $d^\dagger, c^\dagger$, par-

ticularly for the LLL it is obtained,

$$\phi_m(\mathbf{r}) = \langle \mathbf{r}|0;m\rangle = \frac{1}{l^{m+1}\sqrt{2^{m+1}\pi\, m!}} z^m e^{-|z|^2/4l^2}, \quad m \geq 0. \tag{2.17}$$

The important structure of any LLL state is equivalently expressed by the statement, that any LLL wavefunction is represented by a $\mathbb{C}$-analytic function. The analytic structure of any such state is emphasized by writing

$$\psi \propto f(z)e^{-|z|^2/4l^2},\ z = x - iy, \tag{2.18}$$

where $f(z)$ is an arbitrary $\mathbb{C}$-analytic function. This notation will be frequently employed in later chapters. For more detailed discussion, see Appendix A.

2.2.2 Models of disorder

The idealized picture of a 2DES with given translational gauge symmetry described in the previous section is rather contrived and does not allow to interpret properly 2DES transport measurements. "Real" 2D-systems such as electrons on a liquid helium surface or electrons confined in the a semiconductor inversion layer are subjected to the influence of a scattering potential which in the case of a helium surface comes from He-vapor atoms and surface ripplons. In the semiconductor case ionized dopants & impurities and interface roughness constitute the source of scattering. Therefore, the properties of the amended model with Hamiltonian (2.8), will be the scope of the subsequent sections.

It is evident that the immobile source of scattering in semiconductors is described by a static scattering potential, *i.e.*originating from long-range Coulomb forces between the fixed impurity locations and the electrons. As will be discussed in more detail in chapter 3, neutral He-vapor atoms are the dominant source of scattering on liquid helium for relatively high temperatures. Despite their volatility, on relevant times scales for a certain range of physical parameters, their presence is fairly well captured by the description of a static short range potential,

$$V(\mathbf{r}) = \sum_{i=1}^{N} v_i \delta(\mathbf{r} - \mathbf{r}_i), \tag{2.19}$$

where N is the number of vapor-atoms, v_i their effective strength and $\mathbf{r}_i$ their location.

Introducing randomness

For any given realization of a disorder potential (2.19) all properties of the system (2.8) may in principle be derived. Certainly, different realizations of $V(\mathbf{r})$ may result in different derived properties.

Nevertheless, the underlying assumption for all treatments of disorder is, that for the vast majority of realizations of the disorder potential $V(\mathbf{r})$ the predictions will be negligibly different from each other. Certainly, the configuration space of the realizations of $V(\mathbf{r})$ as defined in (2.19) increases factorially with the number N of impurity sites. In almost all cases it is justified to assume, that in the limit $N \to \infty$ the width of the distribution of predictions from different realizations of the random potential shrinks to a sharp peak which is solely characterized by its position (the

mean value).

Consequently, in this limit it seems to be feasible to substitute the predictions from one certain realization $V(\mathbf{r})$, by the averaging over all realizations of the disorder potential. This is the paradigm of physics of disordered systems!

Gaussian random potential

The statistical properties of the disorder potential are fully described by the set of k-point correlation functions. In the model (2.19), the scattering strength v_i describes the effective repulsive force resulting from the interaction of an electron with a neutral ^{4}He-atom. In the simplest model, v_i is considered as a scatterer independent constant. Without lack of generality it is assumed[1]

$$\langle V(\mathbf{r})\rangle = 0. \tag{2.20}$$

Then, the 2-point correlation function is

$$\langle V(\mathbf{r})V(\mathbf{r}')\rangle = \sum_{i,j}^{N}\langle v_i v_j \delta(\mathbf{r}-\mathbf{r}_i)\delta(\mathbf{r}'-\mathbf{r}_j)\rangle = n_s v_0^2 \delta(\mathbf{r}-\mathbf{r}'), \tag{2.21}$$

where averaging takes place for the independent random variables $\mathbf{r}_i$ which are uniformly distributed over the area S. Here, n_s is the impurity density and $v_0^2 = v_i^2$ the site independent scattering strength. Higher correlation functions are most easily

[1] an overall nonzero mean potential $\bar{V} = \langle V(\mathbf{r})\rangle$ causes only a shift in the ground energy.

evaluated by Fourier transform

$$\langle V(\mathbf{r})V(\mathbf{r}')V(\mathbf{r}'')V(\tilde{\mathbf{r}})\rangle = \sum_{i,j,k,n}^{N} \sum_{\mathbf{q}_1,\mathbf{q}_2,\mathbf{q}_2,\mathbf{q}_4} v_0^4 \times$$
$$\langle \exp[i\mathbf{q}_1(\mathbf{r}-\mathbf{r}_i) + i\mathbf{q}_2(\mathbf{r}'-\mathbf{r}_j) + i\mathbf{q}_3(\mathbf{r}''-\mathbf{r}_k) + i\mathbf{q}_4(\tilde{\mathbf{r}}-\mathbf{r}_n)]\rangle, \qquad (2.22)$$

where a nonzero contribution in (2.22) is obtained only for paired summation indices ($\{i=j, k=n\}, \dots$), leading to

$$\langle V(\mathbf{r})V(\mathbf{r}')V(\mathbf{r}'')V(\tilde{\mathbf{r}})\rangle = \langle V(\mathbf{r})V(\mathbf{r}')\rangle\langle V(\mathbf{r}'')V(\tilde{\mathbf{r}})\rangle +$$
$$\langle V(\mathbf{r})V(\mathbf{r}'')\rangle\langle V(\mathbf{r}')V(\tilde{\mathbf{r}})\rangle + \langle V(\mathbf{r})V(\tilde{\mathbf{r}})\rangle\langle V(\mathbf{r}')V(\mathbf{r}'')\rangle + \mathcal{O}(n_s v_0^4). \qquad (2.23)$$

Any 4-point correlation can be decomposed into a product of two-point correlations up to a term of the order $\mathcal{O}(n_s v_0^4)$ which originates from the configuration $\{i=j=k=m\}$. In the high density, weak coupling limit $n_s \to \infty$, $v_0 \to 0$ with the combined property $\sqrt{n_s}v_0 = \text{const.}$, any even k-point correlation function can be decomposed into a product of 2-point correlation functions. This is essentially Wick's theorem.

It is explicitly noted, that any correlation function with an odd number of constituents has to vanish. Either the grouping of constituents into classes larger than 2-point correlation functions will give a zero result by virtue of the high density and weak coupling limit, or the only remaining unpaired part will have a zero mean value (2.20).

Then the statistical properties of this disorder potential are completely determined by the 2-point correlation function alone $\langle V(\mathbf{r})V(\mathbf{r}')\rangle = K^{-1}(\mathbf{r}-\mathbf{r}')$ and its joint

probability distribution

$$\mathcal{P}[V] = \exp\left[-\frac{1}{2}\int\int d\mathbf{r}' d\mathbf{r}\; V(\mathbf{r})K(\mathbf{r}-\mathbf{r}')V(\mathbf{r}')\right]$$

constitutes a gaussian distributed random potential. In the case of a short-correlated random potential (2.19) it is $K = v^{-2}\delta(\mathbf{r}-\mathbf{r}')$ with $v = \sqrt{n_s}v_0$, then

$$\mathcal{P}[V] = \exp\left[-\frac{1}{2v^2}\int d\mathbf{r}\; V^2(\mathbf{r})\right]. \tag{2.24}$$

This distribution (2.24) will be the essential starting point for most analytical calculations.

2.2.3 Density of states of broadened Landau levels

Valuable thermodynamic information, like specific heat and magnetization, is contained in the density of states

$$\rho(E) = -\pi^{-1}\langle \mathrm{Im}\; G(\mathbf{r},\mathbf{r},E)\rangle, \tag{2.25}$$

where $\langle G\rangle$ is the disorder averaged Greens function of the full Hamiltonian (2.8). In contrast to the oversimplified picture of a system with translational gauge symmetry (2.6), it is expected that the δ-peaked density of states (DOS) profile

$$\rho(E) = l^{-2}\sum_n \delta(E-(n+\frac{1}{2})\hbar\omega_c) \tag{2.26}$$

will be broadened by a parameter γ which itself is determined by the scattering potential $V(\mathbf{r})$ and can be associated with a scattering time $\gamma \propto \tau^{-1}$. In principle the averaged Greens function is easily written

$$\langle G \rangle = G_0 + \langle G_0 V G_0 \rangle + \langle G_0 V G_0 V G_0 \rangle + \dots , \tag{2.27}$$

here G_0 is the bare Greens function of the "unperturbed" Hamiltonian (2.6). As it turns out (2.27) is hard to evaluate and a reasonable approximation has to be free from divergences.

General consideration

A crude estimate of the Landau level broadening in the presence of a short range interaction potential can be given in the following simple picture. In a high magnetic field an electron completes $\omega_c \tau$ rotations on the cyclotron orbit before it is scattered. The nature of its trajectory forces an electron to encounter a possible impurity many times, thus the magnetic field effectively increases the probability of the single-site scattering by $\omega_c \tau$,

$$\tau^{-1} \propto (\omega_c \tau) \tau_0^{-1}, \quad \mu = \frac{e}{m^*} \tau_0 \tag{2.28}$$

where τ_0 is the scattering relaxation time and μ the mobility in the absence of a magnetic field. The level broadening γ simply follows then from the uncertainty relation $\gamma \sim \tau^{-1} \propto \sqrt{\omega_c / \tau_0}$.

It is interesting to note that the condition $\omega_c\tau_0 = 1$ allows a fundamental distinction between high and low magnetic fields. For $\omega_c\tau_0 \ll 1$ the broadening of the Landau levels is much bigger than the separation $\hbar\omega_c$ between two adjacent levels $\gamma \gg \omega_c$ and the DOS becomes a smooth function of the energy, whereas in the opposite case $\omega_c\tau_0 \gg 1$ the Landau levels are well separated, $\gamma \ll \omega_c$. Therefore we can distinguish between the following cases [9, 15]:

Table 2.1: Simple classification of different regimes in magnetotransport.

	$\omega_c\tau_0 \leq 1$	classically weak magnetic field
$\omega_c\tau_0 \gg 1,$	$\hbar\omega_c/k_BT \leq 1$	classically strong magnetic field
$\omega_c\tau_0 \gg 1,$	$\hbar\omega_c/k_BT \gg 1$	quantum limit

SCBA density of states

The early work by Ando and Uemura [23, 24, 25, 26] belongs to the best known and most established ones. Using the self-consistent Born approximation (SCBA) where impurity scattering was taken into account in a self-consistent way and to avoid divergences in (2.27), Ando and Uemura obtained for the density of states (DOS) in the high-field limit $\omega_c \gg \gamma$

$$\rho(E) = \frac{1}{2\pi l^2}\frac{2}{\pi\hbar\gamma}\left[1 - \frac{1}{\hbar^2\gamma^2}\left(E - \frac{1}{2}\hbar\omega_c\right)^2\right]^{1/2}, \tag{2.29}$$

where $\hbar\gamma = (2/\pi)^{1/2}v/l$ is the broadening parameter. The singular behavior of the semi-elliptic DOS is the result of an oversimplified single-site approximation. Corrections from multiple-site scattering have also been considered [25].

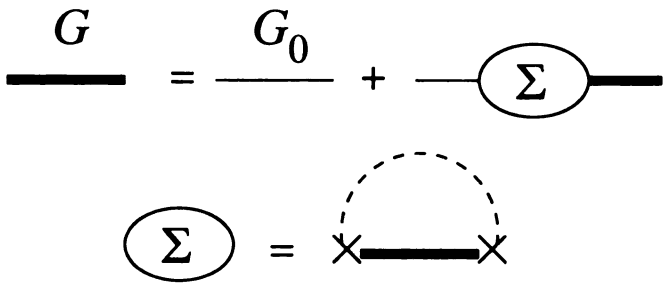

Figure 2.4: A diagrammatic representation of the self-consistent Born approximation. The crosses denote scatterers and the dotted lines represent interactions with them. Since our interaction potential is such that $\langle V \rangle = 0$, the interaction with only one scatterer vanishes in the self- energy Σ.

The perturbation expansion of the disorder averaged Greens function $\langle G \rangle$ in (2.27) can be diagrammatically written Fig. 2.4. In terms of the self energy Σ, the set of irreducible diagrams, it is expressed as

$$G(E) = G_0(E) + G_0(E)\Sigma(E)G(E). \tag{2.30}$$

However, the complete expression for the self energy is not easily obtained.

In the Born approximation only non-intersecting diagrams are included. The dashed line in Fig. 2.4 connects two scattering events. It is easy to see that the depicted rules only lead to a sequence of diagrams with non-intersecting dashed lines which is synonymous for non-intersecting diagrams. Then a closed form for the SCBA self-energy is easily obtained $\Sigma = G(E)/4\Gamma^2$, where $\Gamma = \hbar\gamma$ is the broadening parameter. Hence, (2.30) is a quadratic equation in $G(E)$. With $G_0 = (E - \frac{1}{2}\hbar\omega_c)^{-1}$ and relation (2.25) for the density of states, $\rho \propto \langle \mathrm{Im}G \rangle$, one readily obtains the SCBA density of states (2.29) which is of semielliptic form of width Γ exhibiting an unphysical

cut-off at the edges. In the case of a short range random potential the broadening parameter Γ is independent of the Landau level number. In this approximation scheme, each broadened Landau level has the same shape.

Exact result for the lowest Landau level

Astonishingly, with an elaborate diagram technique, Wegner [5] showed that for the white noise distribution (2.24) the exact density of states of the lowest Landau level could be calculated,

$$\rho(E) = \frac{1}{2\pi l^2}\frac{4}{\pi^{3/2}\hbar\gamma}\,\frac{\exp(w^2)}{1+\left(2\pi^{-1/2}\int_0^w dx\exp(x^2)\right)^2}, \tag{2.31}$$

where

$$w = \frac{2}{\hbar\gamma}\left(E - \frac{1}{2}\hbar\omega_c\right). \tag{2.32}$$

Brézin *et al.* [27] were able to rederive this result avoiding the intricate difficulties of Wegners diagrammatic approach by using a supersymmetric formalism. The tail distribution of (2.31) is gaussian and had been obtained in an earlier work by Ioffe and Larkin [28]. In their work, they used an optimal fluctuation method to determine the shape of the optimal potential as well as the asymptotic tail distribution for $\hbar\gamma \ll E \ll \hbar\omega_c$

$$\rho(E) \propto \exp\left[-\frac{4}{\hbar^2\gamma^2}\left(E - \frac{1}{2}\hbar\omega_c\right)^2\right]. \tag{2.33}$$

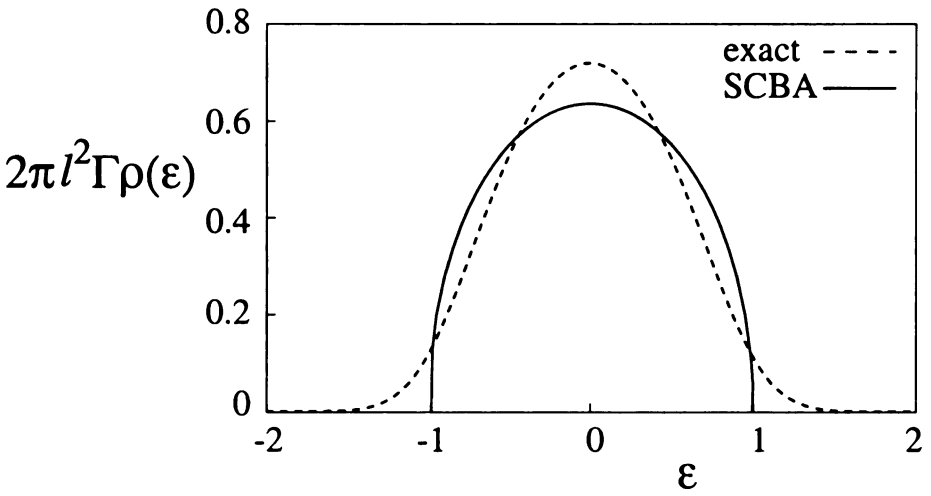

Figure 2.5: The normalized density of states for the lowest Landau level is plotted against the reduced energy $\varepsilon = (E - E_0)/\hbar\gamma$. Here $E_0 = 1/2\hbar\omega_c$ is the ground state energy and $\Gamma = \hbar\gamma$ the SCBA bandwidth. The SCBA approximation shows unphysically sharp edges at $\varepsilon = \pm 1$.

Generalization for potential with finite correlation length

Wegners result (2.31) is valid only for an uncorrelated random potential (2.21). No exact formula is known for gaussian random potentials with a finite correlation length

$$\langle V(\mathbf{r})V(\mathbf{r}')\rangle = (2\pi\lambda^2 l^2)^{-1} \exp\left[(\mathbf{r}-\mathbf{r}')^2/2\lambda^2 l^2\right]. \tag{2.34}$$

A possible technique to obtain the line shape in this case is the method of moments. Böhm *et al.* [29] calculated a finite number of moments of the DOS and restored it for the range $0 \leq \lambda < \infty$ by an efficient continued fraction approach. For the short range correlated potential $\lambda \to 0$, their result agrees with (2.31). The width of the distribution is a function of the correlation length λ. In a similar way, but using a cumulant expansion technique, Kristofferson *et al.* [30] also restored the density of

states for a finite correlation length (2.34).

In all cases the DOS is a smooth function of the reduced energy $\varepsilon = E/\hbar\gamma$ which lacks any signature of a *mobility gap* or other singular features, see Fig. 2.5, to indicate a drastic change in the transport properties whenever the Fermi-energy passes a critical value. The even more arduous task of calculating the conductivity, a two-particle Greens function, in the presence of disorder has to be undertaken.

2.3 SCBA conductivity

The fact that the exact density of states had been obtained [5] almost ten years after the work of Ando and Uemura [23, 24, 25, 26] in 1974, did not render the use of the SCBA as obsolete, in fact much of the transport data from experiments in 2DES are still interpreted on the basis of the SCBA single-electron theory [13, 14, 15]. For electrons on helium and strong quantizing magnetic fields the experimental data is reasonably well described by this single-electron theory. The reason for its persistence is easily explained. The successful application of the diagram technique used by Wegner and its reformulation in a supersymmetric quantum field theory for obtaining the density of states, a one-particle Greens function, could not be easily extended to calculate the conductivity which is a two-particle Greens function. The longitudinal conductivity σ_{xx} is calculated with a Kubo-formula [31],

$$\sigma_{xx} \propto \langle X \mathrm{Im} G(E+i0) \dot{X} \mathrm{Im} G(E+i0) \rangle, \tag{2.35}$$

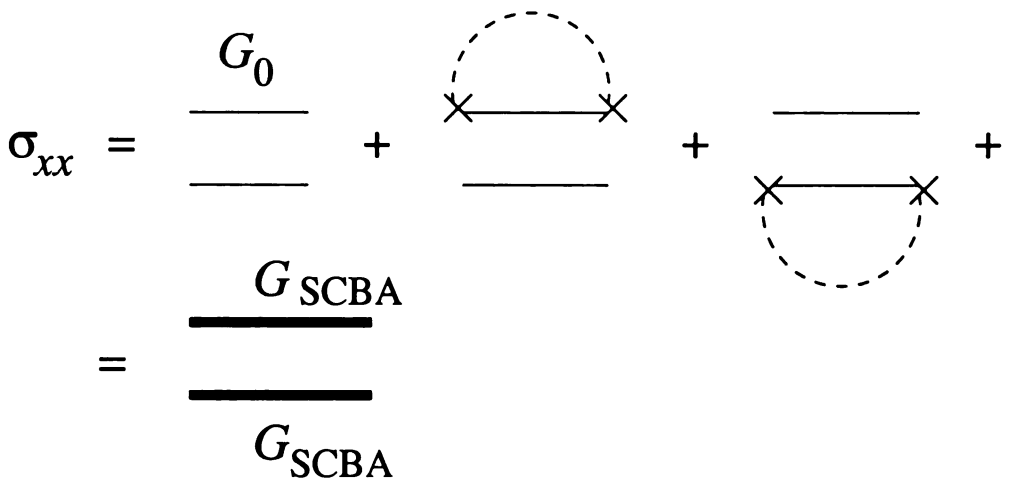

Figure 2.6: SCBA diagrams for the conductivity σ_{xx}. To be consistent with the diagram rules, Fig 2.4, introduced for the single-particle Greens function, no interconnecting and intersecting diagrams are allowed, from which follows that both SCBA-Greens functions are decoupled (mean field).

where X is the operator of the cyclotron orbit center (2.12) and $\dot{X} = (i\hbar)^{-1}[X, H]$ describes the nontrivial time evolution of the orbit centers. Similarly to the density of states the Greens function perturbation technique is used to obtain an infinite series of diagrams. The SCBA-scheme with diagram rules shown in Fig.2.6 allows to sum up an infinite part of the perturbation series. The SCBA diagrams for the conductivity do not contain diagrams which interconnect the two single-particle Greens functions nor do they include any intersecting diagrams of each single strand. This is consistent with the diagram rules, Fig 2.4, for the single-particle SCBA Greens function.

In the case where coupling between Landau levels may be neglected (strong magnetic fields), the magnetoconductivity is obtained for short range interactions [23, 16]

$$\sigma_{xx}(B) = \frac{e^2}{\pi^2\hbar}\int dE\,\left(-\frac{\partial f}{\partial E}\right)\sum_{j=0}^{\infty}(j+1/2)\left[1-\frac{1}{\Gamma^2}(E-E_j)^2\right], \qquad (2.36)$$

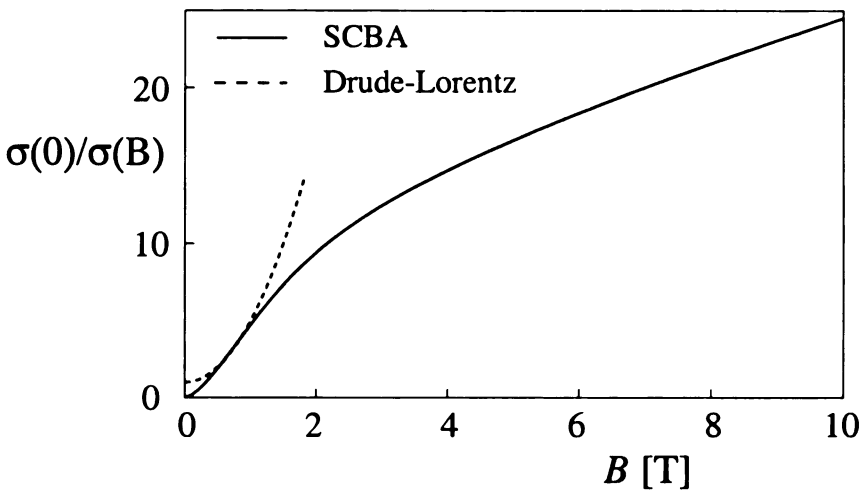

Figure 2.7: The calculated inverse magnetoconductivity in the SCBA approximation (2.37) (solid curve) and for the Drude-Lorentz model (dashed curve).

where $E_j = \hbar\omega_c(j+1/2)$ and $f(E)$ is the distribution function. For a non-degenerate electron system, $f(E)$ obeys the classical Maxwell-Boltzmann distribution and one obtains for the static magnetoconductivity

$$\sigma_{xx}(B) = \frac{n_e e}{B} \frac{\cosh\left(\frac{\Gamma}{k_B T}\right) - \frac{k_b T}{\Gamma}\sinh\left(\frac{\Gamma}{k_B T}\right)}{\frac{\pi}{2} I_1\left(\frac{\Gamma}{k_B T}\right)} \coth\left(\frac{\hbar\omega_c}{2k_B T}\right). \qquad (2.37)$$

Here I_1 is the modified Bessel function of first order, n is the electron density. Figure 2.7 shows the calculated ratio $\sigma_{xx}(0)/\sigma_{xx}(B)$, where $\sigma_{xx}(0) = \mu ne$ is the zero field conductivity, as a function of the magnetic field for typical parameters of the system of electrons on liquid helium. At low fields, the curve shows the Lorentz-Drude like behavior $\sigma_{xx}(B) \propto B^{-2}$, but (2.37) diverges at $B \to 0$. At higher fields the conductivity shows a reduced field dependence $\sigma_{xx}(B) \propto B^{-1/2}$, in the high field

limit

$$\sigma_{xx}^{\mathrm{SCBA}}(B) = \frac{4}{3\pi} n_e e^2 \frac{\gamma l^2}{k_B T}, \tag{2.38}$$

which clearly shows that the static magnetoconductivity in the SCBA approximation is *nonzero* for any finite magnetic field.

The characteristic features of the magnetoconductivity (2.37) can also be understood by a simple diffusion picture [14, 23]. The conductivity can be derived from the Einstein relation $\mu = eD/k_B T$

$$\sigma = \frac{n_e e^2 D}{k_B T}, \tag{2.39}$$

where $D = l_c^2 \tau^{-1}$ is the diffusion constant with characteristic length scale l_c and time for the diffusion process τ. In a magnetic field with $\omega_c \tau \gg 1$ the cyclotron radius becomes the characteristic length. In classically strong fields $\hbar\omega_c \leq k_B T$, the cyclotron radius is given by $l_c = mv/eB \propto \sqrt{mk_B T}/eB$. Then, from (2.39) one obtains the Drude-Lorentz behaviour

$$\sigma_{xx}(B) = \frac{n_e e^2}{m} \frac{1}{\omega_c^2 \tau_0} = \frac{\sigma_0}{(\omega_c \tau)^2} \propto \frac{1}{B^2}. \tag{2.40}$$

In the quantum limit all electrons are barred onto the lowest Landau level, the characteristic length scale is the magnetic length $l = (\hbar/eB)^{-1/2}$ and the characteristic

time is the scattering time γ^{-1}. Then one obtains

$$\sigma_{xx}(B) = \frac{n_e e}{B} \frac{\hbar\gamma}{k_B T} \propto \frac{1}{\sqrt{B}} \tag{2.41}$$

which reproduces the dependence and order of magnitude of the SCBA conductivity (2.38).

In summary, the rather simple perturbational calculation of the dissipative conductivity σ_{xx} does not provide any insight into the transport dynamics of the QHE. The experimental observation of the essential role of a localization-delocalization transition cannot be based on a perturbational approach.

2.4 Localization

The concept of localized states in disordered systems was developed by Anderson [20]. He showed that if a quantum-mechanical system is sufficiently disordered, states have a finite probability of returning to a given site in the long-time limit. This absence of diffusion implies that these states are localized in a finite region of space. The transmission probability decays exponentially on a length scale, which is called the localization length. For localized states the static conductivity vanishes at zero temperature. On the other hand, if the disorder is weak enough, extended states might exist that do not decay exponentially and fill the whole system. Their contribution to the conductivity is finite even at zero temperature. The energy that separates extended from localized states is called the mobility edge. At the mobility edge the

character of eigenstates can be described by fractal measures [32, 33].

The observation that an explanation of the QHE involves both extended and localized states was the more unanticipated, as the scaling theory of localization in zero magnetic fields [34, 35, 36] predicted the absence of extended states in two-dimensional systems. It is the presence of a strong magnetic field that leads to the emergence of nonlocalized states in two dimensions [37, 38]. Chalker [39] showed that these states exist only at a single energy in the limit where scattering between Landau levels can be neglected. At zero temperature the Hall conductivity is thus expected to exhibit sharp steps whenever the Fermi energy passes the critical energy. The longitudinal conductivity vanishes for all energies except at the critical ones.

It is this aspect of localization which constitutes the basic difficulty when one attempts to base the transport properties of such a system on a microscopic theory. The standard machinery, like the SCBA, for dealing perturbationally (diagrammatically) with electron-impurity scattering does not lead to an explanation of the phenomenon of the QHE [40, 41, 42, 43].

2.4.1 Scaling theory

Most what is known about critical properties of the localization-delocalzation transition stems from experiments [6] and numerical simulations [17]. The localization-delocalization transition is understood in terms of the scaling behavior of electron states near the Landau level band centers. For short range scatterers it has been

confirmed numerically that the spatial extent of electron states of the LLL scales as

$$\xi(\varepsilon) \sim l\,|\varepsilon|^{-\nu}, \tag{2.42}$$

where $\varepsilon = E/\hbar\gamma$ and $\nu = 2.33 \pm 0.03$ is the localization exponent [17, 44].

To understand the origin of this scaling one can treat the electron motion semiclassically for a sufficiently small value of the reduced energy $\gamma_0 < \varepsilon < \gamma$. In a strong magnetic field, the guiding center $\mathbf{R} = (X, Y)$ of the electron drifts along equipotential lines of the potential $V(X, Y)$, which is also the Hamiltonian of the system,

$$\dot{X} = \frac{i}{\hbar}[H, X] = -\frac{l^2}{\hbar}\frac{\partial V}{\partial y}, \quad \dot{X} = \frac{i}{\hbar}[H, Y] = \frac{l^2}{\hbar}\frac{\partial V}{\partial x}. \tag{2.43}$$

The problem of finding the wave function of largest extent is similar to the problem of finding the largest connected cluster in a continuum percolation problem [45], which gives the critical exponent, $\nu_p = 4/3$. Tunneling between nearby states at the saddle points modify the critical exponent giving $\nu = 1 + \nu_p = 7/3$ [46]. Even closer at the percolation threshold $\varepsilon \leq \gamma_0$, where tunneling between states becomes strong the semiclassical approximation is not applicable. Numerical simulations with an appropriate random-Landau-matrix model for this regime confirms the persistence of the critical exponent $\nu = 2.33 \pm 0.03$ even out of the range of the semiclassical approach.

Chapter 3

Non-degenerate 2D electron system

3.1 Electrons on ^{4}He: the best conductor

Electrons above the surface of liquid helium provide an example of a nearly ideal two-dimensional (2D) electron system, with mobilities higher than in any solid state conductor have been obtained [16, 47, 48]. For characteristic electron densities $n_e \sim 10^7 - 10^8$ cm^{-2} and temperatures 0.1 K $< T <$ 2 K the interelectron distance $n_e^{-1/2}$ greatly exceeds the de Broglie wavelength $\lambda_T = \hbar/(2mk_BT)^{1/2}$, and therefore the electron system is nondegenerate, see Tab. 3.1. At the same time, the ratio of the characteristic Coulomb energy of the electron-electron interaction to the kinetic

energy, the plasma parameter

$$\Gamma_p = e^2(\pi n_e)^{1/2}/k_B T \tag{3.1}$$

is usually large, $\Gamma_p \gtrsim 10$. Therefore the electron-electron interaction is by no means weak. The system is a strongly correlated normal fluid. For $\Gamma_p \gtrsim 127$ (lower T), the Coulomb energy dominates and the system undergoes a phase transition to the Wigner crystal [49, 50, 51, 52].

Table 3.1: A comparison of some typical physical parameters of two-dimensional electron systems realized by different methods (from [1]). In this table n_e is the electron density, m^*/m the effective to vacuum electron mass ratio, $T_F = E_F/k_B$ the Fermi temperature with $E_F = \pi\hbar^2 n_e/m^*$ and τ the relaxation time with $\mu = e\tau/m^*$ the zero magnetic field mobility.

	electrons on He_4	Si-MOS	GaAs-GaAlAs
$n_e(\mathrm{cm}^{-2})$	10^5 - 10^9	10^{11}–10^{13}	10^{11} - 10^{12}
m^*/m	1.0	0.19	0.067
$T_F(\mathrm{K})$	10^{-6}–10^{-2}	10 - 500	200 - 1000
$\tau(\mathrm{sec})$	10^{-10}–10^{-7}	10^{-12}	10^{-12} - 10^{-11}
$\mu(\mathrm{cm}^2/\mathrm{Vs})$	10^3 - 10^8	10^4	10^5 - 10^7

The normal electron fluid is a special type of many-electron system, which is very different from the much better understood Fermi liquid (and other quantum electron liquids) or low-density electron gas. Analysis of this fluid is complicated by the absence of "good" quasiparticles — the same problem encountered in the physics of liquids. In contrast to atomic or molecular liquids, in an electron fluid the interparticle forces are the long-range Coulomb forces. Another difference from 3D liquids is that relaxation of the total momentum is due to scattering (by ripplons and helium vapor

atoms) of electrons which are inside the electron fluid, not on its boundary. Analysis of electron dynamics and transport phenomena in a normal electron fluid is necessary for understanding a large amount of experimental data on transport accumulated over the last few years [52, 53, 54, 55, 56, 57, 58, 14, 59, 60, 61, 62, 63, 64, 65, 66, 3, 67].

3.1.1 Experimental consideration

Surface State Electrons

Electrons on a surface of dielectric ^{4}He ($\varepsilon = 1.0572$ [68]) are trapped by image charges in the helium film. Additional electric fields from gate electrodes further confine the electron sheet in the experimental area, see Fig.3.1. The confining potential is described by $V(z) = V_{\text{image}}(z) + eE_\perp z, z > 0$, where

$$V_{\text{image}}(z) = -\frac{Qe^2}{4\pi\varepsilon_0 z}, \quad Q = \frac{\varepsilon - 1}{4(\varepsilon + 1)} \ll 1 \tag{3.2}$$

where the dielectric constant of the gaseous ^{4}He-phase is assumed to be unity. Helium is an inert gas, its filled electron shells prevent the electrons from the sheet to penetrate into the liquid bulk material. The steep potential barrier on the interface side, compare Fig.2.1, is a consequence of the Pauli exclusion principle which requires the wavefunction of the electron to be orthogonal to the core electrons of the dielectric. The ground state wave function $Z_0(z)$ (2.5) can be written as

$$Z_0(z) = 2\gamma_\perp^{3/2} z \exp(-\gamma_\perp z) \tag{3.3}$$

with an variational parameter $\gamma_\perp$. In the absence of the external pressing field $E_\perp$, $\gamma_\perp^{(0)}$ is the effective inverse Bohr radius $\gamma_\perp^{(0)} = Q/a_0$ where $a_0 = 4\pi\varepsilon_0\hbar^2/me^2 = 0.53\text{Å}$ is the Bohr radius. The electron remains far from the liquid helium surface, $\langle z\rangle_0 = 3/2a \gg r_0$, ^{4}He ($1/\gamma_\perp^{(0)} = 76\text{Å}$) where r_0 is the interatomic average spacing. The energy gap is determined as $\Delta E = E_1 - E_0 = 0.49\text{meV} = 5.72\text{K}$.

Experimental set-up

One of the problems in measuring transport properties of electrons on a surface of a dielectric is that one cannot attach electrical leads directly to the electron sheet and therefore it is not possible to perform simple dc-current experiments on this system. In common two types of experiments give insight into the electron dynamics. One type of experiments is based on the application of high frequency electro-magnetic fields (radio frequency or microwaves) leading to resonant power absorption by the electron system (plasmon modes, cyclotron resonance). The second type of experiments measures the impedance of an array of electrodes which couple capacitively to the electron sheet, see Fig.3.1.

3.2 Scattering mechanisms

3.2.1 Vapor scattering

The cross-section for scattering of electrons with a helium atom is $b_{\text{He}}^2 \approx 5\text{Å}^2$, and so helium vapor atoms create a nearly ideal δ-correlated potential $V(r) = \sum v_i\delta(\mathbf{r} - \mathbf{r}_i)$ (2.19) arising from the Pauli principle. The explicit form of the squared matrix

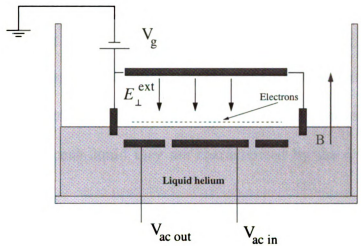

Figure 3.1: Schematic drawing of the experimental liquid helium cell. Capacitors couple to the electron sheet. The mobility μ of the electron system can be determined from the impedance measurement. Gate electrodes supplied by the voltage V_g further confine the electron sheet in the experimental area.

elements of the coupling to the vapor atoms is [69]

$$\overline{|V_{\mathbf{q}}|_v^2} = \int d\mathbf{r}\; K(\mathbf{r}) e^{i\mathbf{q}\mathbf{r}} = \frac{3\pi\hbar^4}{8m^2}\gamma_\perp b_{\mathrm{He}}^2 N_v S^{-1}, \tag{3.4}$$

where $K(\mathbf{r}) = \langle V(\mathbf{r})V(0)\rangle$ is the correlation function (2.21), N_v is the (3D) vapor density, S the surface area and $\gamma_\perp$ as given in (3.3). It is noted that N_v depends on the temperature exponentially,

$$N_v = \left(\frac{Mk_bT}{2\pi\hbar^2}\right)^{3/2} \exp\left(-\frac{Q}{k_BT}\right). \tag{3.5}$$

In this expression M denotes the ^{4}He atom mass and Q the vaporization energy of ^{4}He ($Q/k_B = 7.17$K [69]).

3.2.2 Ripplon scattering

The free surface of a liquid at a finite temperature always oscillates. The surface oscillations of a liquid of depth d are called capillary gravity waves. For a classical incompressible, non-viscous liquid they are characterized by the dispersion relation [70]

$$\omega_{\mathbf{q}}^2 = \left(gq + \frac{\alpha q^3}{\rho} \right) \tanh qd, \tag{3.6}$$

where q is the wave vector of the excitation, $g = 9.81 m/s^2$ the gravity acceleration, $\alpha \approx 0.35$dyn/cm the surface tension and $\rho = 0.145$g/cm^3 the density of the liquid phase.

The excitations of the free surface can be quantized by elementary excitations which are called ripplons [71, 72]. Any arbitrary surface displacement $u(\mathbf{r})$ can be expanded into a series of ripplons

$$u(\mathbf{r}) = \frac{1}{\sqrt{S}} \sum_{\mathbf{q}} Q_{\mathbf{q}} \exp(i\mathbf{qr})(a_{\mathbf{q}} + a_{-\mathbf{q}}^{\dagger}), \; Q_{\mathbf{q}} = \left(\frac{\hbar q \tanh qd}{2\rho\omega_q} \right), \tag{3.7}$$

where $[a_{\mathbf{q}}, a_{\mathbf{q}'}^{\dagger}] = \delta_{\mathbf{q}-\mathbf{q}'}$ are the ripplon creation and annihilation operators. The energy associated with such a surface excitation is easily described by a system of surface bound quasi-particles of Bose type with occupation number $N_{\mathbf{q}}$

$$H_R = \sum_{\mathbf{q}} \hbar\omega_{\mathbf{q}} (a_{\mathbf{q}}^{\dagger} a_{\mathbf{q}} + \frac{1}{2}), \quad N_{\mathbf{q}} = \left(\exp \frac{\hbar\omega_{\mathbf{q}}}{k_B T} - 1 \right)^{-1}. \tag{3.8}$$

Various coupling mechanisms between ripplons and the electron sheet have been proposed, a detailed discussion can be found in Ref. [73]. The following coupling mechanism is experimentally confirmed and generally accepted. The electron wave function adiabatically follows the surface movement. The interaction energy is brought about mainly by two effects. One contribution results from the change in the polarization of the helium as the surface profile is altered by the presence of ripplons. At large interparticle separation R between an electron and a helium atom the polarization potential is proportional to $1/R^4$. The change in polarization energy V_p can be obtained by an integration over the change in the helium volume which as a weakly polarizable medium, $P \propto (\epsilon - 1)E$, where P is the polarization, $P \propto (\epsilon - 1)E$, interacts with the electric field E of an electron

$$V_p(\mathbf{r}, z) = -\frac{Qe^2}{4\pi^2\varepsilon_0} \int d\mathbf{r}' \int_0^{u(\mathbf{r}')} \frac{dz'}{[(\mathbf{r}' - \mathbf{r})^2 + (z' - z)^2]^2}. \tag{3.9}$$

The second contribution $\Delta E_{\text{pot}} = eE_\perp u(\mathbf{r})$ is due to the vertical motion of an electron in the presence of an external electric field $E_\perp$ perpendicular to the unperturbed helium surface as it follows adiabatically the fluctuations of the interface. Since one-ripplon processes are dominating higher order processes by orders of magnitude [74], the interaction between electrons and ripplons can be compactly written as [69]

$$H_{e-R} = \frac{1}{\sqrt{S}} \sum_{\mathbf{q}} Q_{\mathbf{q}} V_{\mathbf{q}}(z) \exp(i\mathbf{qr})(a^\dagger_{-\mathbf{q}} + a_{\mathbf{q}}) c^\dagger_{\mathbf{k}+\mathbf{q}} c_{\mathbf{k}} \tag{3.10}$$

with $Q_{\mathbf{q}}$ as defined in (3.7) and

$$V_{\mathbf{q}}(z) = -\frac{Qe^2q^2}{4\pi\varepsilon_0}\left[\frac{K_1(qz)}{qz} - \frac{1}{(qz)^2}\right] + eE_\perp. \tag{3.11}$$

Here K_1 is the modified Bessel function of the second kind, Q is given by (3.2), and $\{c_{\mathbf{k}}, c^\dagger_{\mathbf{k}'}\} = \delta_{\mathbf{k}+\mathbf{k}'}$ are the anticommuting electron creation and annihilation operators for the electronic ground state $\psi_{\mathbf{k}}(\mathbf{r}, z) = S^{-1/2}Z_0(z)\exp(i\mathbf{kr})$ with a wave vector $\mathbf{k}$ parallel to the surface. The electron-ripplon interaction will be strong only for comparable wave length. Energy and momentum conservation restrict the ripplon wave vectors to values $q \leq 2\lambda\!\!\!^{-}_T \sim 10^5 - 10^6$ cm^{-1} which are of the order of the de Broglie wavelength $\lambda\!\!\!^{-}_T$ [75]. With the electron energy exceeding the ripplon energy $\hbar\omega_{\mathbf{q}} \ll (\hbar\lambda\!\!\!^{-}_T)^2/2m$ the scattering process is quasi-elastic.

It is noteworthy that the electron-ripplon interaction (3.11) depends explicitly on the external pressing field $E_\perp$, therefore one can easily vary its interaction strength. For low enough temperatures $T < 2K$, the electron will remain in its ground state Z_0, the effective ripplon potential is obtained by the projection of (3.11)

$$V_{\mathbf{q}} = \int_0^\infty Z_0(z)V_{\mathbf{q}}(z)Z_0(z)\,dz\,. \tag{3.12}$$

Therefore the effective intensity of the random field of short wavelength ripplons is

of the form [69]

$$\overline{|V_{\mathbf{q}}|_r^2} = S^{-1}\frac{k_B T e^2}{\alpha q^2}\left[E_\perp^2 + 2E_\perp E_{\rm pol} + E_{\rm pol}^2\right], \tag{3.13}$$
$$E_{\rm pol} \equiv E_{\rm pol}(q) = \frac{\hbar^2\gamma_\perp^{(0)}}{2me}q^2\varphi\left(\frac{q}{2\gamma_\perp}\right).$$

Here, $\gamma_\perp$ and $\gamma_\perp^{(0)}$ are the variational parameters of the electron wave function transverse to the layer $Z_0(z) \propto z\exp(-\gamma_\perp z)$, in the presence and absence of the electric field $E_\perp$ that presses the electrons against the helium surface, $\gamma_\perp^{(0)} = (me^2/4\hbar^2)(\varepsilon - 1)/(\varepsilon + 1)$. In Eq. (3.13), α is the surface tension and the function $\varphi(x)$ is given by $\varphi(x) \approx \ln(2/x)$ for $x \ll 1$, [69].

3.3 Magnetoconductivity: current status in theory and experiment

Over the past three decades a huge amount of experimental data on electrons on liquid helium has been amassed and with an equally vast amount of theoretical work a very detailed understanding of the involved scattering processes and transport phenomena has been reached. A comprehensive theory of magnetotransport in the semiclassical regime is given by Mark Dykman [9]. It is the subject of this section to provide a current survey on the theoretical understanding of magnetotransport of electrons on helium with emphasis on the many-electron transport processes. It also will be pointed out the context in which the subject of this Ph. D. thesis has to be placed and where studies have been conducted to reach new insights.

Table 3.2: Regimes for magnetoconductivity theories. The regimes are shown for the values of the given parameters. The last column shows the magnetic field at which the parameter in the first column equals one, for the electron density $n_e = 10^{12}\mathrm{m}^{-2}$ at 1K.

Parameter	Regime	Conductivity behavior	B [T]
$B = 0$	zero field	Drude	0
$\mu B = \omega_c \tau$	< 1 : Classically weak field	Drude	0.01
	> 1 : Classically strong field	Drude	
ω_c/ω_p	$< 1 : eE_f \lambda_T \approx \hbar\omega_p > \hbar\omega_c$	$\approx$ Drude	0.23
	$> 1 : eE_f \lambda_T \approx \hbar\omega_p < \hbar\omega_c$		
$\hbar\omega_c/k_B T$	< 1 : Classical limit	Non-Drude (Many electron classical)	0.74
	> 1 : Quantum limit	Non-Drude (Many electron quantum)	

Magnetoconductivity requires consideration of a multidimensional parameter space, magnetic field, temperature, electron density and particular parameters which are inherent to the scattering mechanisms. Therefore it is natural to specify parameter ranges for which particular effective models can be used to describe the transport phenomena within that range.

Table 3.2 shows a collection of parameter spaces which will be discussed in more detail in the following subsections. In particular one has a very good understanding of the transport processes at relatively low magnetic fields $k_B T > \hbar\omega_c$. Recent experiments utterly confirm the theoretical picture presented in this section, see Fig.3.2 and Ref. [3].

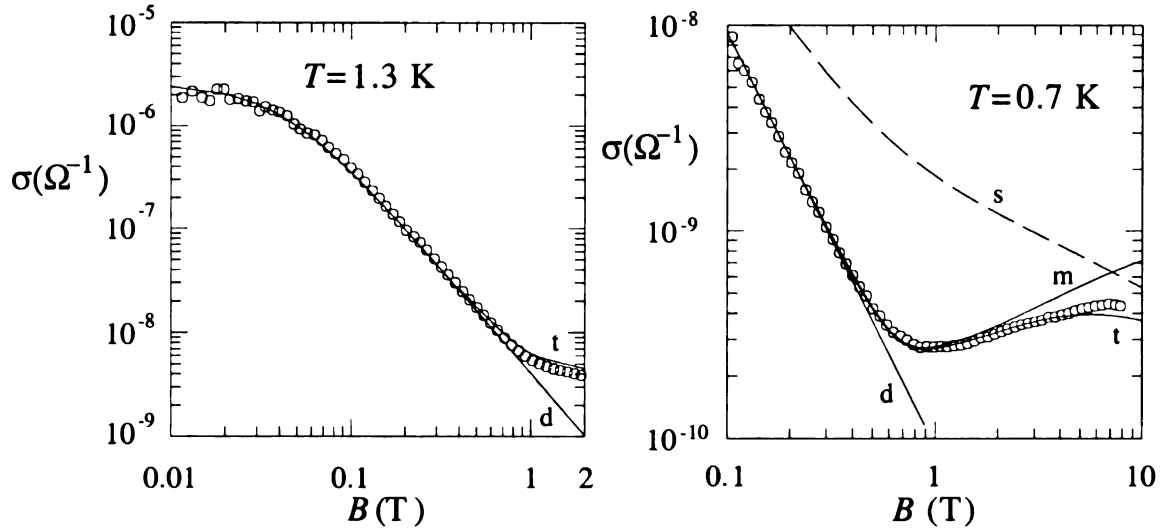

Figure 3.2: The magnetoconductivity $\sigma(B)$ versus B for electrons on bulk liquid helium at (a) 1.3K, $n_e = 2.32 \times 10^8 \mathrm{cm}^{-2}$, $\mu = 24 \mathrm{m}^2/\mathrm{Vs}$ and (b) 0.7K, $n_e = 0.55 \times 10^8 \mathrm{cm}^{-2}$, $\mu = 980 \mathrm{m}^2/\mathrm{Vs}$. Line **d** shows the Drude model, line **s** the SCBA single electron theory, line **m** the many-electron theory and line **t** the total magnetoconductivity (from Lea *et al.*, 1996) [3].

3.3.1 Single-electron explanation

Drude magnetoconductivity, low magnetic field

The simplest theory for the magnetoconductivity is the Drude model which treats the electron-scatterer interaction as well separated in time. The static conductivity is simply derived from the classical equation of motion

$$m\frac{d}{dt}\mathbf{v} = -e\mathbf{v} \times \mathbf{B} - e\mathbf{E} - m\tau_{B=0}^{-1}\mathbf{v}, \tag{3.14}$$

where $\tau_{B=0}^{-1}$ is the scattering rate in the absence of the magnetic field calculated in the approximation where the effect of the electron-electron interaction on collisions with

scatterers is ignored, yielding to

$$\sigma_{xx}(\omega = 0) = \frac{e^2 n_e}{m} \frac{\tau_{B=0}}{1 + \omega_c^2 \tau_{B=0}^2}. \tag{3.15}$$

This simple picture accounts much for the explanation of the experimental data in Fig. 3.2. Certainly, the Drude theory is valid in the weak field limit, $\omega_c \tau < 1$, the broadened Landau levels overlap and thus the scattering will be field independent $\tau = \tau_{B=0}$. As will be discussed in the many-electron section, the Drude theory continues to describe the system even in classically strong magnetic fields $\omega_c \tau \gg 1$ for a certain parameter range (3.26). A conceptual picture can be drawn that in classically strong fields $\omega_c \tau \gg 1$, an orbiting electron repeatedly encounters the same scattering center giving enhanced scattering, therefore τ is expected to be B-field dependent. However, Coulomb interactions with its manifestation of an internal many electron field $\mathbf{E}_{\mathrm{fl}}$ "blows away" the electron during the orbit cycle, and restores the Drude picture of orbiting electrons in which orbit center motion is effectively described by diffusion. In the range of classically strong fields the Drude model is entirely maintained by many-electron effects.

SCBA magnetoconductivity, high magnetic field

Single-electron magnetotransport is usually analyzed using the self-consistent Born approximation (SCBA) [14, 16, 59, 60, 61, 62, 63]. In this approximation the relaxation rate $\tau_{SCBA}^{-1}(B)$ is given by the relaxation rate $\tau_{B=0}^{-1}$ multiplied by the factor of the increase of the density of states that results from "squeezing" of the energy

spectrum into (broadened) Landau levels. This factor, in turn, is given by the ratio between the interlevel distance and the level broadening which is itself due to scattering, $\omega_c/\tau^{-1}_{SCBA}(B)$. The result for the relaxation rate is of the form

$$\tau^{-1}_{SCBA}(B) = \vartheta_{SCBA}\omega_c^{1/2}\tau^{-1/2}_{B=0}, \quad \vartheta_{SCBA} \sim 1, \quad \omega_c \gg \tau^{-1}_{SCBA}(B). \tag{3.16}$$

A simplified derivation for the SCBA conductivity was already given in Section 2.3. Detailed analysis of the SCBA for a nondegenerate 2D system can be found in [14, 61, 62]; an alternative approach to the single-electron theory is based on the method of moments for the frequency-dependent conductivity $\sigma_{xx}(\omega)$ [76]. If one thinks of $\sigma_{xx}(\omega)$ as a function which has a Gaussian-type peak at the frequency $\omega = 0$, then the method of moments gives a result similar to the SCBA.

If $\tau_{SCBA}(B)$ is used instead of $\tau_{B=0}$ in Eq. (3.15), the magnetoconductivity in classically strong fields, $\omega_c\tau_{SCBA} \gg 1$, is $\propto B^{-3/2}$; it differs from the result (3.15) by a large factor $(\omega_c\tau_{B=0})^{1/2} \gg 1$. The experiments also show a big discrepancy between observed data and the single-electron SCBA explanation for the regime of classically strong fields, Fig. 3.2.

However, in the limit of very strong quantizing magnetic fields $\omega_c\tau \gg 1, \hbar\omega_c/k_BT > 1$, the SCBA conductivity $\sigma^{SCBA} \propto B^{-1/2}$ (2.41) seems to deliver a reasonably good picture which qualitatively agrees with experiments [15, 61, 62]. **It is the subject of this thesis to show that even in the strong-field limit the static magnetotransport is entirely due to many-electron effects. The coincidence of having a single-electron theory to describe this regime is only**

fortuitous.

3.3.2 Fluctuational electric field

To a large extent, transport is determined by the momentum exchange between electrons and scatterers. When the electron-electron interaction is strong, as in the fluid or Wigner crystal, it controls the collisions with the scatterers. The effect is expected to be particularly strong when a 2D electron system is placed into a transverse magnetic field B [77, 78, 76]. In the single-electron approximation the electron energy spectrum in the magnetic field is a set of discrete Landau levels with separation $\hbar\omega_c$, and electrons do not have a finite group velocity. Therefore the standard picture of a moving electron with independent elastic or quasielastic collisions does not apply. As a consequence, the scattering is always strong, irrespective of the strength of the electron-scatterer coupling, and the random potential of the scatterers is the only reason for the centers of cyclotron orbits to move.

On the contrary, the energy spectrum of the system of interacting electrons is continuous even in the absence of scatterers. Therefore, although the electron-electron interaction does not change the total momentum of the electron system, it may mediate the momentum transfer to the scatterers and thus strongly affect the transport.

Classical and semiclassical many-electron dynamics

A theory of the dynamics and transport of a normal electron fluid can be formulated for not too low temperatures and/or for small enough electron densities or high magnetic fields, where the major effect of the electron-electron interaction on the electron

dynamics may be described in terms of an electric field $\mathbf{E}_f$ [78] that drives each electron. Unlike the long-wavelength fluctuational field known in plasma physics [79], the field $\mathbf{E}_f$, although also of fluctuational origin, determines the Coulomb force on an individual electron. This force affects the electron motion during collisions with scatterers, and ultimately the momentum transfer from the many-electron system to the scatterers. A special significance of the field $\mathbf{E}_f$ for a 2D electron system in a magnetic field stems from the fact that a cyclotron orbit center drifts transverse to the fields $\mathbf{E}_f$and $\mathbf{B}$. A drifting electron occasionally collides with scatterers, as would a single electron in the absence of a magnetic field, and thus the field $\mathbf{E}_f$ may "restore" the simple Drude picture of electron relaxation that results from collisions which are well separated in time. Clearly, in this case $\mathbf{E}_f$ determines the collision probabilities and thus the transport coefficients.

The field $\mathbf{E}_f$ is particularly useful for characterizing the electron dynamics in a many-electron system provided this field is uniform over the electron wavelength $\lambda\!\!\!^{-}$ (otherwise the nonuniformity of the field would be as important as the field itself). A simple estimate of the field $\mathbf{E}_f$ and of the parameter range where it is uniform can be obtained if one assumes that there is short-range order in the electron system in the interesting range $\Gamma_p \gtrsim 10$, as has been established by Monte Carlo calculations [80, 81, 82, 10, 83, 11, 84, 4]. In this case the electrons are affected by fields due to electron displacements from their (quasi)equilibrium positions (see Fig. 3.3). The characteristic thermal displacement δ and $\mathbf{E}_f$ can be estimated by linearizing electron equations of motion and by setting the potential energy of a displaced electron equal

to k_BT (cf.[78]):

$$eE_f\delta \sim e^2 \left| \frac{\partial^2}{\partial \mathbf{r}_n^2} \sum_m{}' |\mathbf{r}_n - \mathbf{r}_m|^{-1} \right|_{eq} \delta^2 \sim k_BT, \tag{3.17}$$

(the derivative is evaluated for the equilibrium electron positions; clearly, the characteristic values of E_f, δ are independent of n). This gives

$$\langle E_f^2 \rangle \approx F k_B T n_e^{3/2}, \quad \delta \sim (k_BT)^{1/2} n_e^{-3/4} e^{-1} \tag{3.18}$$

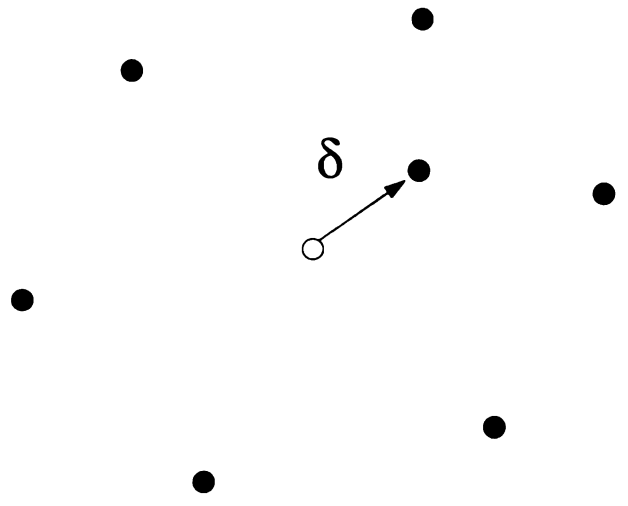

Figure 3.3: Fluctuational electron displacement in a strongly correlated system.

(the coefficient F in (3.18) is discussed below).

It is clear from Fig. 3.3 that the characteristic distance over which the field $\mathbf{E}_f$ varies is given by δ. The field is uniform over the wavelength $\lambda\!\!\!^{-}$ provided that $\lambda\!\!\!^{-} \ll \delta$. In the absence of the magnetic field the characteristic $\lambda\!\!\!^{-}$ is given by the thermal de Broglie wavelength $\lambda\!\!\!^{-}_T = \hbar(2mk_BT)^{-1/2}$, whereas in a strong magnetic field it is given by the quantum magnetic length $l_B = (\hbar/m\omega_c)^{1/2}$. Therefore, with account taken of

(3.17), the condition $\lambda\!\!\!^{-} \ll \delta$ can be written in the form

$$\lambda\!\!\!^{-} \ll \left(\frac{k_B T}{m\omega_p^2}\right)^{1/2}, \ \lambda\!\!\!^{-} = l_B\,(2\bar{n}+1)^{-1/2}, \ \omega_p = \left(\frac{2\pi e^2 n_s^{3/2}}{m}\right)^{1/2}, \tag{3.19}$$

where

$$l_B = (\hbar/m\omega_c)^{1/2}, \ \omega_c = eB/m, \ \bar{n} = [\exp(\hbar\omega_c/k_B T) - 1]^{-1}. \tag{3.20}$$

The condition (3.19) means that the electron motion is classical or, in a strong magnetic field, semiclassical. In the absence of the magnetic field ($\omega_c = 0$) (3.19) reduces to the inequality $k_B T \gg \hbar\omega_p$. It is clear from Fig. 3.3 that ω_p is the frequency of electron vibrations about (quasi)equilibrium positions, and (3.19) is the condition for these vibrations to be classical. It is noted that for $k_B T < \hbar\omega_p$, quantum effects come into play and the normal electron fluid becomes nonclassical. These quantum effects are not related to overlapping of the wave functions of different electrons; it is the motion of an electron in the field of other electrons that gets quantized.

In the presence of the magnetic field the fluid is classical provided

$$k_B T \gg \hbar\omega_p, \ \hbar\omega_c. \tag{3.21}$$

For $\hbar\omega_c > k_B T$ the fluid may be semiclassical. The motion of an electron in the field $\mathbf{E}_f$ is then a superposition of a quantum cyclotron motion with frequencies $\sim \omega_c$ and a semiclassical drift of the center of the cyclotron orbit. The frequency Ω that characterizes the drift can be estimated from Fig. 3.3 if one assumes that the

field $\mathbf{E}_f$ is pointing towards the equilibrium position. Then the "displaced" electron drifts transverse to this field with a velocity $eE_f/m\omega_c$ along a circle of radius δ. The frequency Ω is the reciprocal period of the drift. For

$$k_B T \gg \hbar\Omega, \quad \Omega = \omega_p^2/\omega_c, \tag{3.22}$$

the drift is classical. The inequality (3.22) follows from (3.17) for $\hbar\omega_c \gtrsim k_B T$. It is noted that (3.22) may be fulfilled in a sufficiently strong magnetic field, $\omega_c \gg \omega_p$, even if $k_B T < \hbar\omega_p$, i.e., even if the fluid is non-classical for $B = 0$.

The conditions (3.21) and (3.22) show also where the dynamics of a Wigner crystal are classical and semiclassical, respectively. The spectrum of phonons of a crystal was analyzed in [85]; ω_p is a characteristic Debye frequency of the crystal for $B = 0$, whereas for $\omega_c \gg \omega_p$ the spectrum consists of the optical branch (that starts at ω_c) and a low frequency branch; the widths of the branches are $\sim \Omega$. It is noted that the melting temperature of the crystal T_m as given by the condition $\Gamma \approx 127$ [51, 52] may be greater than or less than $\hbar\omega_p$ depending on the electron density ($T_m \propto n_s^{1/2}$, $\omega_p \propto n_s^{3/4}$; for electrons on helium $\hbar\omega_p/T_m \approx 1.3$ when $n_s = 10^8$ cm^{-2}). From this perspective it is particularly important that the magnetic field can be used to "switch" the 2D system, whether a fluid or a crystal, from the domain of quantum dynamics, $\hbar\omega_p \gg k_B T$, to the semiclassical domain, $k_B T \gg \hbar\Omega$.

Distribution of the fluctuational electric field

For classical and semiclassical electron systems the statistical averaging over the electron coordinates (or the positions of the centers of cyclotron orbits, in quantizing magnetic fields) may be performed independently from the averaging over the electron momenta (the occupation numbers of the Landau levels, for $\hbar\omega_c > k_BT$) [78, 4]. In particular, averaging a function taking into account the distribution of Coulomb fields affecting an electron may be obtained by integrating the over the electron coordinates with the weight $\exp(-H_{\rm ee}/k_BT)$, where

$$H_{\rm ee} = \frac{1}{2}e^2 {\sum_{n,n'}}' |\mathbf{r}_n - \mathbf{r}_{n'}|^{-1} \tag{3.23}$$

By changing to dimensionless coordinates $e\mathbf{r}_n n_e^{3/4} T^{-1/2}$ it is straightforward to show, that the distribution of the dimensionless field $\mathbf{E}_{\rm f}/n_e^{3/4}T^{1/2}$ is determined by the single parameter Γ_p, and in particular the coefficient F in Eq. (3.18) is a function of Γ_p only. It shall be noted that $\langle E_{\rm f}^2 \rangle$ can be expressed in terms of the two-particle distribution function of the electron system $\mathcal{P}(\mathbf{r}_1, \mathbf{r}_2)$:

$$e^2\langle E_{\rm f}^2 \rangle \equiv \langle (\boldsymbol{\nabla}_n H_{\rm ee})^2 \rangle = -ek_BT\langle \boldsymbol{\nabla}_n \mathbf{E}_n \rangle \equiv \frac{e^2 k_B T}{n_e S} \int \frac{\mathcal{P}(\mathbf{r}_1, \mathbf{r}_2)}{|\mathbf{r}_1 - \mathbf{r}_2|^3} d\mathbf{r}_1 d\mathbf{r}_2 \tag{3.24}$$

(S is the area of the system).

The function F in (3.18) and the distribution of the field $\mathbf{E}_{\rm f}$ can be easily found for large Γ_p (low T) where electrons form a Wigner crystal and electron vibrations about equilibrium positions can be described in the harmonic approximation [86].

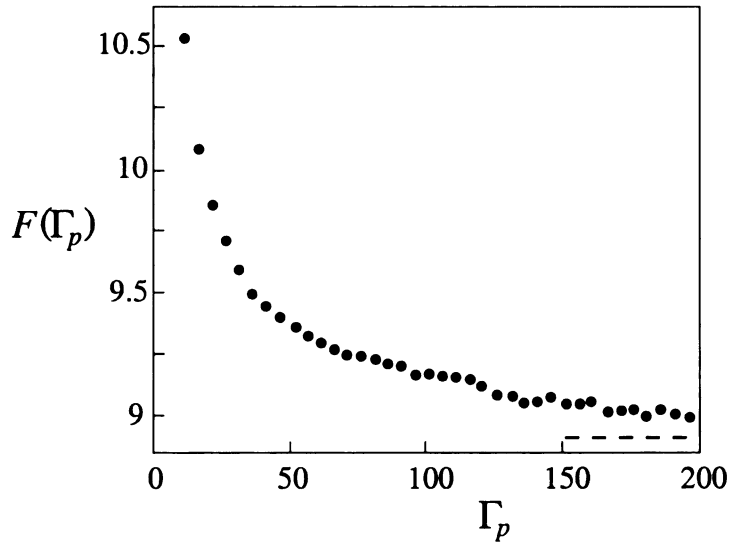

Figure 3.4: The scaled mean square fluctuational field $F(\Gamma_p) = \langle E_f^2 \rangle / k_B T n_e^{3/2}$ from Monte Carlo calculations [4]. The asymptotic value of F for a harmonic Wigner crystal is shown dashed.

Both transverse and longitudinal modes of the crystal contribute to the field, and the numerical value of F is ≈ 8.91. The distribution of the field is Gaussian, which is a standard result for the distribution of the force per particle in a classical solid.

In the opposite limit of small Γ_p the major contribution to the field $\mathbf{E}_f$ comes from pair collisions, and

$$F(\Gamma_p) \approx 2\pi^{3/2}\Gamma_p^{-1}, \quad \Gamma_p \ll 1.$$

In the most interesting range of the electron fluid and the melting transition, the function F and the distribution of the field were obtained from Monte Carlo simulations [4].

The results for the scaled mean square fluctuational field $F(\Gamma_p)$ are shown in Fig. 3.4. For $\Gamma_p \gtrsim 10$, the function F decreases monotonically with increasing Γ_p. Quite remarkably (but in qualitative agreement with the above small-Γ_p estimate which, when extrapolated to $\Gamma_p \sim 1$, gives $F(1) \approx 11$), the variation of F is small in this range, although the structure of the system changes dramatically, from a liquid where correlations in electron positions decay within twice the mean electron separation, to a crystal. The behavior of F is a consequence of $\langle E_f^2 \rangle$ being determined primarily by the short-range order in the system, according to Eq. (3.24).

It is noted that, with account taken of Eqs. (3.17), (3.24) and the above data for $\langle E_f^2 \rangle$, the criterion for the fluctuational field to be uniform over the electron wavelength

$$\lambda\!\!\!^{-} \; |\langle \nabla_n \mathbf{E}_n \rangle| = e\langle E_f^2 \rangle \lambda\!\!\!^{-} \, (k_B T)^{-1} \ll \langle E_f^2 \rangle^{1/2}$$

takes on a form that coincides with the inequality (3.19).

The shape of the distribution of the field in its central part is close to Gaussian for $\Gamma_p > 10$.

$$p(\mathbf{E}_f) = [\pi \langle \mathbf{E}_f^2 \rangle]^{-1} \exp\left[-\mathbf{E}_f^2 / \langle \mathbf{E}_f^2 \rangle\right], \tag{3.25}$$

As Γ_p decreases, the deviation of the field distribution from the Gaussian shape becomes more substantial. However, the difference between the mean reciprocal field $\langle E_f^{-1} \rangle$, which is of interest for transport (see next sections), and its value for a Gaus-

sian distribution $\pi^{1/2}\langle E_f^2\rangle^{-1/2}$ is less than 10% for $\Gamma_p \gtrsim 20$.

3.3.3 Qualitative Picture of Many-Electron Transport

Weak to moderately strong magnetic fields

For several types of 2D electron systems, and for electrons on helium in particular, electron scattering is due to collisions with short-range scatterers, and the scattering is elastic or quasielastic. Clearly, in a strongly correlated electron fluid at most one electron at a time collides with a given short-range scatterer. If the characteristic duration of a collision $t_{\rm coll}$ is small compared to the characteristic time over which the field $\mathbf{E}_f$ varies in order of magnitude (the correlation time in the electron system), the effect of the electron-electron interaction on the collisions may be fully described in terms of $\mathbf{E}_f$. Indeed, in this case the field $\mathbf{E}_f$ is all that an electron "knows" about other electrons during a collision.

Firstly, the effect of the field $\mathbf{E}_f$ on the collisions with short-range scatterers will be analyzed for not too strong magnetic fields where

$$k_B T \gg e\langle E_f^2\rangle^{1/2} \lambda\!\!\!^{-}_T \sim \hbar\omega_p \gg \hbar\omega_c, \ \lambda\!\!\!^{-}_T = \hbar(2mk_BT)^{-1/2}. \tag{3.26}$$

It is noted that (3.26) does not mean that the magnetic field is weak. The field may well be classically strong, i.e., there may hold the inequality $\omega_c\tau \gg 1$, where τ^{-1} is the scattering rate. In what follows the term "moderately strong fields" for classically strong magnetic fields that satisfy condition (3.26) will be used.

In the range (3.26) the electron motion is classical (cf. (3.21)), and an electron

has a well-defined kinetic energy $p^2/2m \sim k_B T$ and a well-defined potential energy in the field of other electrons. Uncertainty of each of these energies is determined by smearing $\lambda\!\!\!^{-}_T$ of the electron wave packet. For an electron in an electric field $\mathbf{E}_\mathrm{f}$ this uncertainty is given by $eE_\mathrm{f}\lambda\!\!\!^{-}_T$ and is small compared to $k_B T$. This means that, in spite of the electron system being strongly correlated, the electron-electron interaction has little effect on collisions with short-range scatterers in the absence of a magnetic field. One can also see this from the following arguments. The duration of a collision is determined by the time it takes an electron to fly past the scatterer. For short-range scatterers and for electrons with thermal velocities $v_T = (2k_B T/m)^{1/2}$ this time is $t_\mathrm{coll} \sim \lambda\!\!\!^{-}_T/v_T \sim \hbar/k_B T$. The acceleration of the electron in the field E_f over this time is $\sim eE_\mathrm{f}\lambda\!\!\!^{-}_T v_T/k_B T \ll v_T$. The condition $k_B T \gg \hbar\omega_p$ guarantees that $t_\mathrm{coll} = \hbar/k_B T$ is small compared to the velocity correlation time ω_p^{-1} [10].

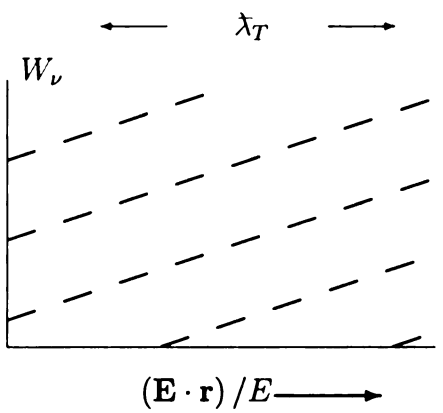

Figure 3.5: Single-electron energy levels W_ν in the electric field $\mathbf{E}$ and transverse magnetic field (tilted Landau levels). Uncertainty of the electron kinetic energy exceeds $\hbar\omega_c$ for the shown size of the electron wave packet $\lambda\!\!\!^{-}_T$.

The role of the field $\mathbf{E}_\mathrm{f}$ becomes very different in the presence of the magnetic field, since the field $\mathbf{E}_\mathrm{f}$ tilts Landau levels and makes the electron energy spectrum

continuous. It is clear from Fig. 3.5 that for an electron wave packet of size $\lambda\!\!\!^{-}_T$, the discreteness of the one-electron energy spectrum due to Landau quantization is washed out by many-electron effects if $eE_f\lambda\!\!\!^{-}_T \gg \hbar\omega_c$. One would therefore expect that even in classically strong magnetic fields, $\omega_c\tau \gg 1$, collisions with scatterers will occur nearly as if there were no magnetic field at all [64, 65]. Then the many-electron system should not display magnetoresistance, and in the whole range (3.26) the static conductivity σ is given by a simple expression

$$\sigma \equiv \sigma_{xx}(\omega = 0) = \frac{e^2 n_s}{m} \frac{\tau_{B=0}}{1 + \omega_c^2 \tau_{B=0}^2}, \quad e\langle E_f^2 \rangle^{1/2} \lambda\!\!\!^{-}_T \gg \hbar\omega_c, \hbar\tau_{B=0}^{-1} \tag{3.27}$$

where $\tau_{B=0}^{-1}$ is the scattering rate in the absence of the magnetic field calculated in the approximation where the effect of the electron-electron interaction on collisions with scatterers is ignored.

It is emphasized that the absence of magnetoresistance in the range (3.26) for *classically strong magnetic fields*, known experimentally since [53], is a purely many-electron effect. In the single-electron approximation, the character of electron scattering for $\omega_c\tau \gg 1$ is qualitatively different from that in the absence of the magnetic field even in the range of high temperatures $k_BT \gg \hbar\omega_c$, where there applies the notion of a classical electron orbit. For an electron colliding with a short-range scatterer the orbit has the shape of a rosette [87]. It is a nearly closed circle, with the characteristic cyclotron radius $R_B \sim (k_BT/m)^{1/2}\omega_c^{-1}$ and with the center slowly rotating around the scatterer. The electron is coming back to the scatterer, over and over again.

Therefore it experiences *multiple* collisions with the same scatterer, in contrast to a single collision in the absence of the magnetic field. In fact, in the single-electron approximation the number of collisions is determined by the probability to find another scatterer while spinning around the given scatterer.

"STRONG" Strong magnetic fields

Onset of magnetoresistance in classically strong magnetic fields, $k_BT > \hbar\omega_c > e\langle E_f^2\rangle^{1/2}\lambda\!\!\!^{-}_T$, can be qualitatively understood in the following way [64, 65]. If there were no fluctuational electric field, an electron in the magnetic field would be moving along a rosette described above, coming back to the scatterer with period $2\pi/\omega_c$. In the presence of the field $\mathbf{E}_f$ the center of the electron cyclotron orbit drifts with a velocity $v_d = E_f/B$. Therefore the number of times the scatterer is encountered is finite. It is clear from Fig. 3.6 that in order of magnitude, this number is $\zeta = \lambda\!\!\!^{-}_T(2\pi E_f/B\omega_c)^{-1}$ (here, $\lambda\!\!\!^{-}_T$ stands for the characteristic "size" of the scatterer; if scatterers are not point-like and their size exceeds $\lambda\!\!\!^{-}_T$, the above expression should be appropriately modified). One would expect classical magnetoresistance to arise in the many-electron system for $\zeta > 1$ which means that the single-site scattering probability is effectively enhanced.

The magnetoconductivity σ can be estimated using the Einstein relation between the conductivity and the diffusion coefficient D, $\sigma = e^2 n_s D/T$. It is seen from Fig. 3.6 that scattering results in a shift of the electron orbit by the cyclotron radius R_B. Therefore $R_B^2/2$ may be associated with the squared diffusion length, and then $D = R_B^2/2\tau$. The scattering rate τ^{-1} is proportional to the encountering factor ζ [88],

and the expression for σ takes on the form

$$\sigma = \frac{e^2 n_s}{2T} R_B^2 \tau^{-1}, \quad \tau^{-1} \sim \zeta \tau_{B=0}^{-1}, \quad \zeta = \lambda\!\!\!^{-}\, \omega_c B / 2\pi \langle E_f^2 \rangle^{1/2}. \tag{3.28}$$

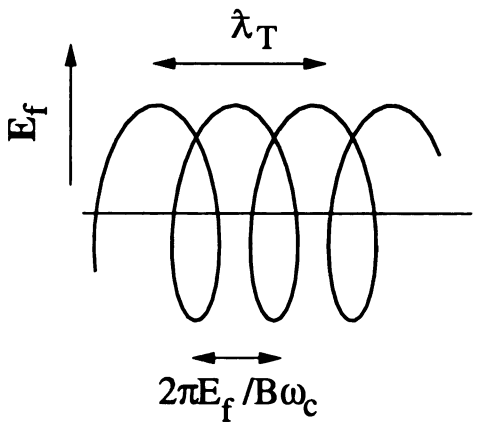

Figure 3.6: Classical electron trajectory in the fluctuational electric field $\mathbf{E}_f$ and transverse magnetic field B. The radius of the spiral $R_B \sim (k_B T/\hbar\omega_c)\lambda\!\!\!^{-}_T$.

A distinctive feature of the many-electron magnetoconductivity (3.28) is its *independence* of the field B for classically strong fields where $R_B \sim (k_B T/\hbar\omega_c)\lambda\!\!\!^{-}_T \propto B^{-1}$ and $\zeta \propto B^2$ ($\lambda\!\!\!^{-} = \lambda\!\!\!^{-}_T$ for $\hbar\omega_c \ll T$).

The arguments used to obtain an estimate of σ apply also if the electron system is in a quantizing magnetic field. For strongly quantizing fields, $\hbar\omega_c \gg k_B T$, an electron is a "hard disk" with characteristic size $l_B = (\hbar/m\omega_c)^{1/2}$. It drifts transverse to the magnetic field with a velocity E_f/B, and the characteristic duration of a collision is [78, 76]

$$t_e = l_B B \langle E_f^{-1} \rangle.$$

The scattering rate is increased compared to $\tau_{B=0}^{-1}$ by the encountering factor $\zeta \sim \omega_c t_e \propto B^{3/2}$ (the same estimate can be obtained using density-of-states arguments: the kinetic energy uncertainty of an electron wave packet of a size l_B in the field E_f is $\sim eE_\mathrm{f} l_B$, and therefore the density of states into which the electron may be scattered is increased by a factor $\zeta \sim \hbar\omega_c / eE_\mathrm{f} l_B$).

In the whole domain $\hbar\omega_c \gtrsim k_B T$, the value of R_B in Eq. (3.28) is given by the characteristic radius of the electron wave function, whereas t_coll is given by the time-of-flight over the wavelength $\lambda\!\!\!^{-}$ (3.26),

$$R_B = l_B(2\bar{n}+1)^{1/2}, \qquad t_\mathrm{coll} = l_B(2\bar{n}+1)^{-1/2} B\langle E_\mathrm{f}^{-1}\rangle. \tag{3.29}$$

It follows from (3.27), (3.28), (3.29) that the magnetoconductivity σ is nonmonotonic as a function of B. It decreases as B^{-2} in the range (3.27), reaches a minimum for "strong" classically strong fields where $\zeta \gg 1$, and then increases as $B^{1/2}$ for $\hbar\omega_c \gg k_B T$.

Eq. (3.28) for τ^{-1} gives also the characteristic value of the halfwidth γ of the peak of cyclotron resonance of a many-electron system in a strong magnetic field. We note that in the classical range $k_B T \gg \hbar\omega_c$ the expressions for γ and for the relaxation rate in Eqs. (3.27), (3.28) for the static conductivity coincide with each other. This is no longer true in the quantum range, although still $\gamma \sim \tau^{-1}$ [4].

Interelectron momentum exchange

The exchange of momentum between electrons does not affect the long-wavelength conductivity directly [89], since it does not change the total momentum of the electron system. However, its role in the transport may be substantial. This is well-known in the theory of low-density electron plasma in semiconductors [90, 91] from the analysis of the case where the single-electron rate of collisions with scatterers $\tau_s^{-1}(\epsilon)$ depends on the electron energy ϵ. In the single-electron approximation the static conductivity σ (for $B = 0$) is a sum of the conductivities of electrons with different energies and therefore different scattering rates; it is given by the averaged (over ϵ) *reciprocal* scattering rate, $\sigma = e^2 n_s \overline{\tau_s(\epsilon)}/m$. The interelectron momentum exchange occurs via pair electron-electron collisions. If the frequency of these collisions greatly exceeds $\tau_s^{-1}(T)$, then $\sigma = e^2 n_s / m\overline{\tau_s^{-1}(\epsilon)}$. These results were applied to 2D electrons on helium in [57, 58].

Based on the discussion in Sec. 3.1 one would expect that similar arguments apply to the static conductivity of a *strongly correlated* classical electron fluid for weak magnetic fields. Here, an electron exchanges its momentum with other electrons not via pair collisions but by being accelerated by the Coulomb force from these electrons. The rate of interelectron momentum exchange τ_{ex}^{-1} is given by the frequency of the electron vibrations ω_p, as it is clear from Fig. 3.3. If $\omega_p \tau \gg 1$, as it was assumed in Eq. (10), the conductivity is determined by the relaxation rate of the total momentum of the many-electron system, i.e., by the average rate $\overline{\tau_s^{-1}(\epsilon)}$.

The role of interelectron momentum exchange in strong fields B, where collisions

with scatterers are mediated by the electron-electron interaction, is clear from the analysis of cyclotron resonance. Resonant absorption at frequency ω_c is due to transitions between neighboring tilted Landau levels in Fig. 3.5, $|\nu\rangle \to |\nu+1\rangle$. "Partial spectra" which correspond to different transitions are broadened because of collisions with scatterers. Prior to averaging over the many-electron ensemble the broadening of a spectrum $\gamma_\nu(\mathbf{E}_f)$ depends both on the level number ν and $\mathbf{E}_f$. Even if all partial spectra are Lorentzian, but with different widths, the total spectrum may be non-Lorentzian (see [92] for a review of the theory of systems with equidistant or nearly equidistant energy levels).

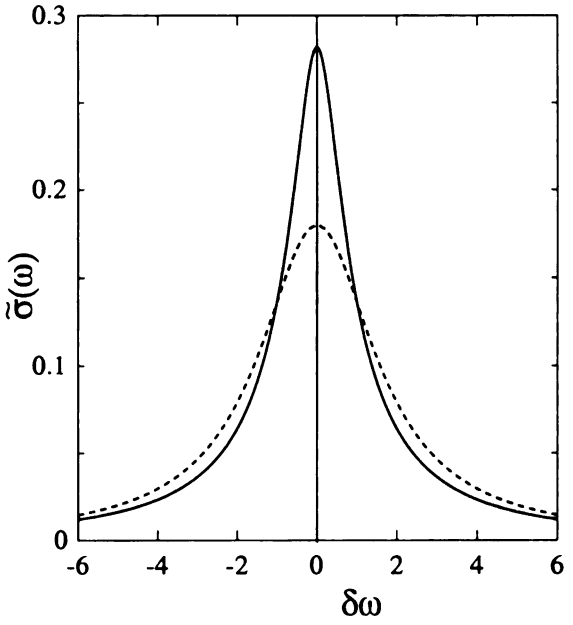

Figure 3.7: Reduced high-frequency conductivity (14) near the cyclotron resonance peak as a function of the reduced frequency $\delta\omega = (\omega - \omega_c)/\gamma_0$ for Gaussian distribution of $\mathbf{E}_f$ (solid line); $\tilde{\sigma}(\omega) = 2m\gamma_0\sigma_{xx}(\omega)/\pi e^2 n_s$ ($\gamma_0 \equiv \gamma_0(\langle E_f^2\rangle^{1/2})$). A Lorentzian distribution with the same area and with the halfwidth $\pi^{1/2}\gamma_0$ is shown with a dashed line (from [4]).

Electron-electron interaction gives rise to transitions between the Landau levels

of individual electrons and to drift of the cyclotron orbit centers. Electron motion results also in averaging of the widths $\gamma_\nu(\mathbf{E}_\mathrm{f})$. The characteristic frequency of the corresponding interelectron momentum exchange is seen from Fig. reffig:displacement to be $\tau_{\mathrm{ex}}^{-1} = \Omega = \omega_p^2/\omega_c$ for $\omega_p \ll \omega_c$. For fast momentum exchange, $\tau_{\mathrm{ex}}^{-1} \gg \tau^{-1}$, this is relaxation of the total momentum of the electron system that determines the shape of the cyclotron resonance spectrum, and the spectrum is Lorentzian with a width given by the appropriately averaged $\gamma_\nu(\mathbf{E}_\mathrm{f}) \propto E_\mathrm{f}^{-1}$ [4]. In the opposite case $\tau_{\mathrm{ex}}^{-1} \ll \tau^{-1}$ the spectrum is non-Lorentzian. For $k_B T \ll \hbar\omega_c$ the conductivity is given by the expression

$$\sigma_{xx}(\omega) \approx \frac{e^2 n_s}{2m} \left\langle \frac{\gamma_0(\mathbf{E}_\mathrm{f})}{\gamma_0^2(\mathbf{E}_\mathrm{f}) + (\omega - \omega_c)^2} \right\rangle . \tag{3.30}$$

The shape of the peak of $\sigma_{xx}(\omega)$ depends on the shape of the distribution of the fluctuational field. For the case of Gaussian distribution it is shown in Fig. 3.7.

3.3.4 Summary

For a broad range of electron densities and relatively low temperatures, the electron system is a strongly correlated electron liquid, $\Gamma_p \gg 1$. The analysis of the fluid is a complicated problem by the absence of "good" quasiparticles, which is in contrast to the much better understood Fermi liquid. Therefore the analysis of electron transport requires a nontraditional approach.

Although the EEI does not change the total momentum of the 2DES, and thus

does not directly affect the long-wavelength conductivity $\sigma_{xx}(\omega)$ (the Kohn theorem), momentum transfer from electrons to defects depends, of course, on electron motion, and so $\sigma_{xx}(\omega)$ is ultimately determined by the EEI.

The concept of the fluctuational electric field is an important picture in the description of the many-electron system [9]. The restoration of the Drude-model in the range of weak to moderately strong magnetic fields is entirely maintained by many-electron effects. The onset of magnetoresistance in classically strong magnetic fields, $k_BT > \hbar\omega_c > e\langle E_f^2\rangle^{1/2}\lambda\!\!\!^{-}_T$, is also a signature of the many-electron magnetoconductivity [9, 93] Much of the features of the many-electron magnetoconductivty relate to the range where the characteristic force on an electron from the random potential is weaker than the force from other electrons. Then the corresponding results could be explained, qualitatively and quantitatively, using lowest order perturbation theory in the random potential [12, 93].

In the opposite limit where the force from the random potential is stronger than that from other electrons, the static conductivity in quantizing magnetic fields could be reasonably well described [13, 14, 15] by the single-electron theory based on the self-consistent Born approximation (SCBA) [16].

Chapter 4

Single-electron conductivity

In this chapter, we calculate the low-frequency ($\omega \ll \omega_c$) conductivity of a non-interacting non-degenerate ($k_BT \gg \hbar\gamma$ and $nl^2 \ll 1$) two-dimensional electron system in a weak delta-correlated disorder potential, meaning the lowest Landau level (LLL) width is $\hbar\gamma \ll \hbar\omega_c$. To be specific, all results are written for the LLL, *i.e.*, they apply directly only for quantizing magnetic fields, $k_BT \ll \hbar\omega_c$. At higher temperatures one has to add the contribution of higher Landau levels weighted with the corresponding Boltzmann occupation factors.

The outline of this chapter is as follows. In Sec. 4.1 calculations of the low-frequency conductivity will be given, the moment technique will be applied to this problem in Sec. 4.2 and Sec. 4.3. From the tail asymptotic and the scaling for small frequencies in Sec. 4.4, 4.5 the conductivity will be reconstructed in Sec. 4.6.

4.1 Kubo-conductivity

The most important advantage of restricting the calculations to a single Landau level in this temperature range is that such states are nearly equally occupied. As a result, the usual Kubo formula for the dissipative conductivity of the system can be written as a simple trace, without the Boltzmann factor,

$$\sigma_{xx}(\omega) = \frac{n\left(1-e^{-\beta\omega}\right)}{\hbar\omega}\,\Re\mathrm{e}\int_0^\infty dt\, e^{i\omega t}\left\langle j_x(t)\, j_x(0)\right\rangle \tag{4.1}$$

$$\approx \frac{n\beta}{2\hbar}\int_{-\infty}^{\infty} dt\, e^{i\omega t}\,\mathrm{Tr}_0\overline{\left\{j_x(t)\, j_x(0)\right\}}, \quad \beta\omega \ll 1. \tag{4.2}$$

Here $j_x \equiv ep_x/m$ is the one-electron current operator, $\beta \equiv \hbar/k_BT$, the angular brackets $\langle\cdot\rangle$ denote statistical averaging over the states followed by an averaging over quenched disorder, while the horizontal line denotes only the disorder averaging. The trace Tr_0 in Eq. (4.2) is performed over all single-particle states of the lowest Landau level; the energies are measured with respect to its center. Eq. (4.1) is written for the case of strongly quantizing magnetic fields, $\exp(\beta\omega_c) \gg 1$, so that only the lowest Landau level is occupied. However, the calculation is readily generalized to the case of arbitrary $\beta\omega_c$ by replacing Tr_0 by the sum of traces over the states of each Landau level n weighted with $\exp(-n\beta\omega_c)[1-\exp(-\beta\omega_c)]$.

The trace over the broadened Landau level is conveniently done using the formalism of guiding center coordinates $\mathbf{R} \equiv (X, Y)$. The dynamics of a particle restricted to a given Landau level is mapped to that of a 1D quantum particle with the generalized

momentum and coordinate X and Y, and with the Hamiltonian

$$H = \hbar\gamma \sum\nolimits_{\mathbf{q}} \tilde{V}_{\mathbf{q}} \exp(i\mathbf{q}\mathbf{R}), \quad [X, Y] = -il^2. \tag{4.3}$$

The dimensionless coefficients

$$\tilde{V}_{\mathbf{q}} \equiv (V_{\mathbf{q}}/\hbar\gamma) \exp(-l^2 q^2/4) \tag{4.4}$$

are proportional to Fourier components of the disorder potential,

$$V_{\mathbf{q}} \equiv S^{-1} \int d^2\mathbf{r}\, V(\mathbf{r}) e^{-i\mathbf{q}\mathbf{r}}, \tag{4.5}$$

where S is the overall area of the system. For higher Landau levels the momentum dependence of $\tilde{V}_{\mathbf{q}}$ is more complicated, see Appendix B [see Eq. (B.16)]. We will assume that $V(\mathbf{r})$ is Gaussian and delta-correlated,

$$\langle V(\mathbf{r})\, V(\mathbf{r}')\rangle = v^2 \delta(\mathbf{r} - \mathbf{r}'), \tag{4.6}$$

in which case [16] $\hbar\gamma = (2/\pi)^{1/2} v/l$.

After the Landau level projection, the cyclotron energy $\hbar\omega_c$ is no longer relevant for low-frequency dynamics, and the only remaining quantities with the dimension of energy are the Landau level width $\hbar\gamma$ and the temperature. In the simplified Kubo formula (4.2) the temperature dependence is factorized, and we can rewrite the

low-frequency conductivity in the form of the generalized Einstein relation

$$\sigma_{xx}(\omega) = \frac{ne^2 D}{k_B T} \frac{1}{8} \tilde{\sigma}(\omega), \tag{4.7}$$

where $D = l^2\gamma$ is the characteristic diffusion coefficient and

$$\tilde{\sigma}(\omega) \equiv \frac{2}{l^2\gamma} \int_{-\infty}^{\infty} dt\, e^{i\omega t} \mathrm{Tr}_0 \Big\{ \overline{\dot{\mathbf{R}}(t) \cdot \dot{\mathbf{R}}(0)} \Big\} \tag{4.8}$$

is the reduced conductivity. It depends on the ratio ω/γ of the only two quantities with the dimension of frequency that remain after projection on one Landau level.

The expression (4.8) for the reduced conductivity at a given Landau level can be written more explicitly after evaluating the guiding center velocity with the help of the Hamiltonian (4.3),

$$\dot{\mathbf{R}}_\mu = il^2\gamma \sum_{\mathbf{q}} \epsilon^{\mu\nu} \mathbf{q}_\nu \tilde{V}_{\mathbf{q}}\, e^{i\mathbf{q}\mathbf{R}}, \tag{4.9}$$

where $\mu, \nu = x, y$ and $\epsilon^{\mu\nu}$ is the usual unit antisymmetric tensor. We obtain

$$\begin{aligned} \tilde{\sigma}(\omega) = \quad & -2l^2\gamma \int_{-\infty}^{\infty} dt\, e^{i\omega t} \sum\nolimits_{\mathbf{q},\mathbf{q}'} (\mathbf{q}\,\mathbf{q}') \\ & \times \mathrm{Tr}_0 \Big\{ \overline{\tilde{V}_{\mathbf{q}} \tilde{V}_{\mathbf{q}'} \exp\left[i\mathbf{q}\,\mathbf{R}(t)\right] \exp\left[i\mathbf{q}'\,\mathbf{R}(0)\right]} \Big\}. \end{aligned} \tag{4.10}$$

This form is particularly convenient for calculating the frequency moments of the reduced conductivity (4.10), see below in Sec. 4.2.

4.2 Method of spectral moments

Because of the Landau level degeneracy in the absence of a random potential, the problem of dissipative conductivity is to some extent similar to the problem of the absorption spectra of Jahn-Teller centers in solids [94], which are often analyzed using the method of spectral moments (MOM). This method can be applied to the conductivity (4.10) as well [95]. It allows, at least in principle, to restore $\sigma_{xx}(\omega)$. In addition, the moments

$$M_k = \frac{1}{2\pi\gamma}\int_{-\infty}^{\infty} d\omega\,(\omega/\gamma)^k \tilde{\sigma}(\omega) \tag{4.11}$$

can be directly found from measured $\sigma_{xx}(\omega)$, and therefore are of interest by themselves.

For $\omega, \gamma \ll k_B T/\hbar$, the states within the broadened lowest Landau level are equally populated and the reduced conductivity is symmetric, $\tilde{\sigma}(\omega) = \tilde{\sigma}(-\omega)$. Then odd moments vanish, $M_{2k+1} = 0$. For even moments, we obtain from Eq. (4.10), (4.11)

$$\begin{aligned} M_{2k} = \quad & -2l^2 \sum (\mathbf{q}_1\,\mathbf{q}_{2k+2}) \left\langle \tilde{V}_{\mathbf{q}_1} \ldots \tilde{V}_{\mathbf{q}_{2k+2}} \right\rangle \\ & \times \left[\left[\ldots \left[e^{i\mathbf{q}_1\mathbf{R}}, e^{i\mathbf{q}_2\mathbf{R}} \right], \ldots \right], e^{i\mathbf{q}_{2k+1}\mathbf{R}} \right] e^{i\mathbf{q}_{2k+2}\mathbf{R}}, \end{aligned} \tag{4.12}$$

where the sum is taken over all $\mathbf{q}_1, \ldots, \mathbf{q}_{2k+2}$. The commutators (4.12) can be eval-

Table 4.1: The number of diagrams to calculate M_{2k} increases factorially, $(2k+2)!!$, among which the disconnected diagrams Fig. 4.1b, and diagrams of type Fig. 4.1c, also factorially increasing in number, can be discarded. Symmetric diagrams remain small in number, allowing us to use the diagram symmetry to reduce the number of diagrams to be calculated by a factor of roughly one-half. The sum of diagrams with paired endpoints, $\mathbf{q}_1 = -\mathbf{q}_{2k+2}$ is overall positive and gives the leading contribution to M_{2k}, the approximate values are given in the column denoted by the prefactor $-\mathbf{q}_1\mathbf{q}_1$. All other add up to a $\sim 12\%$ negative correction, as shown in the last column.

k	total	symmetric	disconnected	$-\mathbf{q}_1\mathbf{q}_1$	$\mathbf{q}_1\mathbf{q}_{2k+2}$
0	1	1	0	1	0
1	3	3	1	0.375	0
2	15	7	5	0.415	-0.0304
3	105	25	31	0.731	-0.0797
4	945	81	239	1.735	-0.2131
5	10395	331	2233	5.124	-0.6459
6	135135	1303	24725	17.964	-2.239
7	2027035	5937	318631	72.559	-8.809

uated recursively using

$$\left[e^{i\mathbf{q}\mathbf{R}},\, e^{i\mathbf{q}'\mathbf{R}}\right] = 2i\sin\left(\frac{1}{2}l^2\mathbf{q}\wedge\mathbf{q}'\right)e^{i(\mathbf{q}+\mathbf{q}')\mathbf{R}}, \tag{4.13}$$

where $\mathbf{p}\wedge\mathbf{q} = p_xq_y - p_yq_x$. Indeed, in MOM the time dependent problem of the electron motion in a random field (4.10) is translated into the evaluation of the correlator (4.12) for $t = 0$.

4.3 Diagram technique

From Eq. (4.6) it is, $\langle\tilde{V}_{\mathbf{q}}\tilde{V}_{\mathbf{q}'}\rangle = (\pi l^2/2S)\exp(-l^2q^2/2)\delta_{\mathbf{q}+\mathbf{q}'}$, where S is the area. The evaluation of the $2k$ th moment comes then to choosing pairs $(\mathbf{q}_{i_n} = -\mathbf{q}_{j_n})$ for

$i_n \neq j_n$, $n = 1 \ldots, k+1$ and integrating over $k+1$ independent $\mathbf{q}_i$. Then,

$$
\begin{aligned}
M_{2k} \;=\; & \left(\frac{-l^2}{2\pi}\right)^{k+1} l^2/2 \sum_{\mathcal{C}(\{\mathbf{q}\})} \int d\mathbf{q}_1 \cdots d\mathbf{q}_{2k+2} \\
& \mathcal{C}(\{\mathbf{q}\})(\mathbf{q}_1\mathbf{q}_{2k+2}) \exp[-\frac{1}{4} l^2(q_1^2 + \ldots + q_{2k+2}^2)] \times \\
& \sin(\frac{1}{2} l^2 \; \mathbf{q}_1 \wedge \mathbf{q}_2) \times \\
& \sin(\frac{1}{2} l^2 (\mathbf{q}_1 + \mathbf{q}_2) \wedge \mathbf{q}_3) \times \\
& \qquad \vdots \\
& \sin(\frac{1}{2} l^2 (\mathbf{q}_1 + \mathbf{q}_2 + \ldots + \mathbf{q}_{2k}) \wedge \mathbf{q}_{2k+1})
\end{aligned}
\tag{4.14}
$$

where the sum is taken over all $(2k+2)!!$ ways to choose pairs out of the set of $\{\mathbf{q}_1, \ldots, \mathbf{q}_{2k+2}\}$ variables. $\mathcal{C}(\{\mathbf{q}\}) = \delta(\mathbf{q}_{i_1} + \mathbf{q}_{j_1}) \ldots \delta(\mathbf{q}_{i_{k+1}} + \mathbf{q}_{j_{k+1}})$ is the *contraction* function. It is convenient to depict the *contraction* procedure graphically in terms of diagrams, Fig. 4.1. These diagrams merely represent the contraction function $\mathcal{C}$ and are not to be confused with ordinary diagrams within the Greens-function technique!

Not all diagrams contribute to the sum in (4.14). We find that any disconnected diagram, Fig. 4.1b, has zero value since one of the sine terms in (4.14) has to vanish. Additionally, diagrams of the type Fig. 4.1c are zero for parity reasons, amounting to less than $(2k-2)!!$, $k > 0$ (to avoid double counting with the former case diagrams). This comes about a special structure of the function in (4.14) which contains a factor

$$
(\mathbf{q}_1\mathbf{q}_{2k+2}) \sin(\frac{1}{2} l^2 \mathbf{q}_{2k+1} \wedge \mathbf{q}_{2k+2})^2 \sin(\frac{1}{2} l^2 \mathbf{q}_m \wedge \mathbf{q}_{2k+2})^2
$$

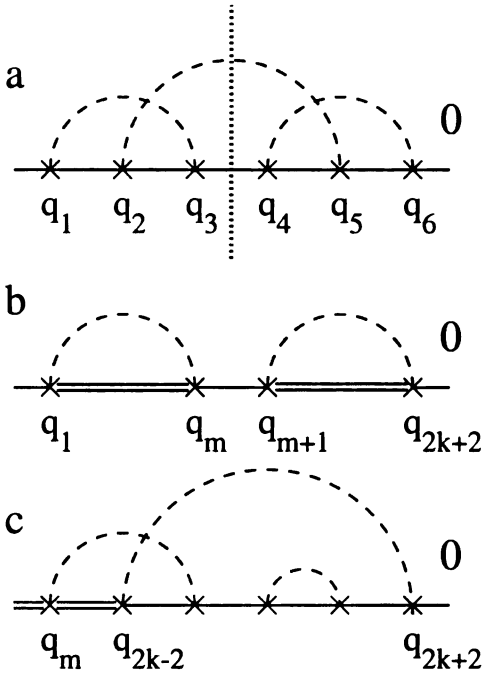

Figure 4.1: a) shows an example of a *symmetric* diagram for the calculation of M_4, its value is zero. Graphically the symmetry manifests itself as a reflection symmetry with respect to the dotted line. The dashed lines indicate which variables are to be paired. b) the value of any *disconnected* diagram is zero, double lines indicate an arbitrary internal pairing structure. c) this particular type of diagrams is zero because the associated function is odd in $\mathbf{q}_{2k+2}$, therefore it vanishes after the integration.

and apparently vanishes after integration over $\mathbf{q}_{2k+2}$. Excluding both types of diagrams in the summation process, reduces the amount of computing time to evaluate M_{2k}, Table 4.2. The more, a symmetry readily seen from (4.12) may be exploited. The arrangement of all $\mathbf{q}_i$ may be reversed without changing the overall value. This implies that diagrams which can be transformed into each other by simply reversing its sequence of variables $\mathbf{q}_i$ are equivalent, Fig 4.1a.

In principle high dimensional gaussian integrals as in (4.14) can be calculated algebraically, however, the associated computational cost is high. The number of diagrams increases factorially, Table 4.2, thus we have devised a fast combinatoric-numeric classification scheme, which allows us to sort diagrams inexpensively into *bins*. Then a representative diagram is evaluated algebraically for each *bin* and finally summed up with its proper multiplicity, giving exact numbers for the moments.

Equation (4.14) can easily be represented by a sum of matrix exponentials,

$$\begin{aligned} M_{2k} &= -2l^2 \left(\frac{l^2}{8\pi}\right)^{k+1} \sum_{C(\{\mathbf{q}\})} \sum_{\{j_1,\ldots,j_{2k}\}} (-1)^{\sigma(\{\mathbf{j}\})} \times \\ &\int d\mathbf{q}_1 \cdots d\mathbf{q}_{2k+2}\, C(\{\mathbf{q}\})(\mathbf{q}_1 \mathbf{q}_{2k+2}) \times \\ &\exp\left[-\frac{l^2}{4}(q_1^2 + \ldots + q_{2k+2}^2) + i\frac{l^2}{4} \sum_{m,n=1}^{2k+2} \hat{B}_{mn}^{\{\mathbf{j}\}} \mathbf{q}_m \wedge \mathbf{q}_n\right], \end{aligned} \tag{4.15}$$

where the inner sum is taken over all binary sequences of length $2k$, $\mathbf{j} = (0, 1, \ldots)$ and $\sigma(\{\mathbf{j}\}) = \sum_i j_i$. The antisymmetric $(2k+2)^2$-dimensional square matrix $\hat{B}^{\{\mathbf{j}\}}$ has

the following structure:

$$\hat{B}^{\{j\}} = \begin{pmatrix} 0 & c_1 & c_2 & \dots & c_{2k} & 0 \\ -c_1 & 0 & c_2 & & c_{2k} & 0 \\ -c_2 & -c_2 & 0 & & & \\ \vdots & & & \ddots & c_{2k} & \vdots \\ -c_{2k} & -c_{2k} & \dots & -c_{2k} & 0 & \\ 0 & & \dots & & & 0 \end{pmatrix}, \tag{4.16}$$

$c_i = (-1)^{j_i}$.

Choosing pairs, i. e. $\{(\mathbf{q}_1 = -\mathbf{q}_2), (\mathbf{q}_3 = -\mathbf{q}_4), \dots\}$, results in the reduction of the matrix $\hat{B}$ to a $(k+1)^2$-dimensional square matrix by means of the following procedure:

The pairing procedure reduces the number of variables by one-half. The results are unaltered by the choice of the independet variables. For the given example, we decide to keep the independent variables $\mathbf{q}_1$, $\mathbf{q}_3$, etc. Then, in the matrix representation of the exponential, row 2 is subtracted from row 1, further row 4 from row 3 and so on. Now, the subtrahend rows (2,4, ...) are discarded, saying that those associated variables don't exist any more. The same subtraction and reduction scheme is applied to the columns of the intermediate rectangular matrix, giving the (weighted with $\mathbf{q}_1\mathbf{q}_{2k+2}$) exponential of the quadratic form $(l^2/2)\sum \mathbf{q}_i \hat{A}_{ij} \mathbf{q}_j$, where $i, j = 1, \dots, k+1$. The matrix elements $\hat{A}_{ij}$ are themselves 2×2 matrices, $\hat{A}_{ij} = -\hat{I}\delta_{ij} + a_{ij}\hat{\sigma}_y$, where $\hat{\sigma}_y$ is the Pauli matrix, and $a_{ij} = -a_{ji} = 0, \pm 1$.

Given any diagram, its value may be calculated by generating the matrices $\hat{B}$ for all

binary sequences **j**, then contracting the matrices according to the rules of its diagram and finally counting the occurrences of the contracted matrices $\hat{A}$ summing up with the proper sign, $(-1)^{\sigma(\{\mathbf{j}\})}$. In order to evaluate the multidimensional gaussian integral (4.15) for a specific contracted matrix $\hat{A}_{ij}$ we use the diagonalization technique, see Appendix C, and obtain the value

$$-4^{-k}\prod_{i=1}^{k+1}(1+\lambda_i^2)^{-1/2}\sum_{m=1}^{k+1}\frac{u_{m,1}u_{m,x}^*}{1+\lambda_m^2}\,, \tag{4.17}$$

where $\hat{U}\hat{A}\hat{U}^\dagger = \mathrm{diag}(\lambda_1,\ldots,\lambda_{k+1})$, $(\hat{U})_{ij} = u_{ij}$. Additionally we have assumed that $\mathbf{q}_1$ and $\mathbf{q}_{2k+2}$ were kept as independent variables in the *pairing* procedure, then $x = k+1$, else if they are paired and dependent, $\mathbf{q}_1 = -\mathbf{q}_{2k+2}$, then we have to take $x = 1$ and (4.17) has to be multiplied by (-1).

Different matrices $\hat{A}$ may result in the same value after the integration in (4.15). Therefore (4.17) serves as an equivalence relation and divides the whole set of matrices $\hat{A}$ into equivalence classes. Each equivalence class is assigned its own bin in which the integer multiplicity (positive or negative) of equivalent matrices $\hat{A}$ is stored.

The exact value for M_{2k} is obtained by simply taking a representative contracted matrix $\hat{A}$ for each equivalence class and calculating the gaussian integral (4.15) algebraically. The result is a rational number which has to be multiplied with its bin content. Calculating algebraically only non-equivalent (4.17) gaussian integrals tremendously reduces computing time which allowed us to obtain moments up to M_{14}. The outline of the program to calculate these moments is given in App. G.

Summing up all bins gives the moment M_{2k}. For $k = 0, 1, \ldots, 7$ we obtain

$$M_{2k} = 1; \frac{3}{8}; \frac{443}{1152}; \frac{25003}{38400}; \frac{13608949709}{8941363200}; \frac{298681273551508807}{66698308912435200}; \frac{566602308094143977186611746328323669809}{360333644526692897267555673086361600000}; \frac{25890089116770493082846170526532875247246693310933727924122704599397 01}{40611974008223423608381355617240666314144290787406293503186042880000} \tag{4.18}$$

and the approximate values,

$$M_{2k} \approx 1; \frac{3}{8}; 0.385; 0.651; 1.522; 4.478; 15.72; 63.75\,.$$

4.4 Method of optimal fluctuation, $\omega \gg \gamma$ asymptotic

To restore the conductivity $\tilde{\sigma}(\omega)$ from the calculated finite number of moments, we need its asymptotic form for $\omega \gg \gamma$. It can be found from the method of optimal fluctuation [28], by calculating the thermal average in Eq. (4.10) on the exact eigenstates $|n\rangle$ of the lowest Landau band of the disordered system,

$$\tilde{\sigma}(\omega) = \frac{4\pi l^2}{\hbar\gamma} \sum_{n,m} \overline{\delta(E_n - E_m - \hbar\omega) \left|\langle n|\boldsymbol{\nabla} V|m\rangle\right|^2}, \tag{4.19}$$

where E_n are the energies of the LLL states $|n\rangle$ in the potential $V(\mathbf{r})$ (again, generalization to the case of several occupied Landau levels is straightforward).

In the neglect of inter-band mixing, the energies E_n are symmetrically distributed around the Landau band center ($E = 0$). The tails of the density of states $\rho(E)$ are known to be Gaussian, $\rho(E) \propto \exp(-4E^2/\hbar^2\gamma^2)$. They are determined by the probability of the optimal (least improbable) potential fluctuation $V_E(\mathbf{r})$ in which the lowest or highest bound state has energy E ($|E| \gg \gamma$) [28, 5, 96].

If we ignore the matrix element in Eq. (4.19) altogether (as we show below, this only affects the prefactor), the tail of the conductivity will be proportional to the probability to find two states E_n, E_m such that $E_n - E_m = \hbar\omega$. The major contribution comes from states at the opposite ends of the energy band with energies close to $E_n = -E_m = \hbar\omega/2$, giving

$$\tilde{\sigma}(\omega) \propto [\rho(\hbar\omega/2)]^2 \propto \exp(-2\omega^2/\gamma^2). \tag{4.20}$$

To check this approximation, we will apply the method of optimal fluctuation [97, 28]. The averaging over disorder in Eq. (4.19) will be done using the path integral representation

$$\overline{\mathcal{F}[V]} \equiv \int \mathcal{D}V(\mathbf{r})\, \mathcal{F}[V(\mathbf{r})] \exp\{-\mathcal{R}[V(\mathbf{r})]\}, \tag{4.21}$$

where, for a delta-correlated Gaussian potential with the correlator (4.6),

$$\mathcal{R}[V] = \frac{1}{2v^2} \int d\mathbf{r}\, V^2(\mathbf{r}). \tag{4.22}$$

For large ω, the leading contribution to the sum (4.19) comes from transitions between

the states $|\psi_t\rangle$ and $|\psi_b\rangle$ with energies E_t and E_b at the top and bottom of the Landau band, respectively,

$$E_{t,b} = \int d\mathbf{r}\, V(\mathbf{r})\, |\psi_{t,b}(\mathbf{r})|^2. \tag{4.23}$$

To logarithmic accuracy, the conductivity is given by the solution of the variational problem of finding the optimal potential $V(\mathbf{r})$ which minimizes the functional $\mathcal{R}[V]$ and maximizes the matrix element of the transition subject to the constraint $E_t - E_b = \hbar\omega$, *i.e.*,

$$\begin{aligned} \tilde{\sigma}(\omega) \;\propto\; \max_V \Big\{ & \exp\left[-\mathcal{R}[V] + \lambda\left(E_t - E_b - \hbar\omega\right)\right] \\ & \times |\langle\psi_t|\boldsymbol{\nabla} V|\psi_b\rangle|^2 \Big\}, \end{aligned} \tag{4.24}$$

where λ is a Lagrange multiplier. Variation with respect to $V(\mathbf{r})$ gives the equation

$$\frac{V(\mathbf{r})}{v^2} = \lambda\left(|\psi_t|^2 - |\psi_b|^2\right) + \frac{\delta}{\delta V(\mathbf{r})} \ln |\langle\psi_t|\boldsymbol{\nabla} V|\psi_b\rangle|^2. \tag{4.25}$$

We have analyzed the variational problem using a simple and tractable direct variational method, and also by finding the maximum in Eq. (4.24) numerically. To see the qualitative features of the solution, we first discuss it ignoring the contribution of the matrix element. In this case the Lagrange multiplier λ is given by the consistency

equation,

$$\hbar\omega = E_{\rm t} - E_{\rm b} = v^2\lambda \int d\mathbf{r}\, \left(|\psi_{\rm t}|^2 - |\psi_{\rm b}|^2\right)^2, \tag{4.26}$$

and then the conductivity (4.24) is

$$|\ln\tilde{\sigma}(\omega)| = \hbar^2\omega^2 \left[2v^2 \int d\mathbf{r}\, \left(|\psi_{\rm t}|^2 - |\psi_{\rm b}|^2\right)^2\right]^{-1}. \tag{4.27}$$

The solution (4.25) corresponds to a potential of the form of a well and a hump, far away from each other (cf. Fig. 4.5). The potential is antisymmetric, the well and the hump have the same Gaussian shape [$\propto \exp(-r^2/2l^2)$, with $\mathbf{r}$ counted off from the corresponding extremum] and opposite signs. The wave functions ψ_t and ψ_b are localized at the hump and the well of $V(\mathbf{r})$, respectively, and are given just by the most "localized" wave function of the lowest Landau level, namely that with zero angular momentum, $\psi_{00}(\mathbf{r}) \propto \exp(-r^2/4l^2)$, centered at the appropriate potential extremum. The overlap of these wave functions is negligibly small, and Eqs. (4.26), (4.27) give

$$\hbar\omega = 2v^2\lambda\, A, \quad |\ln\tilde{\sigma}(\omega)| = \frac{\hbar^2\omega^2}{4v^2\, A} = \frac{\omega^2}{2\pi\,\gamma^2 l^2\, A},$$

with $A \equiv \int d\mathbf{r}\, |\psi_{\rm t,b}|^4 = (4\pi l^2)^{-1}$. In this way we recover the expression (4.20) for the conductivity tail. For higher Landau levels ($N \geq 1$), the wave functions have the form [96] $\psi_{\rm t,b} \propto r^N \exp(-iN\phi)\exp(-r^2/4l^2)$, in which case the corresponding constant $A_N = (4\pi l^2)^{-1}(2N)!/2^{2N}(N!)^2$.

The prefactor in Eq. (4.24) prevents the well and the hump of $V(\mathbf{r})$ from being

too far away from each other. Nevertheless, the full variational equation (4.25) has a solution with an antisymmetric optimal potential $V(\mathbf{r}) = -V(-\mathbf{r})$ and symmetric wave functions $\psi_t(\mathbf{r}) = \psi_b(-\mathbf{r})$; respectively, $E_t = -E_b = \hbar\omega/2$. To estimate the role of the overlap integral we used the direct variational method in which we sought the potential in the form $V(\mathbf{r}) = \tilde{V}(|\mathbf{r} - \mathbf{r}_0|) - \tilde{V}(|\mathbf{r} + \mathbf{r}_0|)$ with $\tilde{V}(r) = V_0 \exp(-r^2/2l^2)$. The distance $2r_0$ separating the hump and the well was used as a variational parameter. Given the potential, one has to solve the Schrödinger equation, looking for the wave functions projected on the lowest Landau level. We took the functions $\psi_{t,b}$ in the simplest form of orthogonal combinations of the zero-momentum wave functions centered close to $\pm\mathbf{r}_0$ (the positions were found using a variational procedure). The distance r_0 scales with frequency logarithmically. The overall asymptotic expression for the exponent in $\tilde{\sigma}$ was the same as in Eq. (4.20); the overlap integral gave only a prefactor,

$$|\langle\psi_t|\boldsymbol{\nabla}V|\psi_b\rangle|^2 \sim (\hbar\gamma^2/l\omega)^2 \ln(\omega/\gamma).$$

To further check the accuracy of the asymptotic behavior of $\tilde{\sigma}(\omega)$, we maximized (see App. D) the functional in Eq. (4.24) numerically. We used the variational equation (D.4) to represent the optimal potential as a bilinear combination of the LLL wave functions $\psi_{0m}(\mathbf{r}) \propto r^m \exp(im\phi)\exp(-r^2/4l^2)$ with different magnetic quantum numbers $m \geq 0$,

$$V(\mathbf{r}) = \sum_{m,m'} u_{mm'}\, \psi^*_{0m}(\mathbf{r})\, \psi_{0m'}(\mathbf{r}).$$

The corresponding eigenfunctions $\psi_{t,b}$ were written as linear combinations of the same functions $\psi_{0m}(\mathbf{r})$.

Both the exponent and the prefactor of the variational functional (4.24) calculated numerically become close to the result of the direct variational method for $\omega/\gamma \gtrsim 3$. The shape of the optimal potential found numerically for two values of ω/γ is illustrated in Fig. 4.2.

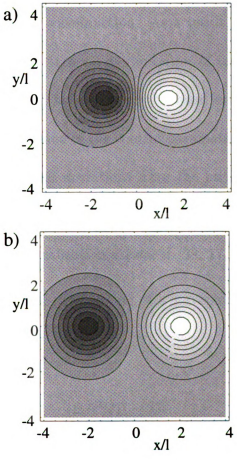

Figure 4.2: Density plot of the optimal potential for $\omega = 3\gamma$ (a) and $\omega = 8\gamma$ (b). The distances are measured in units of the magnetic length l.

4.5 Single electron scaling for $\omega \to 0$

An entirely different set of states defines the conductivity for very small frequencies, $\omega \ll \gamma$. In this regime the constraint imposed by conservation of energy is not very restrictive, and it is the matrix element that determines relative contributions of different pairs of states.

Close to the static limit the contribution to the conductivity increases dramatically with the typical size of a wavefunction. As a result, $\tilde{\sigma}$ [Eq. (4.2)] is primarily determined by a narrow energy interval at the center of the Landau band where the states are nearly delocalized. The energy of the band center ($E = 0$) is a critical energy, similar to the critical value of the control parameter in the theory of classical percolation transition. At small deviations from the critical energy (parametrized by the dimensionless energy $\varepsilon \equiv E/\hbar\gamma$) the correlation length diverges, $\xi_\varepsilon \sim l\,|\varepsilon|^{-\nu}$, where $\nu = 2.33 \pm 0.03$ is the localization exponent [98, 17, 44].

Were it not for localization, propagation of a wavepacket in a random potential would be diffusive,

$$\langle \Delta R^2(t) \rangle \sim Dt. \tag{4.28}$$

Localization corrections are least important near the critical energy, but even there they modify the form of a wavepacket at very large times [99].

However, for not too large times the r.m.s. displacement, which is primarily determined by small momenta, retains the diffusive form. This can be used to find the

conductivity at small frequencies. To this end, let us rewrite Eq. (4.8)

$$\tilde{\sigma}(\omega) = -\frac{2\omega^2}{l^2\gamma} \lim_{\delta\to+0} \Re\mathrm{e} \int_0^\infty dt\, e^{i\omega t-\delta t}\, \mathrm{Tr}_0\, \overline{\Delta R^2(t)}, \tag{4.29}$$

in terms of the squared displacement $\Delta R^2(t) \equiv [\mathbf{R}(t) - \mathbf{R}(0)]^2$, where $\mathbf{R}(t) \equiv e^{iHt}\mathbf{R}\, e^{-iHt}$ is the Heisenberg operator of the guiding center. For an eigenstate $|n\rangle$ of the Hamiltonian (4.3) randomly chosen not too far from the critical energy, $\langle n|\Delta R^2(t)|n\rangle$ has the diffusive form (4.28) at small enough t, but it eventually saturates at the distance of the order of the localization length ξ_{ε_n}.

Replacing the trace by the integral over energy weighted with the (non-critical) density of states, we obtain the overall long-time ($\gamma t \gg 1$) r.m.s. displacement

$$\begin{aligned} \mathrm{Tr}_0\overline{\Delta R^2(t)} &\sim \hbar\gamma \int d\varepsilon\, \rho(\hbar\gamma\varepsilon)\, \min(Dt, \xi_\varepsilon^2) \\ &\propto l^2\, (\gamma t)^{1-1/(2\nu)}. \end{aligned} \tag{4.30}$$

This average is determined by the states with energies $|\varepsilon| \leq (\gamma t)^{-1/2\nu}$; the integral rapidly converges outside this region.

With asymptote (4.30), time integration in Eq. (4.29) gives:

$$\tilde{\sigma}(\omega) = C\, (\omega/\gamma)^\mu, \quad \mu \equiv (2\nu)^{-1}. \tag{4.31}$$

The same result can be obtained from the scaling form [100, 101] of the zero-temperature conductivity of the non-interacting system at a given chemical potential,

which can be written as

$$\sigma_{xx}(\varepsilon,\omega) = \frac{e^2}{\hbar}\,\mathcal{G}_0\left(\frac{\omega\xi_\varepsilon^2}{\gamma l^2}\right), \tag{4.32}$$

where the dimensionless scaling function $\mathcal{G}_0(X)$ rapidly vanishes for $X \to 0$ and approaches a constant value for large X. Indeed, the conductivity for $\beta\omega \ll 1$ can be written as a convolution of the scaling function (4.32) with the derivative of the Fermi distribution function

$$\tilde{\sigma}(\omega) = \frac{8\,k_B T}{ne^2\,l^2\gamma}\int d\varepsilon\left(-\frac{dn_F}{d\varepsilon}\right)\sigma_{xx}(\varepsilon,\omega) \tag{4.33}$$

[cf. Eq. (4.7)]. For $k_B T \gg \hbar\gamma$, all energies within the stripe of width $\delta\varepsilon \sim (\omega/\gamma)^\mu$ contribute equally, and in the limit $\omega \to 0$ we obtain Eq. (4.31) with the coefficient

$$C = 16\pi\mu\int_{-\infty}^{\infty}\frac{dX}{|X|^{1+\mu}}\,\tilde{\mathcal{G}}_0(X). \tag{4.34}$$

Here we have assumed that $\varepsilon^\nu\xi_\varepsilon \to$ const for $\varepsilon \to 0$, and $\tilde{\mathcal{G}}_0(X) \equiv \lim_{\varepsilon\to 0}\mathcal{G}_0(X\,\varepsilon^{2\nu}\xi_\varepsilon^2/l^2)$. The integration converges both at zero and infinity.

Therefore with $\nu \approx 2.33$ we conclude,

$$\tilde{\sigma}(\omega) \propto \omega^\mu\ (\omega \to 0),\quad \mu = (2\nu)^{-1} \approx 0.215. \tag{4.35}$$

4.6 Reconstruction technique

4.6.1 Hermite polynomial reconstruction

Since the conductivity is asymptotically Gaussian, one is tempted to restore $\tilde{\sigma}(\omega)$ from the moments M_n in a standard way, writing an expansion in Hermite polynomials $\tilde{\sigma}(\gamma x) = \sum_n B_n H_n(\sqrt{2}x)\exp(-2x^2)$. The coefficients B_n can be easily expressed in terms of higher-order moments. However, for the moments (4.18), this expansion does not converge rapidly, which indicates a possible *nonanalyticity* of the conductivity at $\omega = 0$, see Fig. 4.3.

4.6.2 Laguerre polynomial reconstruction

The arguments given in Sec. 4.5 strongly suggest that a scaling relation $\sigma(\omega) \propto \omega^\mu$ for $\omega \to 0$ exists. The attempted reconstruction by Hermite polynomial supports the indication of a nonanalyticity at $\omega = 0$. Given the exponent μ, the conductivity $\tilde{\sigma}(\omega)$ can be restored from the moments (4.18) by using an expansion in terms of appropriate orthogonal polynomials. With Eqs. (4.20), (4.35), the conductivity can be written as

$$\tilde{\sigma}(\omega) = x^\mu G(x)\exp(-2x^2),\ x = |\omega|/\gamma. \tag{4.36}$$

The function $G(x)$ $(x \geq 0)$ can be expanded in Laguerre polynomials $L_n^{(\mu-1)/2}(2x^2)$, which are orthogonal for the weighting factor in Eq. (4.36). We have restored the corresponding expansion coefficients from the moments (4.18). The resulting con-

ductivity calculated with $\mu = 0.215$ is shown in Fig. 4.5. The estimated deviation from the exact value due to a finite number of terms we preserved in the expansion is smaller then the width of the line. The expansion for $\tilde{\sigma}$ converges rapidly for μ between 0.19 and 0.28, whereas outside this region the convergence deteriorates, Fig. 4.4.

4.7 Summary

In summary, the low-frequency single-electron magnetoconductivity of a nondegenerate 2D electron liquid in a quantizing magnetic field has been studied well beyond the known SCBA results. The universal shape of the reduced magnetoconductivity $\tilde{\sigma}(\omega)$ has been obtained with good accuracy, see Fig.4.6, using the above asymptotic expressions and the method of moments [95]. It follows from those results that for strong coupling to short-range scatterers the conductivity $\sigma_{xx}(\omega)$ is nonmonotonic. The static conductivity is found to be zero which is in contrast to the SCBA result. In the limit of small frequencies, $\omega \to 0$, the single-electron conductivity can be found from scaling arguments described with QHE critical exponents known from localization properties of a 2DES.

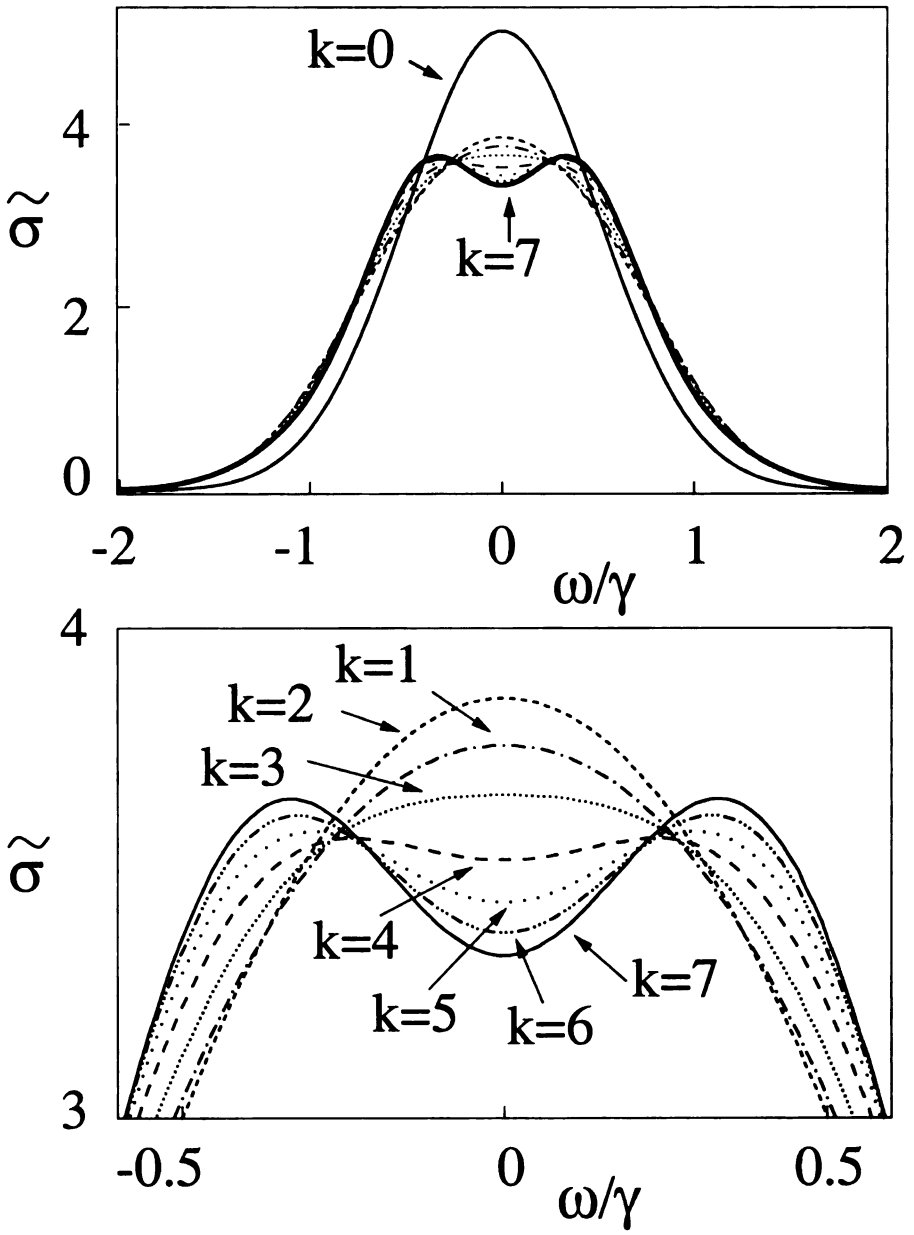

Figure 4.3: Approximating $\tilde{\sigma}$ with Hermite polynomials. With increasing number of moments M_{2k} the tail, $\omega \geq \gamma$, converges rapidly. Interestingly enough, the overall conductivity $\tilde{\sigma}$ is nonmonotonic for small ω. At the bottom, the magnification shows a rather slow convergence at $\omega = 0$, which indicates a possible *nonanalyticity* of the conductivity.

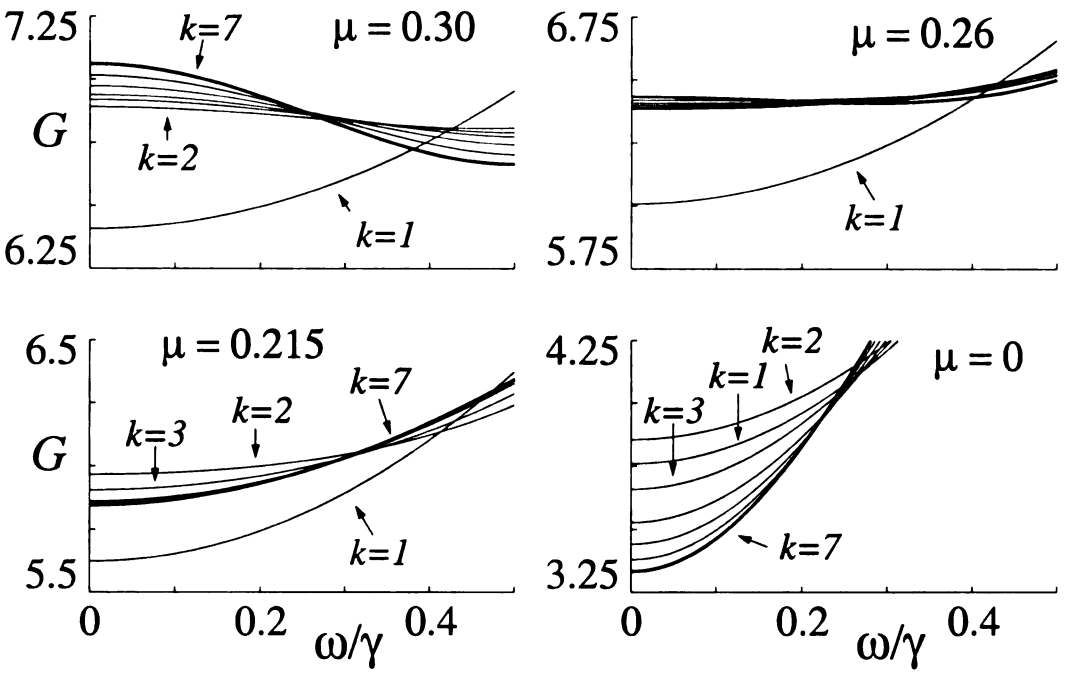

Figure 4.4: The expansion of the prefactor G (4.36) in Laguerre polynomials $L_n^{(\mu-1)/2}(2x^2)$, in dependence of the exponent μ. The expansion converges rapidly for μ between 0.19 and 0.28 and deteriorates significantly outside of this interval.

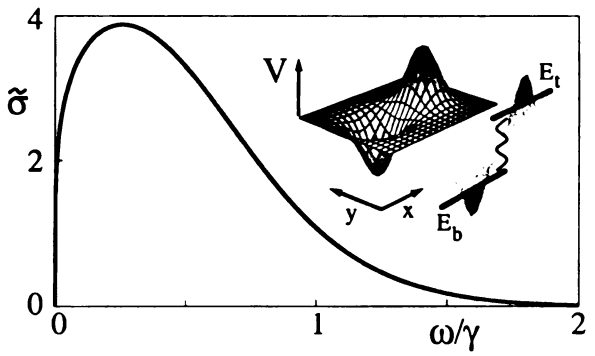

Figure 4.5: Reduced microwave conductivity (4.10) of a non-interacting 2DES in a short-range disorder potential for $k_BT \gg \hbar\gamma$ (solid line). For small frequencies, $\omega \ll \gamma$, the singular part of the conductivity $\sigma_{xx} \sim \omega^{\mu}$ is determined by spatially large, nearly delocalized states. For large frequencies, $\omega \gg \gamma$, the conductivity is determined by large optimal fluctuations of the disorder potential as illustrated in the inset. The corresponding optimal potential $V_{\rm opt}(\mathbf{r})$ should be such that $\hbar\omega$ be equal to the energy difference $E_{\rm t} - E_{\rm b}$ between the top and bottom bound states $|t\rangle$, $|b\rangle$, and at the same time these states be maximally overlapping.

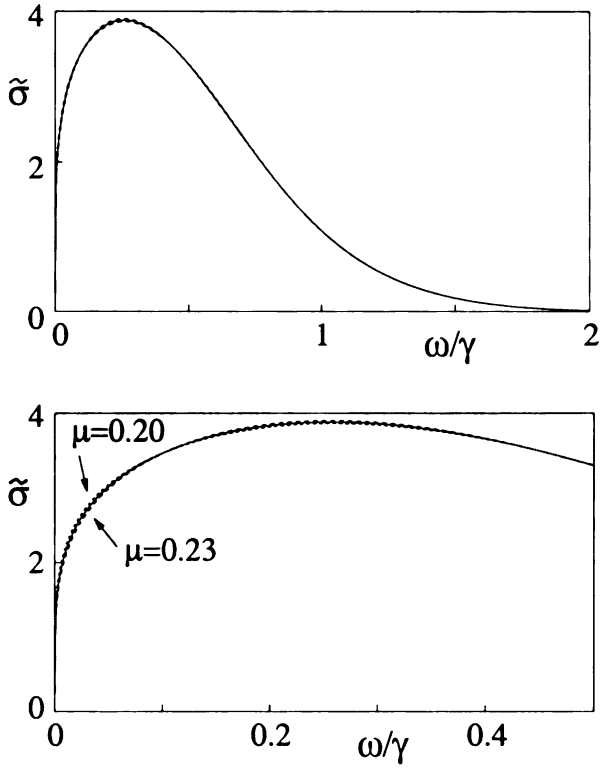

Figure 4.6: Comparison of the reduced conductivity $\tilde{\sigma}(\omega)$ for different values of $\mu = 0.23, 0.215$ (solid line), 0.20. The curves dependence is only sensitive against the scaling exponent μ for a narrow frequency region $\omega < 0.5\gamma$.

Chapter 5

Cyclotron Resonance

The single electron conductivity at cyclotron frequency is determined by the correlation function of the Landau level raising and lowering operator

$$\sigma_c(\omega) = \frac{ne^2}{2m} \int_{-\infty}^{\infty} dt\, e^{i\omega t}\, \langle p_-(t) p_+(0) \rangle, \tag{5.1}$$

where we used Eq. (4.1) and assumed that $\exp(\hbar\omega_c/k_BT) \gg 1$, in which case only the lowest Landau level is occupied for small densities. If the disorder is weak, $\gamma \ll \omega_c$, it only weakly mixes different Landau levels, the primary effect being lifting the degeneracy of each level. Then, the problem of optically-induced transitions between different Landau levels resembles that of transitions between degenerate electronic terms of impurities in solids in the presence of the electron-phonon coupling which gives rise to Jahn-Teller effect [94]. One of the effective methods of the theory of absorption spectra of Jahn-Teller centers is the method of moments.

The MOM formalism can be transferred to the case of inter-Landau-level tran-

sitions [76]. For $\hbar\gamma \ll k_B T$, quenched disorder can be described in the same way as scattering by thermally excited phonons. The major difference is infinite level degeneracy.

In the neglect of disorder-induced scattering between Landau levels, one should keep only the part H_d of the disorder potential $V(\mathbf{r})$, which is diagonal in the Landau level representation,

$$H_d = \sum_N H_d^{(N)} P_N = \hbar\gamma \sum_{\mathbf{q}} \tilde{V}_q e^{i\mathbf{qR}} \sum_N L_N\Big(\frac{q^2 l^2}{2}\Big) P_N, \tag{5.2}$$

where $\tilde{V}_q$ is defined by Eq. (4.4) and $P_N = P_N^2$ is the operator of projection to the N th Landau level, as in Eq. (B.15). With the Hamiltonian (5.2), oscillations at the cyclotron frequency can be singled out in Eq. (5.1),

$$p_\pm(t) = e^{\pm i\omega_c t} e^{iH_d t/\hbar} p_\pm e^{-iH_d t/\hbar}. \tag{5.3}$$

Then, from Eq. (5.1), we can write

$$\sigma_c(\omega) = \frac{ne^2}{2m\gamma}\, \tilde{\sigma}_c(\omega), \tag{5.4}$$

where

$$\tilde{\sigma}_c(\omega) = \gamma \int_{-\infty}^{\infty} dt\, e^{i\Delta\omega t}\, \mathrm{Tr}_0 \overline{[e^{iH_d t/\hbar} p_- e^{-iH_d t/\hbar} p_+]} \tag{5.5}$$

is the reduced conductivity, and $\Delta\omega \equiv \omega - \omega_c$ is the frequency detuning, $|\Delta\omega| \ll \omega_c$.

5.1 Cyclotron moments

The major difference of Eq. (5.5) from its counterpart (4.8) for the low-frequency conductivity is that the Hamiltonians for direct and inverse time propagation (corresponding to the factors $e^{\pm iH_d t}$) are now different, which is again familiar from the theory of impurity absorption spectra. The reduced cyclotron conductivity can be conveniently written in a form conventional for this theory by introducing the "perturbation" Hamiltonian

$$\delta H_d \equiv H_d^{(1)} - H_d^{(0)} = -\hbar\gamma \sum_{\mathbf{q}} \frac{q^2 l^2}{2} \tilde{V}_{\mathbf{q}}\, e^{i\mathbf{q}\mathbf{R}}. \tag{5.6}$$

In the interaction representation, $\tilde{\sigma}_c$ can be then simply expressed in terms of a time-ordered exponential,

$$\tilde{\sigma}_c(\omega) = \gamma \int_{-\infty}^{\infty} dt\, e^{i\Delta\omega t}\, \mathrm{Tr}_0 \overline{\left[\mathrm{T}_\tau \exp\left(-\frac{i}{\hbar} \int_0^t d\tau\, \delta H_d(\tau) \right) \right]}. \tag{5.7}$$

Here, time dependence of the operator δH_d,

$$\delta H_d(\tau) \equiv e^{iH\tau/\hbar}\, \delta H_d\, e^{-iH\tau/\hbar}, \quad H \equiv H_d^{(0)}, \tag{5.8}$$

is generated by the disorder Hamiltonian projected on the LLL, which is given by Eq. (4.3) of the previous chapter.

We can now define the spectral moments of the cyclotron peak as

$$M_k^c = \frac{1}{2\pi\gamma}\int_{-\infty}^{\infty} d\omega \left(\frac{\omega-\omega_c}{\gamma}\right)^k \tilde{\sigma}_c(\omega). \tag{5.9}$$

Using Eq. (5.7) we write

$$M_k^c = \overline{\mathrm{Tr}_0\left(\frac{i}{\gamma}\frac{d}{dt}\right)^k \mathrm{T}_\tau \exp\Big(-\frac{i}{\hbar}\int_0^t \delta H_d(\tau)\, d\tau\Big)\Big|_{t=0}}. \tag{5.10}$$

We note that, similar to the case of the peak of low-frequency conductivity discussed in the previous chapter, we are calculating here the moments of the cyclotron peak only, whereas the small ($\propto \gamma/\omega_c$) background from the correlators neglected in obtaining Eq. (5.1) is projected away, as are also the peaks of $\sigma_{xx}(\omega)$ at $\omega \approx n\omega_c$ with $n \neq 1$.

We will now calculate the spectral moments. Because all states of the lowest Landau level are equally populated, the reduced conductivity (5.7) is symmetric with respect to ω_c, *i.e.*, $\tilde{\sigma}_c(\omega_c + \Delta\omega) = \tilde{\sigma}_c(\omega_c - \Delta\omega)$. Therefore all odd moments vanish, $M_{2k+1}^c = 0$. We obtain the general structure of the expression for even moments which follows from Eq. (5.10) and shows a similar structure to that of Eq. (4.15). The main difference is that the prefactor now is a complicated polynomial, a combination of products of terms which are linear in the squared wave numbers q_k^2,

$$\begin{aligned} M_{2k}^c = \quad & \sum_{\{\mathbf{q}\}} \langle \tilde{V}_{\mathbf{q}_1} \ldots \tilde{V}_{\mathbf{q}_{2k}} \rangle \ \left(a_1 q_1^2 + \ldots + a_m q_1^2 q_2^2 \ldots q_{2k}^2\right) \times \\ & \exp\left[\frac{i}{2} l^2 \left(\mathbf{q}_1 \wedge \mathbf{q}_2 + \ldots + (\mathbf{q}_1 + \ldots + \mathbf{q}_{2k-1}) \wedge \mathbf{q}_{2k}\right)\right], \end{aligned} \tag{5.11}$$

where the sum is taken over the quasicontinuous spectrum of all wavenumbers $\mathbf{q}_1, \ldots, \mathbf{q}_{2k}$.

Unlike in the case for the low-frequency conductivity $\tilde{\sigma}(\omega)$ we couldn't find any easy diagram rules to reduce the computational overhead resulting from diagram symmetries. Secondly the resulting high dimensional oscillating gaussian integrals could not easily be computed numerically by a diagonalization technique. This is because of the nontrivial prefactor in (5.11). To obtain exact values for those integrals we developed the computer algebra package *GaussInt* [102] for Mathematica, which is capable of handling the integration of highly dimensional gaussian integrals in a manageable time frame. For $k = 0, 1, \ldots, 5$ we obtain for M_{2k}^c

$$M_{2k}^c = 1; \frac{1}{2}; \frac{37}{64}; \frac{52043}{55296}; \frac{4750893001499}{2488320000000}; \frac{2969405418835327520783195071649605468 7}{648069633391411761172111687680000000 0} \tag{5.12}$$

and their approximate values

$$M_{2k}^c \approx 1; \frac{1}{2}; 0.578; 0.941; 1.909; 4.582\,.$$

5.2 Asymptotic behavior

To restore the conductivity $\tilde{\sigma}_c(\omega)$ from its moments (5.12) we also need its asymptotic form. The method of optimal fluctuation provides the asymptotic gaussian ω-dependence. If we introduce the exact eigenstates of the Hamiltonian (5.2) for the

lowest $|0,m\rangle$ and the first excited $|1,m\rangle$ Landau levels, with energies $E_m^{(0)}$ and $E_m^{(1)}$, respectively, the expression (5.5) for the reduced conductivity can be written in the form

$$\tilde{\sigma}_c(\omega) = 2\pi\hbar\gamma \sum_{m,n} \overline{\delta(E_m^{(1)} - E_n^{(0)} - \hbar\omega)|\langle 1,m|p_+|0,n\rangle|^2}. \tag{5.13}$$

As for the low-frequency conductivity considered in the previous chapter, the conductivity tail is determined by large optimal fluctuations of the disorder potential. The problem of finding the optimal potential for the cyclotron resonance had already been considered by Ioffe and Larkin [28]. They found the optimal potential was realized by a rotational-symmetric potential

$$V_{\rm opt}^{\rm Larkin} = 2\pi V_0|\Phi_0|^2 + 2\pi V_1|\Phi_1|^2 \tag{5.14}$$

where

$$\Phi_0 = \psi_{0,0}(\mathbf{r}) = (2\pi l^2)^{-1/2}\exp[-r^2/4l^2],$$

$$\Phi_1 = \psi_{1,-1}(\mathbf{r}) = (4\pi l^4)^{-1/2} r e^{i\varphi}\exp[-r^2/4l^2].$$

are the functions of the lowest and first excited Landau levels centered at the *same* origin, with magnetic quantum numbers 0 and -1 respectively. This resulted in the asymptotic form of the cyclotron resonance absorption peak $\sigma_c \propto \exp(-8\,\Delta\omega^2/\gamma^2)$, for the range $\hbar\gamma \ll k_B T$.

We argue that the transition probability between the states with energy separation $E_m^{(1)} - E_n^{(0)} = \Delta\omega + \omega_c$ is exponentially increased if the cyclotron orbit centers of these states are permitted to shift with respect to each other. This happens despite the associated decrease of the overlap integral.

The calculation of the tails of the cyclotron resonance absorption peak is very similar to that in Sec. 4.4. We begin by writing the averaging in terms of a functional integral (4.21), with the energy conservation taken into account using a Lagrange multiplier [as in Eq. (4.24) but with *different* Hamiltonians for E_t and E_b]. If we neglect the dependence of the transition matrix element on $V(\mathbf{r})$, then for the optimal potential we obtain an equation similar to Eq. (5.14). However, in contrast to Ref. [28], we permit the centers of the wave functions Φ_0 and Φ_1 to be shifted with respect to each other.

A remarkable feature of this simplified variational problem is that, in the neglect of overlapping of the displaced wave functions, the *same* value of the variational functional [except for the overlap term] is obtained for the trial wave functions of the first Landau level with the magnetic quantum numbers -1 or 0, *i.e.*, $\psi_{1,-1}$ or $\psi_{1,0}$, or for any of their linear combinations.

For a displacement R between the centers of the hump and well of the optimal potential, the transition matrix element is $|\langle\psi_1|p_+|\psi_0\rangle| \sim \exp(-R^2/4l^2)$. The optimal distance $R^2 \approx 4l^2 \ln[(\omega - \omega_c)^2/\gamma^2]$ is found by maximizing the expression with the matrix element present. As in the case of the low-frequency conductivity, this distance increases as the frequency is tuned away from resonance.

The variational result for the conductivity tail is

$$\tilde{\sigma}_c(\omega) \propto \exp\Big(-\frac{8}{3\gamma^2}(\omega-\omega_c)^2\Big). \tag{5.15}$$

This tail is much broader, with the exponent reduced by a factor of 3, compared to the result of Ref. [28].

5.3 Restoration

5.3.1 Reconstruction with Hermite polynomials

The result of the standard reconstruction of $\tilde{\sigma}_c$ from its moments (5.12) by $\tilde{\sigma}_c(\gamma x) = \sum_n B_n H_n(\sqrt{8/3}x)\exp(-8/3x^2)$ is shown in Fig. 5.1. The coefficients B_n can be easily expressed in terms of higher-order moments. Although the tail of the conductivity converges rapidly, it is noticeably slower close to the center [it is emphasized, however, that convergence is reached, in contrast to the similar expansion for the low-frequency conductivity in Fig. 4.3, where the convergence was not reached for 14 moments]. Within this approach, the number of calculated moments is apparently insufficient for restoring the entire function $\tilde{\sigma}_c$ with desired accuracy.

5.3.2 Continued fraction reconstruction

Continued fraction expansions are known to be reliable source for powerful and fast approximations. Analogous to the reconstruction of the density of states for an arbitrary correlated random potential [29], we employ this powerful technique to restore

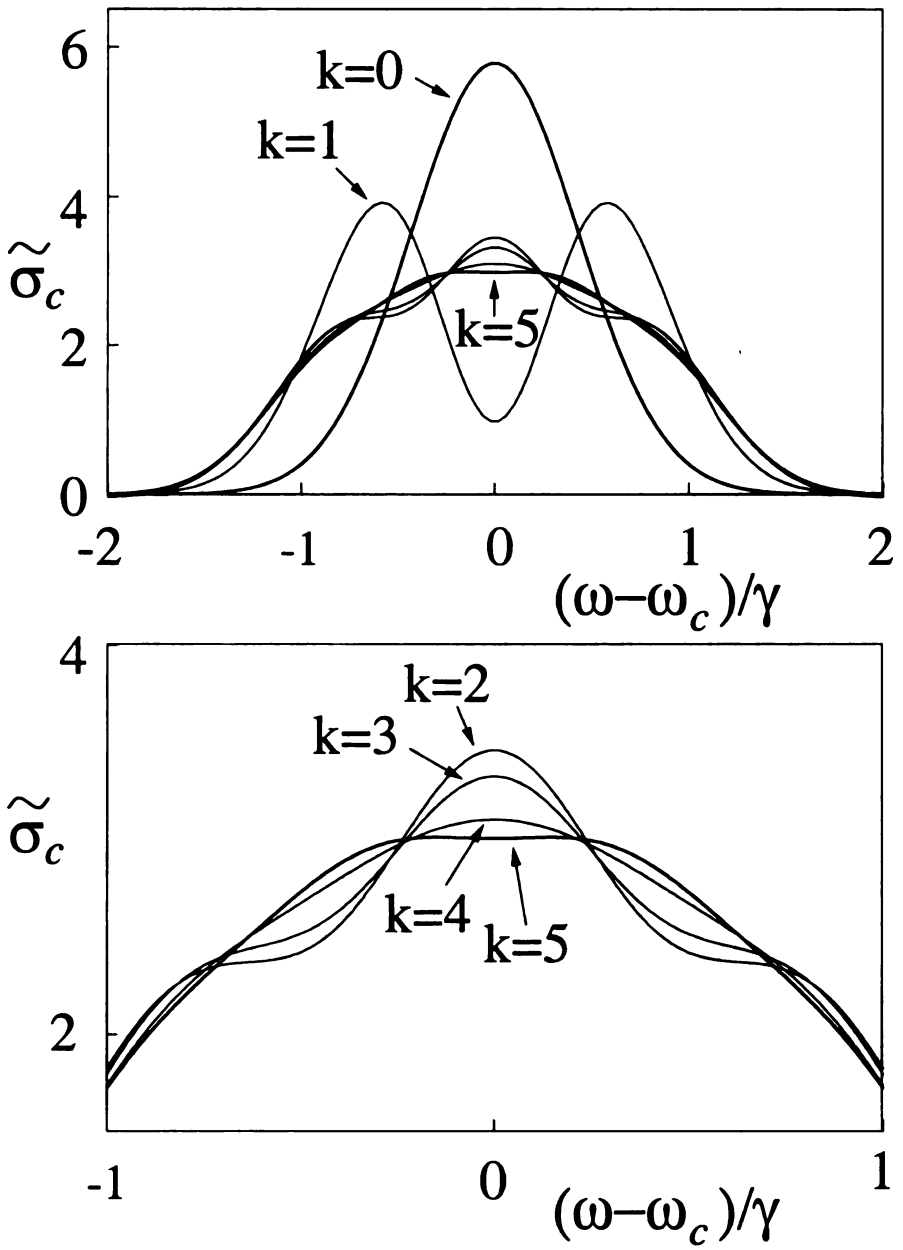

Figure 5.1: Approximating $\tilde{\sigma}_c$ with Hermite polynomials. With increasing number of moments M_{2k}^c the tail, $\omega \geq \gamma$, converges rapidly. Interestingly enough, this approximation scheme doesn't show fast convergence.

$\tilde{\sigma}_c$ from its moments (5.12). In the following we give a brief summary of the important steps involved in this process.

The Stieltjes transform of the conductivity $\tilde{\sigma}_c$

$$R(z) = \frac{1}{2\pi\gamma} \int_{-\infty}^{\infty} d\omega \, \frac{\tilde{\sigma}_c(\omega + \omega_c)}{z - i\omega/\gamma}, \quad \Re\mathrm{e}\, z > 0, \tag{5.16}$$

with its inverse transformation

$$\tilde{\sigma}_c(\omega + \omega_c) = 2 \lim_{\varepsilon \to 0+} \Re\mathrm{e}\,[R(\varepsilon + i\omega/\gamma)], \tag{5.17}$$

is related to the moments,

$$R(z) = \sum_{k=0}^{\infty} i^k M_k^c \, z^{-k-1}. \tag{5.18}$$

We now construct an approximation to (5.16) which applies for an even function $\tilde{\sigma}(\omega + \omega_c) = \tilde{\sigma}(-\omega + \omega_c)$, allows for the Gaussian asymptotics (5.15)

$$\lim_{\omega \to \pm\infty} \frac{\gamma^2}{\omega^2} \ln \tilde{\sigma}_c(\omega + \omega_c) = -\frac{1}{2\alpha}, \quad \alpha = \frac{3}{16}, \tag{5.19}$$

and requires only a finite number of moments.

According to Stieltjes classic theory [103, 104], R can be expanded into a Jacobi-type continued fraction. For normalized even moments we can write

$$R(z) = \underset{j=1}{\overset{\infty}{\mathrm{K}}} \left(\frac{\Delta_j}{z}\right), \quad \Delta_j \geq 0, \tag{5.20}$$

where we use the notation

$$\underset{j=1}{\overset{\infty}{\mathrm{K}}}\left(\frac{\Delta_j}{z}\right) := \cfrac{1}{z + \cfrac{\Delta_1}{z + \cfrac{\Delta_2}{z + \ddots}}} \tag{5.21}$$

for the continued fraction with coefficients Δ_j and variable z. The first J continued-fraction coefficients $\Delta_1, \ldots, \Delta_J$ are obtained from the normalized moments $M_2^c, \ldots, M_{2J}^c$ by expanding the power series (5.18) into the continued fraction (5.20) using an efficient recursive algorithm [103]. Having obtained only a finite number of coefficients Δ_j, we need to estimate the remaining ones. Fortunately however, the asymptotic behavior (5.19) implies [105] the following asymptotically linear growth for the continued-fraction coefficients

$$\lim_{j\to\infty} \frac{\Delta_j}{j} = \alpha. \tag{5.22}$$

Therefore it is natural to match this linear growth to the first $J < \infty$ coefficients $\Delta_1, \ldots, \Delta_J$ to construct the approximations $R^{(J)}(z)$ to $R(z)$ by means of

$$R^{(J)}(z) = \underset{j=1}{\overset{\infty}{\mathrm{K}}}\left(\frac{\Delta_j^{(J)}}{z}\right), \tag{5.23}$$

where

$$\Delta_j^{(J)} = \begin{cases} \Delta_j & \text{for} \quad j \leq J \\ \Delta_J + \alpha(j-J) & \text{for} \quad j > J \end{cases} . \tag{5.24}$$

A continuous fraction with a linearly increasing coefficient can be written in terms of the Whittaker parabolic cylinder function D_ν,

$$T(\beta, \alpha, z) \equiv \underset{j=1}{\overset{\infty}{\mathrm{K}}} \left(\frac{\beta + \alpha j}{z} \right) = \frac{D_{-(\beta/\alpha)-1}(\alpha^{-1/2} z)}{\alpha^{1/2} D_{-\beta/\alpha}(\alpha^{-1/2} z)}, \tag{5.25}$$

which is valid if $\alpha > 0$, $\beta + \alpha > 0$ and $\Re\mathrm{e}\, z > 0$, so that we can write Eq. (5.23) as

$$R^{(J)}(z) = \cfrac{1}{z + \cfrac{\Delta_1}{z + \ddots + \cfrac{\Delta_{J-1}}{z + \Delta_J T(\Delta_J, \alpha, z)}}} . \tag{5.26}$$

Applying the inversion formula (5.17) immediately gives the restored cyclotron resonance absorption $\tilde{\sigma}_c(\omega)$ as shown in Fig.5.2.

5.4 Summary

From very general arguments is seems to be clear that the singular behavior of transistions within the lowest Landau level states may not affect the cyclotron resonance absorption. The suppression of the low-frequency conductivity for $\omega \to 0$ may be

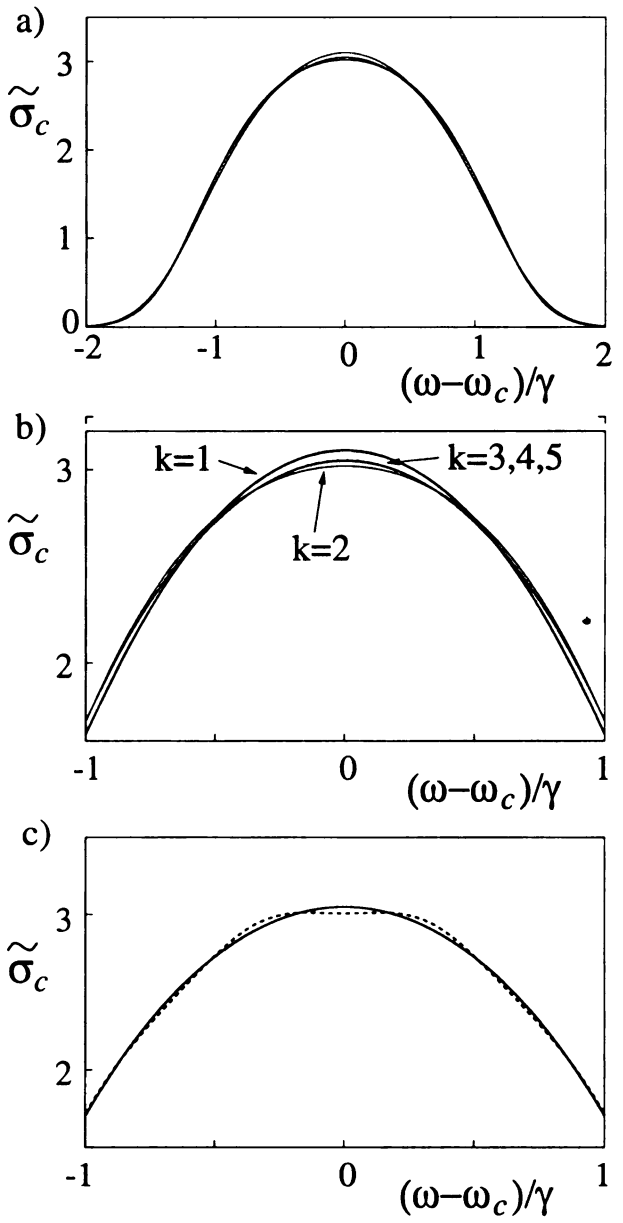

Figure 5.2: Approximating $\tilde{\sigma}_c$ with continued fractions. The convergence is astoundingly fast, with increasing number of moments M^c_{2k}. For $k = 3, 4, 5$ the curves lie on top of each other Fig.5.2b. The convergence can be compared to the standard Hermite polynomials approximation. Fig.5.2c shows a comparison between the continued-fraction (solid line) and the Hermite polynomial approximation (dashed line) for $k = 5$. Interestingly, though a non-critical behavior of the cyclotron resonance absorption is expected, the Hermite reconstruction fails to converge quickly.

attributed to level repulsion between overlapping localized states. This repulsion is comparatively small for states of relatively large radii, with energies close to the band center. Indeed, only such states contribute to the low-frequency conductivity, as we saw in Sec. 4.5. On the other hand, resonant cyclotron absorption is due to transitions between *different* Landau levels. Although the central part of the absorption peak is formed by transitions between strongly overlapping states, the involved states are eigenstates of *different* Hamiltonians, with random parts $H_d^{(0)}$ and $H_d^{(1)}$. Their wave functions have different spatial structures and their energies are essentially uncorrelated, except for states deep in the tails of the Landau levels. Consequently, we expect no suppression of transitions at frequencies close to ω_c. This argument is in agreement with the results of the method of moments presented in this chapter Fig. 5.2.

Chapter 6

Many-electron conductivity

In the present chapter we show that the electron-electron interaction (EEI) in a correlated 2DES gives rise to a nonzero static magnetoconductivity and to a low-frequency plateau in $\sigma_{xx}(\omega)$. We obtain the value of $\sigma_{xx}(0)$ and the width of the plateau, which for a weakly nonideal Fermi gas would be determined by the dephasing rate [106]. This allows us to reconcile the results on the QHE and the data on the strong-field magnetoconductivity of electrons on helium.

The EEI also dramatically changes the tail of $\sigma_{xx}(\omega)$ for $\omega \gg \gamma$. In the single-electron approximation, this tail is formed by the transitions between localized states with energies lying on the opposite tails of the disorder-broadened Landau level. Since the tail of the density of states is Gaussian [5, 28], so is also the tail of $\sigma_{xx}(\omega)$.

The EEI makes it possible for an electron to absorb a photon by changing its position with respect to other electrons. The photon energy then goes to the potential energy of the correlated many-electron system. In a quantizing transverse magnetic field $\mathbf{B}$, an electron displacement by $\delta\mathbf{r}$ requires the momentum transfer $(e/c)\delta\mathbf{r} \times \mathbf{B}$.

This momentum is provided by the disorder potential, via multiple scattering by defects - the mechanism which is somewhat similar to the one that gives rise to anomalous tunneling transverse to a magnetic field [107]. As a result, the many-electron $\sigma_{xx}(\omega)$ falls much slower than in the single-electron approximation, with a nonanalytic exponent $\omega^{2/3}$ [108].

Below, in Sec. 6.1, the magnetoconductivity of a nondegenerate electron fluid in the limit of weak short-range disorder is analyzed. It is shown that, for finite frequencies ($\omega \ll \omega_c$), the conductivity in quantizing fields becomes a nonmonotonic function of B. In Sec. 6.2 the low-frequency conductivity for strong disorder is considered.

6.1 Many-electron magnetoconductivity for weak short-range disorder

The force on an electron wave packet of size l from the disorder potential is $\sim \hbar\gamma/l$. Therefore the limit of weak disorder compared to the electron-electron interaction corresponds to

$$\hbar\gamma/l \ll e\langle \mathbf{E}_f^2 \rangle^{1/2}. \tag{6.1}$$

This condition can be interpreted also in terms of energies. It is seen from Eq. (4.6) that the quantity γ characterizes the distance between the single-electron states, of spatial extent l, localized on the same potential fluctuation. The fluctuational field gives rise to mixing of these states. The strength of this mixing is characterized by

$e\langle \mathbf{E}_f^2 \rangle^{1/2} l/\hbar\gamma$. When the mixing is strong (6.1), it is appropriate to speak of scattering of an electron, which moves in the fluctuational field, by disorder. As we will see, the scattering rate is small compared to the reciprocal duration of an individual scattering event (i.e., the reciprocal collision time).

6.1.1 General expresion for the low-frequency conductivity

In the range of temperatures $\hbar\omega_c \gg k_B T \gg \hbar\gamma$ and for $k_B T \gg \hbar\omega$, the low-frequency magnetoconductivity of a nondegenerate 2D electron liquid can be written in the form of an Einstein-type relation, see also Sec. 4.1

$$\sigma_{xx}(\omega) = ne^2 D_s (8k_B T)^{-1} \tilde{\sigma}(\omega), \quad D_s = l^2\gamma. \tag{6.2}$$

Here, D_s is a characteristic single-electron diffusion coefficient: in a scattering by a short-range defect an electron is displaced by $\sim l$, and the single-electron scattering rate is γ. The reduced conductivity $\tilde{\sigma}$ is given by the expression [93]

$$\begin{aligned} \tilde{\sigma}(\omega) = \quad & -2(\hbar m\gamma\omega_c)^{-1} \int_{-\infty}^{\infty} dt\, e^{i\omega t} \sum\nolimits_{\mathbf{q},\mathbf{q}'} (\mathbf{q}\,\mathbf{q}') \\ & \times \left\langle V_{\mathbf{q}} V_{\mathbf{q}'} \exp\left[i\mathbf{q}\,\mathbf{r}_n(t)\right] \exp\left[i\mathbf{q}'\,\mathbf{r}_n(0)\right] \right\rangle. \end{aligned} \tag{6.3}$$

Eqs. (6.2), (6.3) were obtained from the standard Kubo formula for $\sigma_{xx}(\mathbf{k},\omega)$ applied to a many-electron system in the limit $k \to 0$. First, in the Heisenberg equations of motion for the total electron momentum $\hat{\mathbf{P}}$ the term $d\hat{\mathbf{P}}/dt \sim \omega\hat{\mathbf{P}}$ was neglected compared to $\omega_c\hat{\mathbf{P}}$. Then $\hat{\mathbf{P}}$ is expressed in terms of the parameters of the disorder

Hamiltonian

$$H_i = \sum_n \sum_{\mathbf{q}} V_{\mathbf{q}} \exp(i\mathbf{q}\,\mathbf{r}_n) \tag{6.4}$$

($\mathbf{r}_n$ is the nth electron coordinate). The correlator of two $\hat{\mathbf{P}}$ operators is given by the sum over n, n' of the correlators $\langle V_{\mathbf{q}} V_{\mathbf{q}'} \exp[i\mathbf{q}\,\mathbf{r}_n(t)] \exp[i\mathbf{q}'\,\mathbf{r}_{n'}(0)]\rangle$. Only the terms with $n = n'$ were kept in this sum because, for a short-range potential (4.6) and for a correlated electron system, the typical wave numbers $q, q' \sim l^{-1}$ largely exceed the interelectron distance $n^{-1/2}$, or in other words, a short-range defect is interacting only with one electron at a time.

For weak disorder, the conductivity $\tilde{\sigma}(\omega)$ should be evaluated to the lowest order in $V_{\mathbf{q}}$, which corresponds to neglecting the disorder potential when calculating $\mathbf{r}_n(t)$. We will find the appropriate conditions later. At this point we will only assume that the range of times that contribute to the integral (6.3) are $|t| \ll \Omega^{-1}$, where Ω was defined in (3.22). In this case the fluctuational electric field $\mathbf{E}_n$ on the nth electron is time-independent and uniform over the electron wavelength l.

6.1.2 Electron density correlator

We will calculate the density correlator (6.3) using the lowest Landau level wave functions $\psi^{(0)}_{k_y}(\mathbf{r})$ of an electron in a uniform electric field $\mathbf{E}_{\mathrm{f}}$,

$$\begin{aligned} \psi^{(0)}_{k_y}(\mathbf{r}) \quad &= (L_y l)^{-1/2} \pi^{-1/4} \\ &\times \exp\left[ik_y y - \frac{1}{2l^2}\left(x - k_y l^2 + \frac{eE_{\mathrm{f}} l^2}{m\omega_c^2}\right)^2\right]. \end{aligned} \tag{6.5}$$

Here, L_y is the size of the system in the y-direction, and we chose the x-axis in the direction of $\mathbf{E}_\mathrm{f}$, i.e. $\mathbf{E}_\mathrm{f} = E_\mathrm{f}\hat{\mathbf{x}}$.

We will count the electron energy $E^{(0)}(k_y)$ off from $(1/2)\hbar\omega_c - (e^2\mathbf{E}_\mathrm{f}^2/2m\omega_c^2)$, in which case

$$E^{(0)}(k_y) = e\mathbf{E}_\mathrm{f}k_y l^2 \tag{6.6}$$

(the energy spectrum of the many-electron system is continuous, and so is the energy spectrum of an electron in the field of other electrons).

From Eqs. (6.5) and (6.6), the diagonal matrix element of the operator in (6.3) is

$$\begin{aligned}&\langle\psi_k^{(0)}\,|\exp[i\mathbf{q}\,\mathbf{r}(t)]\exp[-i\mathbf{q}\,\mathbf{r}(0)]|\,\psi_k^{(0)}\rangle \\ &\quad = \exp\left[-\frac{1}{2}q^2l^2\right]\exp\left[i\frac{et}{m\omega_c}\mathbf{E}_\mathrm{f}\,\hat{}\,\mathbf{q}\right]\end{aligned} \tag{6.7}$$

(for chosen axes, the wedge product is just $E_\mathrm{f}q_y$).

Calculation of the density correlator in Eq. (6.3) requires averaging of the matrix element (6.7) over electron states in the electron liquid. It can be done just by averaging (6.7) over the fluctuational field $\mathbf{E}_\mathrm{f}$, using the field distribution (3.25). This gives

$$\langle e^{i\mathbf{q}\,\mathbf{r}_n(t)}e^{-i\mathbf{q}\,\mathbf{r}_n(0)}\rangle = \exp\left[-\frac{1}{2}q^2l^2\left(1+\frac{\pi t^2}{2t_e^2}\right)\right], \tag{6.8}$$

where

$$t_e = l(B/c)\,\langle E_{\rm f}^{-1}\rangle = \frac{\hbar\pi^{1/2}}{el\sqrt{\langle \mathbf{E}_{\rm f}^2\rangle}} \sim (\Omega k_B T/\hbar)^{-1/2}. \tag{6.9}$$

The quantity t_e has a simple meaning: this is the time of flight of an electron wave packet, of size l, in the crossed fields $\mathbf{E}_{\rm f}, \mathbf{B}$, past a short-range defect, i.e. t_e is the duration of a collision. For typical $q \sim l^{-1}$, it determines the time over which the correlator (6.8) decays. In terms of t_e, the weak-disorder condition (6.1) has a simple form $\gamma t_e \ll 1$ which, in the single-electron transport theory, corresponds to the condition that the collision duration is small compared to the reciprocal "strength" of the random potential. In other words, collisions occur successively in time.

For $\hbar\Omega \ll k_B T$ we have $t_e \ll \Omega^{-1}$, which means that the fluctuational field on the electron does not vary during the collision, as assumed in the derivation above. On the other hand, for an electron fluctuating about its quasiequilibrium position, the time interval between successive collisions with the same scatterer is $\sim (\delta/l)^2\Omega^{-1}$, where δ was introduced in (3.17). It largely exceeds the time Ω^{-1} it takes for an electron to exchange energy with other electrons and thus to loose coherence. This shows that for weak scattering interference effects leading to weak localization in the single-electron approximation are not important.

6.1.3 Analysis of the conductivity

Eqs. (4.6), (6.8) give an extremely simple expression for the reduced conductivity $\tilde{\sigma}(\omega)$ of the correlated 2D electron liquid,

$$\tilde{\sigma}(\omega) = \sqrt{\frac{\pi}{2}}\gamma t_e \left(1 + \frac{2\omega t_e}{\sqrt{2\pi}}\right) \exp\left(-\frac{2\omega t_e}{\sqrt{2\pi}}\right) \tag{6.10}$$

In the quasi-static limit of small ωt_e Eqs. (6.2), (6.10) give $\sigma_{xx}(0) = (\pi/2)^{1/2} n e^2 l^2 \gamma^2 t_e / 8 k_B T$, as obtained earlier [93, 12] using different approaches (but still based on the notion of the fluctuational field). Thus, $\sigma_{xx}(0)$ has a form of the single-electron conductivity in a magnetic field, with the scattering rate $\tau^{-1} = \gamma^2 t_e$ which is quadratic in the disorder potential and is determined by the EEI.

The frequency dependence of $\tilde{\sigma}$ is shown in Fig. 6.1. Although it has a maximum at $\omega = 0$, it is very different from the standard Drude form $(1 + \omega^2\tau^2)^{-1}$. The characteristic width of the peak t_e^{-1} is given not by the rate of scattering by disorder (which is determined by γ), but by the many-electron time t_e. The tail of the peak is exponential in ω, following the Urbach rule.

The shape of the tail can be understood by noticing that the conductivity is formed by processes in which the **energy** of the absorbed photon $\hbar\omega$ goes to the many-electron system through a process in which the absorbing electron shifts by the distance $\delta r = \hbar\omega / e E_{\mathrm{f}}$ along the fluctuational electric field. The associated **momentum** $\hbar/\delta r$ is provided by short-range scatterers. Since the size of the electron wave packet is l, the probability to transfer momentum bigger than $\hbar/l$ is exponentially small. Therefore the conductivity decays for $\omega \gg e E_{\mathrm{f}} l/\hbar$, or $\omega t_e \gg 1$.

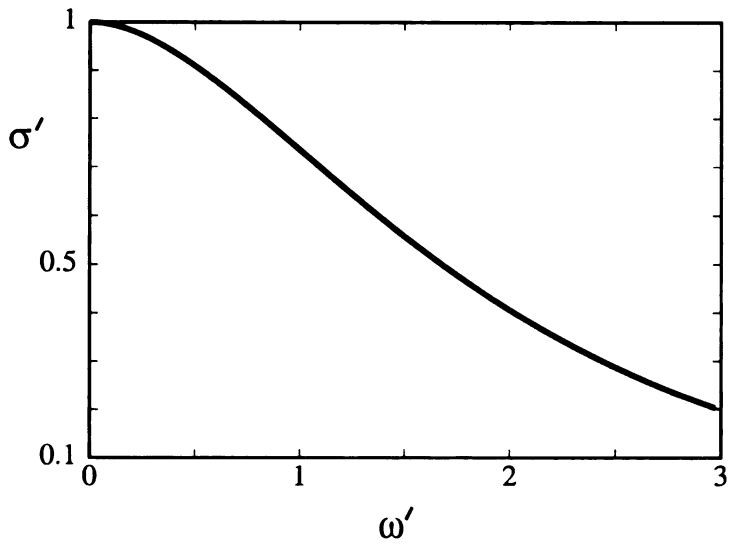

Figure 6.1: (a) The dependence of the reduced conductivity $\sigma'(\omega) = (2/\pi)^{1/2}\tilde{\sigma}(\omega)/\gamma t_e$ on the reduced frequency $\omega' = \omega t_e(2/\pi)^{1/2}$ in the limit of weak disorder (6.10).

An interesting and specific feature of the many-electron microwave conductivity $\sigma_{xx}(\omega)$ is its nonmonotonic dependence on the magnetic field. Since $\gamma \propto 1/l \propto B^{1/2}$ (4.6), and $t_e \propto B^{1/2}$ (6.9), the static conductivity $\sigma_{xx}(0) \propto B^{1/2}$ is *increasing* with the magnetic field for quantizing fields. This is a consequence of the fast increase, with the increasing B, of the characteristic scattering rate $\gamma^2 t_e$. The latter happens because, as B increases, the electron wave function becomes more localized, thus increasing the effective strength of coupling to short-range scatterers. At the same time, the characteristic collision duration t_e is also increasing, which further increases the scattering rate [93, 12]. The increase of $\sigma_{xx}(0)$ with the increasing B has been quantitatively confirmed by the experiment [15].

For finite frequencies $\sigma_{xx}(\omega)$ displays a peak as a function of B, see Fig. 6.2. The position of the peak is given by the expression

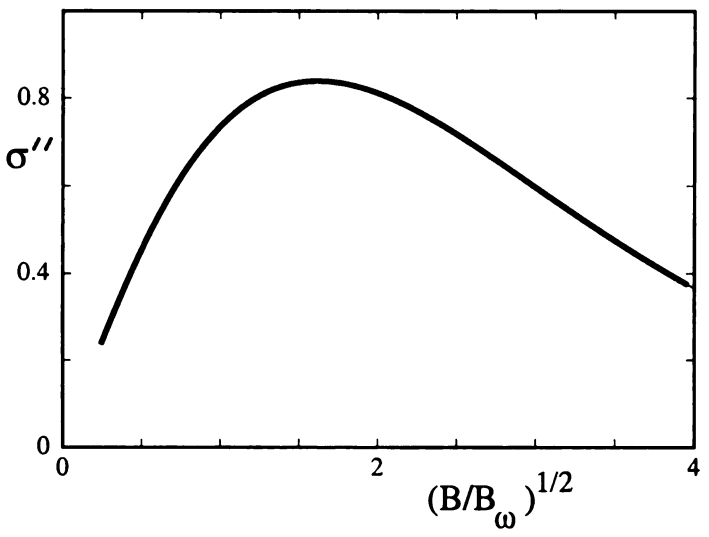

Figure 6.2: (a) The dependence of the reduced microwave conductivity $\sigma''(\omega) = (ne^2v^2/8\hbar^2\omega k_BT)^{-1}\sigma_{xx}(\omega)$ on the magnetic field, $B_\omega = \omega t_e(2/\pi B)^{1/2}$, in the limit of weak disorder.

$$(\omega t_e)_{\max} = (\pi/8)^{1/2}(1+\sqrt{5}), \quad B_{\max} \propto \omega^{-2}. \tag{6.11}$$

The onset of the peak is due to competition between the increase of the scattering rate with increasing B and the decrease of the probability to absorb a photon for $\omega t_e > 1$ explained above (t_e increases with B).

6.2 Low-frequency conductivity for strong disorder

We now consider the opposite case of comparatively strong disorder where the characteristic force on an electron originates from the defects,

$$\hbar\gamma/l \gg e\langle \mathbf{E}_i^2 \rangle^{1/2} \quad \text{or} \quad \gamma t_e \gg 1. \tag{6.12}$$

In this case collisions with defects "overlap" in time. One might expect therefore that the electron-electron interaction (EEI) would not affect the conductivity, and one could use the single-electron theory. In fact, this was done on several occasions for a correlated system of electrons on helium [13, 14, 15], using the self-consistent Born approximation (SCBA), although the existence of the parameter (6.12) was not always appreciated.

The SCBA conductivity is incompatible with the single-electron phenomenology of the quantum Hall effect (QHE), in which all but one (or maybe a few) states in the broadened Landau band are localized [17]. As a consequence, for $k_BT \gg \hbar\gamma$, where **all** states in the band are equally occupied, the single-electron static conductivity should be equal to zero, in contrast to the SCBA result.

6.2.1 Many-electron conductivity for $\omega \to 0$

Self-diffusion in the electron liquid, which is present in the temperature range of interest $k_BT \gg \hbar\gamma$, eliminates the single-electron localization. As a result, the static

conductivity of the liquid has a nonzero value. However, in the strong-disorder limit $\gamma t_e \gg 1$, because of multiple scattering by defects, the coefficient of self-diffusion is very different from that in the free electron liquid. In this subsection we obtain an estimate of this coefficient and of $\sigma_{xx}(\omega)$ for small ω/γ.

For strong disorder (6.12) but for $e^2 n^{1/2} \gg k_B T \gg \hbar\gamma$, electrons remain correlated, and one can think of the fluctuational electric field as a smooth perturbation superimposed on the disorder. The energy distance between the states of size $\sim l$ localized on the same disorder-potential fluctuation is $\sim \hbar\gamma$ and is large compared to $e|\mathbf{E}_\mathrm{f}|l$. For such states, the field $\mathbf{E}_\mathrm{f}$ is a perturbation, which nevertheless causes interstate transitions. On the other hand, for the states near the Landau band center, which have large radii and small interlevel distances, the effect of $\mathbf{E}_\mathrm{f}$ is very strong.

As a result of the EEI, the energy of an electron in the potential of defects $V(\mathbf{r})$ is not conserved. An electron displacement by a distance δL leads to change of the reduced energy $\delta\varepsilon \sim e|\mathbf{E}_\mathrm{f}|\delta L/\hbar\gamma \sim \delta L(\gamma t_e)^{-1}$. By setting δL equal, to the order of magnitude, to the correlation length ξ_ε, one obtains the width $|\varepsilon_\mathrm{f}|$ of the band of long-range states which "survive" in the presence of the fluctuational field

$$\varepsilon_\mathrm{f} \sim (\gamma t_e)^{-1/(\nu+1)}. \tag{6.13}$$

One can easily check that the displacement $\delta L = \hbar\gamma\varepsilon_\mathrm{f}/e|\mathbf{E}_\mathrm{f}| \sim l(\gamma t_e)^{\nu/(\nu+1)}$ is much less than the thermal displacement δ for $\hbar\gamma \ll k_B T$, which justifies the approximation of a uniform fluctuational field.

The motion of each electron gives rise to modulation of energies of all other elec-

trons. The overall change of the Coulomb energy of the electron system over a small time interval is given by $\sum_n e\,(\mathbf{E}_{\mathrm{f}n}\,\delta\mathbf{r}_n)$, where $\delta\mathbf{r}_n$ is the displacement of the nth electron due to the potential of defects, and $\mathbf{E}_{\mathrm{f}n}$ is the electric field on the nth electron from other electrons. Clearly, $\mathbf{E}_{\mathrm{f}n}$ and $\delta\mathbf{r}_n$ are statistically independent. This allows us to relate the coefficient of energy diffusion of an electron D_ϵ to the coefficient D of spatial diffusion in the potential $V(\mathbf{r})$ [108],

$$D_\epsilon = (e^2/2)\,\langle E_{\mathrm{f}}^2\rangle\,D \sim \gamma(\hbar/t_e)^2. \tag{6.14}$$

Energy diffusion eliminates electron localization which caused vanishing of the single-electron static conductivity. The low-frequency boundary ω_l of the range of applicability of the single-electron approximation can be estimated from the condition that the diffusion over the energy layer of width $\sim \delta\varepsilon_l = (\omega_l/\gamma)^\mu$ [which forms the single-electron conductivity (4.35) at frequency $\omega_l \ll \gamma$] occurred over the time $1/\omega_l$. For $\mu = 1/(2\nu)$, this gives

$$\omega_\ell/\gamma = C_{\mathrm{l}}\,(\gamma t_e)^{-2\nu/(\nu+1)}, \quad C_{\mathrm{l}} \sim 1. \tag{6.15}$$

Clearly, $\delta\varepsilon_l = (\omega_l/\gamma)^\mu$ as given by Eq. (6.15) coincides with the estimate (6.13) obtained using different arguments. All states with energies $|\varepsilon| \lesssim \delta\varepsilon_l$ contribute to the conductivity for frequencies $\omega < \omega_l$. Therefore the many-electron conductivity may

only weakly depend on ω for $\omega < \omega_l$, as shown in Fig. 6.3, and the static conductivity

$$\sigma_{xx}(0) \approx \sigma_{xx}(\omega_l) \sim (ne^2\gamma l^2/k_BT)(\gamma t_e)^{-1/(\nu+1)}. \tag{6.16}$$

We note a similarity between the EEI-induced energy diffusion, which we could here quantitatively characterize for a correlated nondegenerate system, and the EEI-induced phase breaking in QHE [109, 110]. The cutoff frequency ω_ℓ can be loosely associated with the dephasing rate [Eq. (6.16) can be obtained also as a conductance of a system of noninteracting electrons of size L_{ω_ℓ} at given temperature $k_BT \gg \hbar\gamma \gg \hbar\omega_\ell$]. In the range $\gamma t_e \sim 1$, Eq. (6.16) matches the many-electron theory [12] where $\sigma_{xx}(0) = (2\pi)^{1/2}ne^2\gamma^2 t_e l^2/16k_BT$. The results are shown by the solid line in Fig. 6.3.

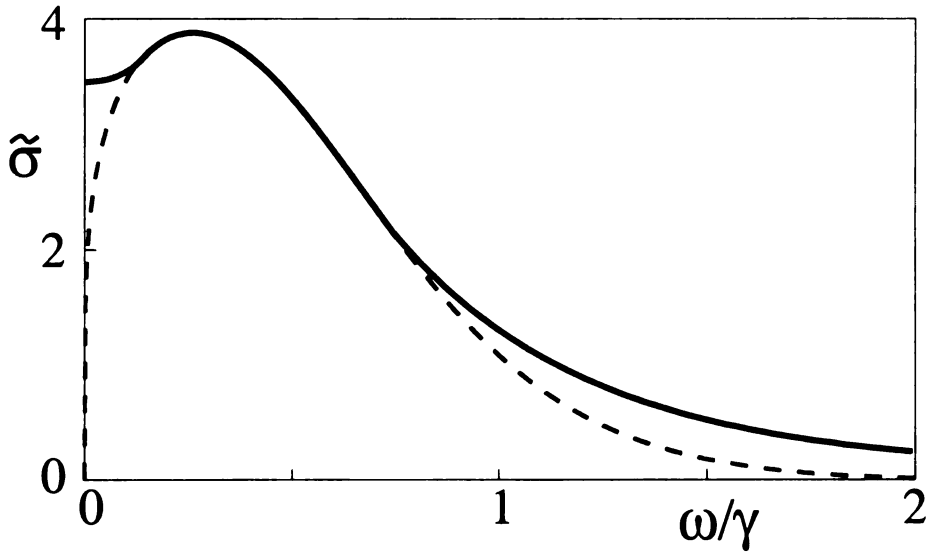

Figure 6.3: Reduced microwave conductivity (6.3) of a nondegenrate electron liquid for strong disorder, $\gamma t_e \gg 1$ and $k_BT \gg \hbar\gamma$ (solid line). The single-electron conductivity (dashed line) goes to zero for $\omega \to 0$. The electron-electron interaction results in flattening of $\tilde{\sigma}(\omega)$ for $\omega \lesssim \omega_l$ (6.15), and in a much slower decay of $\tilde{\sigma}$ for $\omega \gg \gamma$.

Chapter 7

Suggestions for an experiment

The many-electron 2D system that we investigated is characterized by several parameters. Some of them (the electron densitry n, temperature T, and the magnetic field B) can be easily controlled. For electrons on helium, the Landau level broadening by the disorder potential $\gamma = (2/\pi\hbar^2)^{1/2}v/l$, can also be controlled independently. It follows from our results that, in the broadly investigated domain $\hbar\omega_c > kT > \hbar\gamma$, different regimes of the conductivity are determined by the **single parameter** γt_e, where the many-electron time $t_e \propto n^{-3/4}T^{-1/2}B^{1/2}$. In the strong-coupling regime $\gamma t_e \gg 1$, our results predict the occurrence of a new behavior of the conductivity, the peak of $\sigma(\omega)$ at a finite frequency $\omega \sim \gamma$. We also predict a very specific dependence of the static conductivity on the control parameters n, B, T, as specified below. All of these phenomena can be used to unambiguously detect the physical properties of the disordered many-electron system that we investigate.

The results obtained from the single-electron theory in chapter 4 and 5 with their many-electron modification in chapter 6 directly apply to electrons on helium.

Although the many-electron theory of the static conductivity for comparatively weak coupling has been fully confirmed by the experiment, so far only a limited number of experiments has been conducted in the range of strong coupling, or extremely strong magnetic fields, which is of primary interest for the present work. Much of the available data was interpreted in terms of the single-electron theory (SCBA) which, as we have shown, is inconsistent. We expect that new experiments on the static conductivity in low-density electron systems will reveal the many-electron effects that we predict. Particularly revealing would also be the frequency resolved experiments in low-density systems, either on helium or in semiconductor heterostructures.

A new type of feasible experiments that may be particularly revealing is the investigation of the magnetoconductivity at a given nonzero frequency ω as a function of the external magnetic field B. The corresponding representation of our results is given in Fig. 7.1 for the scaled conductivity $\sigma_*(B;\omega)$,

$$\sigma_* \equiv \sigma_*(B;\omega) = \left[\frac{B_0(\omega)}{B}\right]^{1/2} \frac{\tilde{\sigma}(\omega)}{\tilde{\sigma}(\gamma)}, \tag{7.1}$$

where the scaling factor $\tilde{\sigma}(\gamma) \approx 1.08$, and the scaling field $B_0(\omega)$ is defined by the equation $\gamma(B_0) = \omega$. The magnetoconductivity σ_{xx} is related to $\sigma_*(B;\omega)$ by a factor which is independent of B (but depends on ω),

$$\sigma_{xx}(\omega) = \frac{\tilde{\sigma}(\gamma)}{4\pi} \frac{\hbar}{k_B T} \frac{n e^2}{m\omega\tau_0} \sigma_*(B;\omega). \tag{7.2}$$

Here, $\tau_0^{-1} = mv^2/\hbar^3$ is the rate of electron scattering by the short-range potential (4.6)

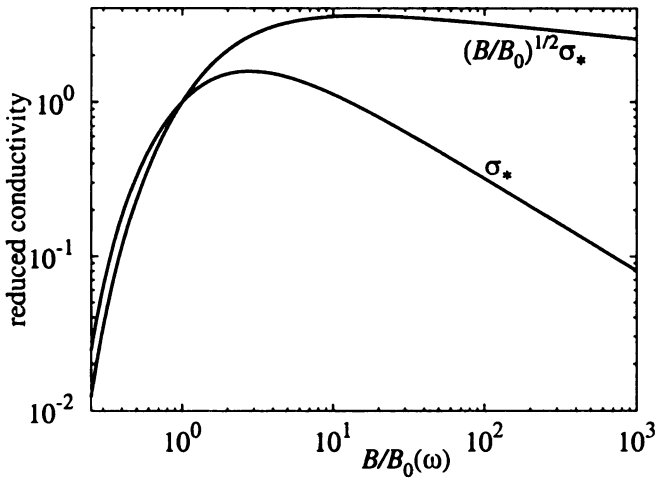

Figure 7.1: Reduced ac magnetoconductivity σ_* (7.1) at a nonzero frequency ω as a function of the reduced magnetic field $B/B_0(\omega) \propto B\,\omega^{-2}$. In order to demonstrate the anomalous single-electron behavior, σ_* is also plotted with an extra factor $(B/B_0)^{1/2}$. For large B, the single-electron conductivity displays scaling behavior, $B^{1/2}\sigma_* \propto B^{-\mu/2}$.

in the absence of the magnetic field. The frequency-dependent scaling field in Eq. (7.1) is related to ω and τ_0 by the expression $B_0(\omega) = \pi mc\tau_0\omega^2/2e$.

In the self-consistent Born approximation, the function $\sigma_*(B;\omega)$ decays with the increasing magnetic field as $B^{-1/2}$, for $B \gg B_0(\omega)$. With the localization effects taken into account, this dependence becomes steeper, with $B^{1/2}\sigma_* \propto B^{-\mu/2}$, as illustrated in Fig. 7.1.

The most restrictive limitation on the single-electron theory is imposed by many-electron effects. Even where the electrons do not form a Wigner crystal and the 2DES is nondegenerate, these effects can determine magnetotransport phenomena [111, 12]. Many electron effects strongly modify the behavior of both, low-frequency magnetoconductivity and cyclotron resonance absorption [112, 113]. However, for sufficiently strong magnetic fields, the effective coupling to a short-range disorder potential becomes in some sense stronger than the electron-electron interaction. Therefore the

single-electron approximation describes certain features of the magnetoconductivity for strong fields.

In particular, for strong coupling to short-range scatterers the full many-electron conductivity $\sigma_{xx}(\omega)$ is nonmonotonic. Observation of the peak of $\sigma_{xx}(\omega)$ and/or its counterpart in the magnetic field dependence of the weighted ac conductivity $B^{1/2}\sigma_{xx}(\omega)$ (cf. Fig. 7.1) would be a clear demonstration of single-electron localization effects in quantizing magnetic fields.

The ω-dependence of the low-frequency many-electron conductivity in the weak disorder regime $\gamma t_e < 1$, t_e being the many electron collision time, is significantly different. The magnetoconductivity σ_{xx} is *maximal* for $\omega = 0$ and decreases monotonically with the increasing ω, see Fig. 6.1.

Both regimes, the weak disorder regime and the strong coupling to scatterers, can be explored by increasing the magnetic field B, since γ and t_e increase with B. The obtained results strongly suggest new experiments in the low-density regime to explicitly observe the many-electron effects on the dynamical magnetoconductivity.

Chapter 8

Conclusion

In conclusion, we have analyzed the low-frequency single-electron magnetoconductivity and the single-electron cyclotron resonance absorption of a nondegenerate 2D electron liquid in quantizing magnetic field, well beyond the known SCBA results. We considered the experimentally important parameter range where the width of the Landau levels is less than temperature, so that all states within the lowest Landau level are equally populated. In this range, by combining the ideas of the scaling theory of the IQHE, the method of optimal fluctuation, and the method of spectral moments, we obtained highly accurate numerical results throughout the frequency domain where the conductivity displays peaks.

We found that, in contrast to the prediction of the SCBA or other mean-field theories [114], the low-frequency conductivity displays a peak at a *nonzero* frequency, as shown in Fig. 4.5. For short-range disorder, the position of the peak is given by $\omega_{\rm m} \approx 0.26\gamma$. For $\omega \to 0$, the single-electron conductivity displays a *universal* power-law dispersion $\sigma_{xx} \propto \omega^{\mu}$, which is related to the scaling behavior of the localization

length as a function of the distance in energy from the center of the disorder-broadened Landau level. On the other hand, the peak of the cyclotron resonance does not display such singular behavior and is not shifted away from ω_c, as seen from Fig. 5.2. Both peaks have Gaussian tails, with different exponents [see Eqns. (4.20), (5.15)].

The application of the single-electron theory is very much limited by many-electron effects. It was found that many electron effects strongly modify the low-frequency dynamical magnetoconductivity, even when the effective coupling to a short-range disorder potential becomes in some sense stronger than the electron-electron interaction.

In the developed theory, the dimensionless parameter γt_e, t_e being the many electron collision time, distinguishes between two different conductivity regimes. In the strong coupling regime, $\gamma t_e > 1$, the full many-electron dynamical conductivity $\sigma_{xx}(\omega)$ is nonmonotonic. This is directly a consequence of the localization effects of a random potential of defects which in the single-electron case would lead to a vanishing static conductivity. Yet for not too large γt_e, the static many-electron conductivity $\sigma_{xx}(0)$ is still of the same order as the single-electron SCBA conductivity $\sigma_{xx}^{\mathrm{SCBA}}(0) = 4ne^2\gamma l^2/3\pi k_B T$ [14]. This is a consequence of a comparatively large value of the exponent ν and the related steep frequency dependence of the single-electron conductivity (4.35) for $\omega \to 0$, see Fig. 4.5. However, for very large γt_e the ratio $\sigma_{xx}(0)/\sigma_{xx}^{\mathrm{SCBA}}(0)$ is small.

On the contrary, the ω-dependence of the low-frequency many-electron conductivity in the weak disorder regime, $\gamma t_e < 1$, is significantly different. The magnetoconductivity σ_{xx} is *maximal* for $\omega = 0$ and decreases monotonically with the increasing

ω, see Fig. 6.1. The characteristic width of the peak t_e^{-1} is given not by the rate of scattering by disorder (which is determined by γ), but by the many-electron time t_e. The tail of the peak is exponential in ω.

Appendices

Appendix A

Coherent states

The lowest Landau level subspace is endowed with a "chiral" structure, of which any state is represented by a linear combination of basis states like the ones in (2.17), meaning that only states with a negative angular momentum, $z^m = r^m e^{-im\varphi}$, $m \geq 0$, are present. Equivalently one can describe those state by $\mathbb{C}$-analytic functions. Here, the analytic structure of any such state is emphasized by writing

$$\psi \propto f(z) e^{-|z|^2/4l^2}, \tag{A.1}$$

where $f(z)$ is an arbitrary $\mathbb{C}$-analytic function. It is worth to study the aforementioned level degeneracy caused by the translational gauge invariance in the framework of canonical coherent states [115]. Since our focus lies on the properties of states within the LLL, we will drop the Landau level index, $|0; m\rangle \equiv |m\rangle$.

A state $|\alpha\rangle$ which is the result of the following operation is called a coherent state

$$|\alpha\rangle = T(\alpha)|0\rangle = e^{\alpha c^\dagger - \alpha^* c}|0\rangle \qquad \alpha \in \mathbb{C}\,.$$

We can rewrite the coherent state in terms of the eigenfunctions

$$\begin{aligned} |\alpha\rangle &= e^{\alpha c^\dagger - \alpha^* c}|0\rangle \\ &= e^{\alpha c^\dagger} e^{-\alpha^* c} e^{-\frac{|\alpha|^2}{2}[c,c^\dagger]}|0\rangle \\ &= e^{-\frac{|\alpha|^2}{2}} \sum_{n=0}^{\infty} \frac{\alpha^n}{n!}(c^\dagger)^n|0\rangle = e^{-\frac{|\alpha|^2}{2}} \sum_{n=0}^{\infty} \frac{\alpha^n}{\sqrt{n!}}|n\rangle. \end{aligned} \tag{A.2}$$

The probability of finding a state $|n\rangle$ in a coherent state $|\alpha\rangle$ is poisson distributed

$$|\langle n|\alpha\rangle|^2 = e^{-|\alpha|^2}\frac{|\alpha|^{2n}}{n!}\,.$$

Coherent states have the property to be minimal uncertainty states. It is equally well justified to represent the generated states $|n\rangle$ (2.13) by conjugate variables X, Y (2.12) as eigenfunctions of a harmonic oscillator. Notice however, the Hamiltonian (2.6) does not depend on those operators, thus

$$\begin{aligned} \psi_n(X) = \langle X|n\rangle &= \frac{(-i)^n}{\sqrt{\sqrt{\pi}2^n n! l}} H_n(X/l) e^{-X^2/2l^2} \\ \psi_n(Y) = \langle Y|n\rangle &= \frac{1}{\sqrt{\sqrt{\pi}2^n n! l}} H_n(Y/l) e^{-Y^2/2l^2}\,. \end{aligned}$$

To evaluate the function $\langle X|\alpha\rangle$ we use the the property that $|\alpha\rangle$ is an eigenfunction

of the annihilation operator c,

$$\begin{aligned} c|\alpha\rangle &= e^{-|\alpha|^2/2}\sum_{n=0}^{\infty}\frac{\alpha^n}{\sqrt{n!}}c|n\rangle \\ &= e^{-|\alpha|^2/2}\sum_{n=1}^{\infty}\frac{\alpha^n}{\sqrt{(n-1)!}}|n\rangle \\ &= \alpha e^{-|\alpha|^2/2}\sum_{n=0}^{\infty}\frac{\alpha^n}{\sqrt{n!}}|n\rangle = \alpha|\alpha\rangle\ . \end{aligned} \tag{A.3}$$

Using (2.11), (2.12) and $[X,Y] = il^2$, then Eq. (A.3) can be written as

$$\left(l^2\frac{\partial}{\partial X} + X\right)\langle X|\alpha\rangle = -l\sqrt{2}\alpha\langle X|\alpha\rangle,\ i\left(l^2\frac{\partial}{\partial Y} + Y\right)\langle Y|\alpha\rangle = l\sqrt{2}\alpha\langle Y|\alpha\rangle,$$

which immediately leads to the normalized solution for $\alpha = \alpha_1 + i\alpha_2$,

$$\langle X|\alpha\rangle = \frac{e^{-\alpha_2^2}}{\pi^{1/4}l^{1/2}}e^{-(X/l-\sqrt{2}\alpha)^2/2},\quad \langle Y|\alpha\rangle = \frac{e^{-\alpha_1^2}}{\pi^{1/4}l^{1/2}}e^{-(Y/l+i\sqrt{2}\alpha)^2/2}. \tag{A.4}$$

and verifies that the coherent state $|\alpha\rangle$ is a minimum-uncertainty state,

$$\langle\Delta X\rangle\langle\Delta Y\rangle = l^2/2.$$

It is also useful to obtain the real-space representation $\psi_\alpha(\mathbf{r})$ of $|\alpha\rangle$, using

$$\left(\frac{\bar{z}}{2} + 2l^2\frac{\partial}{\partial z}\right)\langle\mathbf{r}|\alpha\rangle = \sqrt{2}\alpha l\langle\mathbf{r}|\alpha\rangle,\quad \mathbf{r} = (x,y),$$

for which the normalized solution is found

$$\psi_\alpha(\mathbf{r}) = \frac{1}{l\sqrt{2\pi}} \exp[-(x - \sqrt{2}\alpha_1 l)^2/4l^2 - (y - \sqrt{2}\alpha_2 l)^2/4l^2 + \frac{i}{l\sqrt{2}}(x\alpha_2 - y\alpha_1)],$$

or equivalently for $\sqrt{2}\alpha l = x_0 + iy_0$ and $\mathbf{r}_0 = (x_0, y_0)$ we simply obtain

$$\psi_\alpha(\mathbf{r}) = \frac{1}{l\sqrt{2\pi}} \exp[-(\mathbf{r} - \mathbf{r_0})^2/4l^2 + i\mathbf{r} \wedge \mathbf{r_0}/2l^2] \,. \tag{A.5}$$

From the general point of a gauge transformation, it is easy to derive (A.5) without the use of coherent states. However, the coherent state formulation reveals easily the analytic structure of the LLL. As seen from (A.2) one can write

$$\psi(\alpha) \equiv \langle \alpha | \psi \rangle = e^{-|\alpha|^2/2} f(\alpha^*), \tag{A.6}$$

where $|\alpha\rangle$ is a coherent state and $f(\alpha^*)$ an $\mathbb{C}$-analytic function in α^*. Accordingly to (A.5), if we identify $z^*/l\sqrt{2} = \alpha$, then the analytic representation (A.1) is obtained. A few more remarks shall be made on the properties of coherent states. As evident from the continuous parameter $\alpha \in \mathbb{C}$ in contrast to the discreteness of the ladder operators $c, c^\dagger$, the set of coherent states has to be overcomplete, meaning

$$\int d\alpha |\alpha\rangle\langle\alpha| = \pi, \quad \langle\beta|\alpha\rangle = e^{-|\beta|^2/2 + \beta^*\alpha - |\alpha|^2/2}, \tag{A.7}$$

which clearly shows the lack of orthogonality among those states. A set of characteristic points $\alpha = \sqrt{\pi}(m + in)$, $m, n = 0, \pm 1, \pm 2, \ldots$, the von Neumann lattice [116],

may be chosen to eliminate the overcompleteness, yielding an infinitely discrete basis set of wavefunctions. Pictorially, this corresponds to localized states (A.5) with centers at $\mathbf{r}_0 = l\sqrt{2\pi}(m,n)$. Each state occupies the area $2\pi l^2$, the Landau- level degeneracy is $(2\pi l^2)^{-1}$.

Gauge transformation

The appearance of the gauge factor, $\exp[i\ \mathbf{r} \wedge \mathbf{r}_0]$, in (A.5) is the result of a gauge transformation in the vector potential $\mathbf{A}$,

$$\mathbf{A} \rightarrow \mathbf{A} + \nabla\Lambda \ \Rightarrow\ \psi \rightarrow \psi \exp[-i\frac{e}{\hbar}\Lambda]\ . \tag{A.8}$$

Certainly, $\psi(\mathbf{r}) \propto \exp[-(\mathbf{r}-\mathbf{r}_0)^2/4l^2]$ is a solution to H_0 (2.6) with $\mathbf{A} = B/2(y_0 - y, x - x_0, 0)$, then with (A.8) it readily follows that (A.5) is a solution to H_0 with $\mathbf{A} = B/2(-y, x, 0)$.

Appendix B

Kubo-conductivity of non-degenerate 2DES

The Kubo-conductivity for a system of non-degenerate electrons in the regime $\omega \ll \omega_c$ and $\beta\omega \ll 1$ was given in (4.1)

$$\sigma_{xx}(\omega) = \frac{ne^2\beta}{2m^2} \int_{-\infty}^{\infty} dt\, e^{i\omega t}\, \langle p_x(t) p_x(0) \rangle\,, \tag{B.1}$$

where $\mathbf{p} = (-i\hbar\nabla - (e/c)\mathbf{A})$ is the electron momentum operator in a magnetic field. In the single-electron approximation the time evolution of $\mathbf{p}(t)$ is guided by

$$\frac{d}{dt}\mathbf{p} = i\hbar^{-1}\,[H_0 + V(\mathbf{r}),\ \mathbf{p}], \quad H_0 = \frac{\mathbf{p}^2}{2m}, \tag{B.2}$$

where $V(\mathbf{r})$ is the time independend scattering potential. We define the Landau level raising and lowering operators

$$[p_-, p_+] = 1, \quad p_\pm = (p_x \mp i\kappa p_y)/\sqrt{2\hbar m\omega_c},$$

where $\kappa = eB_z/m\omega_c = \pm 1$. In the absence of defects the electron Hamiltonian is then

$$H_0 = \hbar\omega_c(p_+p_- + \frac{1}{2}).$$

Further we define the guiding center algebra

$$X = x + \frac{\kappa p_y}{m\omega_c}, \quad Y = y - \frac{\kappa p_x}{m\omega_c}, \quad q_\pm = \frac{q_x \mp i\kappa q_y}{\sqrt{2}},$$

with commutation relations $[X, Y] = -i\kappa l^2$ and $[\mathbf{R}, \mathbf{p}] = 0$ where $\mathbf{R} = (X, Y)$. Now $V(\mathbf{r})$ can be expanded in a Fourier series

$$\begin{aligned} V(\mathbf{r}) &= \sum_{\mathbf{q}} V_{\mathbf{q}} e^{i\mathbf{qr}} = \sum_{\mathbf{q}} V_{\mathbf{q}} \exp[i\mathbf{qR} + l(q_-p_+ - q_+p_-)] \\ &= \sum_{\mathbf{q}} V_{\mathbf{q}} \exp[i\mathbf{qR} - q^2l^2/4] e^{l\,q_-p_+}\, e^{-l\,q_+p_-}. \end{aligned} \tag{B.3}$$

To evaluate equation (B.2) it is advantagous to use the relation $[p_\pm, e^{i\mathbf{qr}}] = lq_\pm e^{i\mathbf{qr}}$ readily seen from (B.3), thus leading to

$$\begin{aligned}
\frac{d}{dt}p_x &= \kappa\omega_c p_y - i\sum_{\mathbf{q}} q_x V_{\mathbf{q}} e^{i\mathbf{qr}} = \kappa\omega_c p_y - \frac{\partial}{\partial x}V(\mathbf{r}), \\
\frac{d}{dt}p_y &= -\kappa\omega_c p_x - i\sum_{\mathbf{q}} q_y V_{\mathbf{q}} e^{i\mathbf{qr}} = -\kappa\omega_c p_x - \frac{\partial}{\partial y}V(\mathbf{r}).
\end{aligned} \tag{B.4}$$

With the modest assumption that the momentum correlator asymptotically decouples $\langle p_x(t)p_x(0)\rangle \to 0$ for $t \to \infty$, we can use

$$\begin{aligned}
\langle \frac{d}{dt}p_x(t)p_x(0)\rangle_\omega &= \int_{-\infty}^{\infty} dt\; e^{i\omega t}\langle \frac{d}{dt}p_x(t)p_x(0)\rangle \\
&= -i\omega \int_{-\infty}^{\infty} dt\; e^{i\omega t}\langle p_x(t)p_x(0)\rangle = -i\omega\langle p_x(t)p_x(0)\rangle_\omega,
\end{aligned} \tag{B.5}$$

and rewrite (B.4) as

$$\begin{aligned}
i\omega\langle p_x(t)p_x(0)\rangle_\omega &= -\kappa\omega_c\langle p_y(t)p_x(0)\rangle_\omega + \langle \frac{\partial}{\partial x}V(\mathbf{r})p_x(0)\rangle_\omega, \\
i\omega\langle p_y(t)p_x(0)\rangle_\omega &= \kappa\omega_c\langle p_x(t)p_x(0)\rangle_\omega + \langle \frac{\partial}{\partial y}V(\mathbf{r})p_x(0)\rangle_\omega.
\end{aligned} \tag{B.6}$$

Equations (B.6) can easily be decoupled leading to

$$\left[1-\left(\frac{\omega}{\omega_c}\right)^2\right]\langle p_x(t)p_x(0)\rangle_\omega = \\ -\frac{\kappa}{\omega_c}\langle\frac{\partial}{\partial y}V(\mathbf{r}(t))p_x(0)\rangle_\omega + i\frac{\omega}{\omega_c^2}\langle\frac{\partial}{\partial x}V(\mathbf{r}(t))p_x(0)\rangle_\omega, \tag{B.7}$$

in the limit $\frac{\omega}{\omega_c}\to 0$ we may identify p_x with

$$p_x(t) = -\frac{\kappa}{\omega_c}\frac{\partial}{\partial y}V(\mathbf{r}(t)) = -i\frac{\kappa}{\omega_c}\sum_{\mathbf{q}} q_y V_{\mathbf{q}} e^{i\mathbf{qr}}. \tag{B.8}$$

We also note that the time evolution of the guiding center $\mathbf{R}(t)$ is determined by

$$\begin{aligned}\dot{X} &= i\hbar^{-1}[H,X] = -i\kappa\frac{l^2}{\hbar}\sum_{\mathbf{q}} q_y V_{\mathbf{q}} e^{i\mathbf{qr}},\\ \dot{Y} &= i\hbar^{-1}[H,Y] = i\kappa\frac{l^2}{\hbar}\sum_{\mathbf{q}} q_x V_{\mathbf{q}} e^{i\mathbf{qr}},\end{aligned} \tag{B.9}$$

where the commutation relation $[X,Y] = -i\kappa l^2$ has been used. From (B.9) and (B.8) we conclude, $p_x(t) = m\dot{X}(t)$, similarily the relation holds for $p_y(t) = m\dot{Y}(t)$. The conductivity $\sigma(\omega)$ is an averaged quantitiy which is spatially uniform, $\langle j_x(t)j_x(0)\rangle_\omega = \langle j_y(t)j_y(0)\rangle_\omega$. We obtain the Kubo-conductivity for $\omega \ll \omega_c$, $\beta\omega \ll 1$:

$$\sigma_{xx}(\omega) = \frac{ne^2\beta}{4}\int_{-\infty}^{\infty} dt\, e^{i\omega t}\,\mathrm{Tr}\Big\{\overline{\dot{\mathbf{R}}(t)\cdot\dot{\mathbf{R}}(0)}\Big\}. \tag{B.10}$$

The trace in (B.10) is understood as a trace over the Landau level index as well as the position degeneracy of the orbit centers. The trace over the Landau level index is

taken before averaging over the random potential is carried out upon which the left trace over the orbit centers will be trivial. Essentially we have to consider

$$\xi_N(\mathbf{q},\mathbf{q}',\omega) = \int_{-\infty}^{\infty} dt\; e^{i\omega t} \;\times \sum_M \langle N|e^{i\mathbf{q}\,\mathbf{r}(t)}|M\rangle\langle M|e^{i\mathbf{q}'\,\mathbf{r}(0)}|N\rangle, \tag{B.11}$$

where

$$\int_{-\infty}^{\infty} dt\; e^{i\omega t} \left\langle \dot{\mathbf{R}}(t)\cdot\dot{\mathbf{R}}(0)\right\rangle \propto \sum_N e^{-\beta E_N}\mathrm{Tr}\Big\{\overline{\sum_{\mathbf{q},\mathbf{q}'} V_{\mathbf{q}}V_{\mathbf{q}'}\;(\mathbf{q}\mathbf{q}')\;\xi_N(\mathbf{q},\mathbf{q}',\omega)}\Big\}.$$

Here, $|N\rangle$ denotes only the Landau level index and E_N its engery. For quantizing magnetic fields $k_BT \ll \hbar\omega_c$, we may assume that only LLL-states $|0\rangle$ are occupied, then the thermal averaging in (B.10) is easily achieved by projecting the correlation function onto the LLL, $|N=0\rangle$ in (B.11).

The fast cyclotron motion is described by the ladder operators $p_\alpha(t)$, $\alpha = \pm 1$. Time evolution is guided by (B.4),

$$\frac{d}{dt}\,p_\alpha(t) = \alpha i\omega_c p_\alpha(t) - l\hbar^{-1}\sum_{\mathbf{q}} q_\alpha V_{\mathbf{q}} e^{i\mathbf{q}\mathbf{r}(t)}. \tag{B.12}$$

If we consider the case $\gamma \ll \omega_c$ we may effectively decouple p_α from the slow motion of the orbit centers $\mathbf{R}$ (adiabatic approach), then $p_\alpha(t) = p_\alpha \exp(\alpha i\omega_c t)$. The matrix element $\langle N|\exp[i\mathbf{q}\mathbf{r}(t)]|M\rangle \propto \exp(i(N-M)\omega_c t)$ contains a highly oscillating factor

for $M \neq N$, therefore we need only to consider the Landau level transition amplitudes of the form

$$\langle N|e^{i\mathbf{q}\mathbf{r}(t)}|N\rangle = L_N(\frac{l^2q^2}{2})e^{-l^2q^2/4}\exp[i\mathbf{q}\mathbf{R}(t)], \tag{B.13}$$

where $L_N(x)$ is the Laguerre polynomial of degree N. As follows easily with (B.13), the correlator (B.11) can be written as

$$\begin{aligned}\xi_N(\mathbf{q},\mathbf{q}',\omega) &= \int_{-\infty}^{\infty} dt\, e^{i\omega t}\, L_N(\frac{l^2q^2}{2})L_N(\frac{l^2q'^2}{2}) \times \\ &\exp[i\mathbf{q}\mathbf{R}(t)]\exp[i\mathbf{q}'\mathbf{R}(0)]\, e^{-l^2(q^2+q'^2)/4},\end{aligned} \tag{B.14}$$

where the time evolution of $\mathbf{R}$ is guided by the onto the N-th Landau level projected Hamiltonian,

$$\tilde{V}^{(N)}(\mathbf{r}) \equiv P_N\, V(\mathbf{r}) P_N = \hbar\gamma\, P_N \sum_{\mathbf{q}} \tilde{V}_{\mathbf{q}}^{(N)} e^{i\mathbf{q}\mathbf{R}}, \tag{B.15}$$

$$\tilde{V}_{\mathbf{q}}^{(N)} = (V_q/\hbar\gamma)\, L_N(q^2\, l^2/2)\exp(-q^2l^2/4). \tag{B.16}$$

In quanziting magnetic fields, $k_BT \ll \hbar\omega_c$, the low-frequency conductivity $\sigma_{xx}(\omega)$ $\omega \ll \omega_c$, is determined by transition of states within the lowest Landau level. Therefore, the low-frequency correlator simply is

$$\begin{aligned}\xi_0(\mathbf{q},\mathbf{q}',\omega) &= \int_{-\infty}^{\infty} dt\, e^{i\omega t} \times \\ &\exp[i\mathbf{q}\mathbf{R}(t)]\exp[i\mathbf{q}'\mathbf{R}(0)]\, e^{-l^2(q^2+q'^2)/4},\end{aligned} \tag{B.17}$$

where the time evolution of $\mathbf{R}$ is guided by the projected Hamiltonian, $H = \sum_{\mathbf{q}} \tilde{V}_{\mathbf{q}} \exp[i\mathbf{q}\mathbf{R}]$. Finally the reduced conductivity $\tilde{\sigma}$, (4.10), follows easily from (B.10) and (B.17).

Appendix C

Diagonalization technique

We consider the integral with a real and antisymmetric matrix a_{kl}

$$\int_{-\infty}^{\infty} d\mathbf{q}_1 \cdots d\mathbf{q}_n \; \mathbf{q}_1 \mathbf{q}_j \exp(-\frac{1}{2}\sum_{k=1}^{n} q_k^2 + \frac{1}{2} i \sum_{k,l=1}^{n} a_{kl}\, \mathbf{q}_k \wedge \mathbf{q}_l). \tag{C.1}$$

The integration for each variable $\mathbf{q}$ with its two components, $dq_x dq_y$, is performed over the entire infinite plane. Integral (C.1) is a quadratic form in $\mathbf{q}$, which is solved by diagonalization. By changing variables $q_\pm = (q_x \mp i q_y)/\sqrt{2}$ the integration is done by

$$\int d\mathbf{q} = \int dq_x dq_y \to \int dq_+ dq_-.$$

Using vectors $\mathbf{Q}_\pm$ and matrices $\tilde{\mathbf{A}}, \tilde{\mathbf{E}}, \tilde{\mathbf{M}}$, with components

$$(\mathbf{Q}_+)_k = q_{+_k},\ (\mathbf{Q}_-)_k = q_{-_k},$$

$$\tilde{\mathbf{A}}_{kl} = ia_{kl},\ \tilde{\mathbf{E}}_{kl} = \delta_{k,l},\ \tilde{\mathbf{M}}_{kl} = \delta_{k,1}\delta_{l,j},$$

integral (C.1) is easily written as

$$\int dq_{+_1} \cdots dq_{+_n} dq_{-_1} \cdots dq_{-_n} \, (\mathbf{Q}_+^\dagger \mathbf{M} \mathbf{Q}_+ + \mathbf{Q}_-^\dagger \mathbf{M} \mathbf{Q}_-) \times$$
$$\exp(-\frac{1}{2}\mathbf{Q}_+^\dagger(\tilde{\mathbf{E}} - i\tilde{\mathbf{A}})\mathbf{Q}_+) \exp(-\frac{1}{2}\mathbf{Q}_-^\dagger(\tilde{\mathbf{E}} + i\tilde{\mathbf{A}})\mathbf{Q}_-). \tag{C.2}$$

The coefficient matrix a_{kl} is real and antisymmetric, thus $\tilde{\mathbf{A}}$ is hermitian and can easily be diagonalized,

$$\tilde{\mathbf{U}}\tilde{\mathbf{A}}\tilde{\mathbf{U}}^\dagger = \tilde{\mathbf{D}},\ \mathbf{T} = \tilde{\mathbf{U}}\mathbf{Q}_+,\ \mathbf{V} = \tilde{\mathbf{U}}\mathbf{Q}_-, \tag{C.3}$$

where $\tilde{\mathbf{U}}$ is the unitary transformation matrix and $\tilde{\mathbf{D}}$ the diagonal matrix with real entries λ_k. Integral (C.2) can be transformed into

$$\int dt_1 \cdots dt_n dv_1 \cdots dv_n (\mathbf{T}^\dagger \tilde{\mathbf{U}} \tilde{\mathbf{M}} \tilde{\mathbf{U}}^\dagger \mathbf{T} + \mathbf{V}^\dagger \tilde{\mathbf{U}} \tilde{\mathbf{M}} \tilde{\mathbf{U}}^\dagger \mathbf{V}) \times$$
$$\exp(-\frac{1}{2}\mathbf{T}^\dagger\mathbf{T} + \frac{1}{2}i\mathbf{T}^\dagger\tilde{\mathbf{D}}\mathbf{T}) \exp(-\frac{1}{2}\mathbf{V}^\dagger\mathbf{V} - \frac{1}{2}i\mathbf{V}^\dagger\tilde{\mathbf{D}}\mathbf{V}). \tag{C.4}$$

Here, we used the fact that the Jacobian of any unitary transformation is one. Further,

$$\mathbf{T}^{\dagger}\tilde{\mathbf{U}}\tilde{\mathbf{M}}\tilde{\mathbf{U}}^{\dagger}\mathbf{T} = t_k^* u_{k,1} u_{l,j}^* t_l \,,\ \mathbf{T}_l = t_l \,,\ \tilde{\mathbf{U}}_{k,l} = u_{k,l},$$

a similar expression holds for $\mathbf{V}$ in (C.4). Since t_k and v_k are independed complex variables the necessary condition for (C.4) not to vanish is that $k = l$, thus leading to

$$\int dt_1 \cdots dt_n dv_1 \cdots dv_n (|t_k|^2 + |v_k|^2) u_{k,1} u_{k,j}^* \times$$
$$\exp(-\frac{1}{2}|t_k|^2(1 + i\lambda_k)) \exp(-\frac{1}{2}|v_k|^2(1 - i\lambda_k)). \tag{C.5}$$

Finally, integral (C.5) is readily integrated,

$$(2\pi)^n \prod_{k=1}^{n} (1 + \lambda_k^2)^{-1/2} \sum_{l=1}^{n} 2 \frac{u_{l,1} u_{l,j}^*}{1 + \lambda_l^2}. \tag{C.6}$$

Appendix D

Optimal potential configuration

The asymptotic ($\gamma \ll \omega \ll \omega_c$) conductivity $\sigma(\omega)$ is determined by transitions between exponentially rare, spatially close pairs of states with the energy separation ω. In functional form the conductivity is

$$\begin{aligned} \tilde{\sigma}(\omega) &= \frac{4\pi l^2}{\hbar^2 \gamma} \frac{1}{Z} \int DV(\mathbf{r}) \exp(-R[V]) \times \\ &\quad \delta(E_t - E_b - \omega) |\langle \psi_t | \nabla V | \psi_b \rangle|^2 , \end{aligned} \tag{D.1}$$

where ψ_t (t = top) denotes bound state with the largest energy E_t, whereas ψ_b (b= bottom) denotes the one with the lowest energy E_b. The fluctuational weight for a δ-correlated gaussion potential has the form

$$R[V] = \int \frac{V^2(\mathbf{r})}{2v^2} d\mathbf{r} . \tag{D.2}$$

The wavefunctions ψ_t, ψ_b are within the LLL, *i.e.*, in the circular gauge they can be written as $P(z)\exp(-|z|^2/4)$, where $P(z)$ is an arbitrary polynomial and $z = x - iy$. The δ-function with the help of a Lagrange multiplier as well as the overlap prefactor in (D.1) can be incorporated into the exponent using the auxiliary functional,

$$\begin{aligned}\tilde{R}[V] &= \int \frac{V^2(\mathbf{r})}{2v^2} d\mathbf{r} + \lambda\omega - 2\ln\left|\int \psi_t^* \nabla V(\mathbf{r}) \psi_b \, d\mathbf{r}\right| - \\ &\lambda \iint \left(\psi_t^*(\mathbf{r}) - \psi_b^*(\mathbf{r})\right) \tilde{V}(\mathbf{r};\, \mathbf{r}') \left(\psi_t(\mathbf{r}') + \psi_b(\mathbf{r}')\right) d\mathbf{r} d\mathbf{r}',\end{aligned} \tag{D.3}$$

where $\tilde{V}$ is the projected potential (B.16) and $\psi_{t,b}$ are eigenfunctions within the LLL, $\tilde{V}\psi_{t,b} = E_{t,b}\,\psi_{t,b}$. The optimal fluctuation $V_{\rm opt}$ is found by

$$\begin{aligned}\frac{\delta \tilde{R}}{\delta V(\mathbf{r})} = 0 \;\rightarrow\; \frac{V_{\rm opt}(\mathbf{r})}{v^2} &= \lambda\left(|\psi_t|^2 - |\psi_b|^2\right) + \\ &\frac{1}{\left|\int V(\mathbf{r}) \nabla\left(\psi_t^* \psi_b\right) \, d\mathbf{r}\right|^2} \frac{\delta}{\delta V(\mathbf{r})} \left|\int V(\mathbf{r}) \nabla\left(\psi_t^* \psi_b\right) \, d\mathbf{r}\right|^2,\end{aligned} \tag{D.4}$$

from which follows that $V_{\rm opt}$ may be expanded into a product of LLL basis wavefunctions ϕ_m,

$$V_{\rm opt}(\mathbf{r}) = \sum_{m,n} u_{mn} \phi_m^*(\mathbf{r}) \phi_n(\mathbf{r}). \tag{D.5}$$

The solution to (D.4) in general is not amenable to analytic techniques. However, from general arguments we can assume that $V_{\rm opt}$ is realized by an antisymmetric

potential $V(\mathbf{r}) = -V(-\mathbf{r})$. With constraints imposed upon u_{mn} (D.5) numerical results can be obtained which strongly support the following picture for the limit $\omega/\gamma \gg 1$: The overlap term $\propto \psi_t^* \psi_b$ remains small and the major contribution comes from the fluctuational weight to localize the states, therefore the scaling $\lambda \propto \omega$ holds. Though it seems, that the overlap term can be completely neglected in this limit, its influence on the solution V_{opt} is more subtle. In genral, lowest Landau level states in an antisymmetric potential $V(\mathbf{r}) = -V(-\mathbf{r})$ may be represented by

$$\begin{aligned} \psi_t(\mathbf{r}) &= f(z - z_0) \exp(-|z - z_0|^2/4l^2 + i/2\ \mathbf{r} \wedge \mathbf{r}_0), \\ \psi_b(\mathbf{r}) &= f(-z - z_0) \exp(-|z + z_0|^2/4l^2 - i/2\ \mathbf{r} \wedge \mathbf{r}_0), \end{aligned} \tag{D.6}$$

where f is analytic in $z = x - iy$ and $z_0 = x_0 - iy_0$, the further, $\mathbf{r} = (x, y)$, $\mathbf{r}_0 = (x_0, y_0)$, (these wavefunctions actually solve the SE $(-i\nabla + e/2\ \mathbf{B} \times \mathbf{r})^2/2m\ \psi = \omega_c/2\ \psi$). Thus, we simply can state $\psi_t(\mathbf{r}) = \psi_b(-\mathbf{r})$ as a general property of lowest Landau level wavefunctions in any antisysmmetry potential $V(\mathbf{r})$. If we were to neglect the overlap integral in (D.4), then the much simplier result would apply,

$$V_{\text{opt}} = v^2 \lambda \left(|\psi_t|^2 - |\psi_b|^2 \right). \tag{D.7}$$

To lowest order in perturbation theory we find,

$$\begin{aligned} \omega = E_t - E_b &= v^2\lambda \int (|\psi_t|^2 - |\psi_b|^2)^2 \, d\mathbf{r} + \\ &= 2v^2\lambda \left(A - \int |\psi_t|^2 |\psi_b|^2 \, d\mathbf{r} \right), \end{aligned} \tag{D.8}$$

with $A = \int |\psi_t|^4 d\mathbf{r} = \int |\psi_b|^4 d\mathbf{r}$, the *inverse participation number.* Clearly, from (D.8), (D.7) it follows

$$R[V_{\text{opt}}] = \frac{\omega^2}{4v^2} \left(A - \int |\psi_t|^2 |\psi_b|^2 \, d\mathbf{r} \right)^{-1}. \tag{D.9}$$

The global minimum of (D.9) is reached for a maximum A with zero overlap between the wavefunction ψ_t and ψ_b. A simple scaling argument allows us to identify the maximum value of A,

$$\psi \propto \frac{1}{\sqrt{S}} \;\Rightarrow\; A = \int |\psi|^4 d\mathbf{r} \propto \frac{1}{S}. \tag{D.10}$$

The most "localized" state in the lowest Landau level is the wavefunction (D.6) with $f = (2\pi)^{-1/2}$. The minimal overlap requirement is fulfilled when $r_0 \to \infty$, thus giving the value $\exp(-R) = \exp(-2\omega^2/\gamma^2)$ found in (4.20). For large ω/γ the small correction to R (D.4) from the overlap $|\langle \psi_t | \nabla V | \psi_b \rangle|$ moves the global minimum of R to a finite interpotential distance $2\mathbf{r}_0$. The overall shape of potential and the wavefunctions ψ_t and ψ_b is barely perturbed. Numerically we find confirmation for this behavior, see Appendix E. Accordingly, a direct variational method with $V_{\text{opt}} \propto$

$-V_{-E}(\mathbf{r}-\mathbf{r_0}) - V_E(\mathbf{r}+\mathbf{r_0})$ as in (D.7) can be used to find the optimal distance $\mathbf{r}_0$ and the overlap parameter $K = \exp(-r_0^2/l^2)$. We find the functional $\tilde{R}$ (D.3) as a function of the interpotential distance r_0

$$\tilde{R}(r_0) = 2(\omega/\gamma)^2\left(1+e^{-r_0^2/l^2}\right) + 2\frac{r_0^2}{l^2} - \ln\left(\left(\frac{\hbar\omega}{l}\right)^2 \frac{r_0^2}{l^2}\right). \qquad \text{(D.11)}$$

The optimal distance is $r_0 = l\sqrt{\ln(\omega/\gamma)^2}$ where (D.11) is only valid for $r_0/l \gg 1$.

Appendix E

Finding numerically the optimal potential

We will numerically find the antisymmetric *optimal* potential, $V(\mathbf{r}) = -V(-\mathbf{r})$, which minimizes

$$\tilde{\mathcal{R}}[V] = \frac{1}{2v^2} \int V^2 \, d\mathbf{r} - \lambda(E_t[V] - E_b[V] - \omega) - \ln\left(\int \frac{\partial V}{\partial x} \psi_t^* \psi_b \, d\mathbf{r}\right)^2 , \qquad \text{(E.1)}$$

where $E_t[V] - E_b[V] = \omega$, is the constrained energy difference between the top and bottom-level eigenstates. Necessary condition for the minimum is

$$\frac{\delta \tilde{\mathcal{R}}}{\delta V(\mathbf{r})} = 0 \;\Rightarrow\; \frac{V(\mathbf{r})}{v^2} = \lambda(|\psi_t(\mathbf{r})|^2 - |\psi_b(\mathbf{r})|^2) + \frac{2}{\int \frac{\partial V}{\partial x} \psi_t^* \psi_b \, d\mathbf{r}} \frac{\delta}{\delta V(\mathbf{r})} \int \frac{\partial V}{\partial x} \psi_t^* \psi_b \, d\mathbf{r}. \qquad \text{(E.2)}$$

Applying the scaling relation, $V(\mathbf{r}) = vU(\mathbf{r})$, we may solve for

$$U(\mathbf{r}) = v\lambda(|\psi_t(\mathbf{r})|^2 - |\psi_b(\mathbf{r})|^2) + \frac{2}{\int \frac{\partial U}{\partial x}\psi_t^*\psi_b \, d\mathbf{r}} \frac{\delta}{\delta U(\mathbf{r})} \int \frac{\partial U}{\partial x}\psi_t^*\psi_b \, d\mathbf{r}, \qquad \text{(E.3)}$$

as well, such that

$$\tilde{\mathcal{R}}[V] = \frac{1}{2}\int U^2 \, d\mathbf{r} - \ln\left(\int \frac{\partial U}{\partial x}\psi_t^*\psi_b \, d\mathbf{r}\right)^2 - \ln v^2 \,, \quad \int U(\mathbf{r})|\psi_t(\mathbf{r})|^2 \, d\mathbf{r} \; = \frac{\omega}{2v} = E_t. \qquad \text{(E.4)}$$

For convenience we may now choose $v = 1$, in which case $\omega' = \omega/v$ and $\lambda' = v\lambda$ coincide. In summary, we have to minimize the constrained functional

$$\tilde{\mathcal{R}}[U] = \frac{1}{2}\int U^2 \, d\mathbf{r} - \lambda'(E_t[U] - E_b[U] - \omega') - \ln\left(\int \frac{\partial U}{\partial x}\psi_t^*\psi_b \, d\mathbf{r}\right)^2 , \qquad \text{(E.5)}$$

where $E_t[U] - E_b[U] = \omega'$. We can simplify the notation in our problem of an antisymmetric potential, $E = E_t[U] = \langle\psi_t|U|\psi_t\rangle$ and $-E = E_b[U] = \langle\psi_b|U|\psi_b\rangle$. The minimization procedure applicable to (E.5) will be briefly outlined here.

We will seek the solution to (E.3) by the application of a conjugate gradient method. The formulation of an unconstrained problem is advantageous for the use of such method. We notice that $\omega'/2E$ is the proper scale factor for $U(\mathbf{r})$, as seen from (E.4), therefore

$$\tilde{\mathcal{R}}[U] = \frac{\omega'^2}{4E^2}\int \frac{U^2}{2} \, d\mathbf{r} - \ln\left(\frac{\omega'}{2E}\int \frac{\partial U}{\partial x}\psi_t^*\psi_b \, d\mathbf{r}\right)^2 , \qquad \text{(E.6)}$$

constitutes our *basic* unconstraint functional equation. As can be shown, the minimal solution to (E.6) coincides with the solution to (E.3)

Upon having obtained a numerically close solution by a conjugate gradient method, we will solve for the optimal potential $U(\mathbf{r})$ to any arbitrary accuracy by iterating equation (E.3). Here, it shall be remarked that this procedure will converge *superlinearly.*

E.1 Formulas for the conjugate gradient method

Let us work in the symmetric gauge, $H_0 = (-i\nabla + \frac{m\omega_c}{2}\mathbf{e}_z \times \mathbf{r})^2/2m$, where ω_c is the cyclotron frequency, eB/m, $-e$ the electron charge. The angular momentum wave functions (WF) of the LLL are $\psi_k(\mathbf{r}) = (2^{k+1}\pi k!)^{-1/2} r^k \exp[-r^2/4 - i\varphi k]$, $k \geq 0$. We may expand $U(\mathbf{r})$ in the form $U(\mathbf{r}) = \sum_{m,n} u_{m,n}\psi_m^*\psi_n$, (E.3). Since $U(\mathbf{r})$ is real and antisymmetric we have $u_{m,n} = u_{n,m}^*$ and $u_{m,n} = 0$ when $n - m$ is even. Using

$$\int \psi_m^*\psi_j^*\psi_n\psi_l \, d\mathbf{r} = \delta_{m+j-n-l} \, \frac{1}{4\pi} \, 2^{-m-j} \sqrt{\binom{m+j}{j}} \sqrt{\binom{m+j}{l}}, \quad m, j, n, l \geq 0 \tag{E.7}$$

we obtain for

$$\int \frac{U^2}{2} \, d\mathbf{r} = \frac{1}{4\pi} \sum_{\substack{n>m\geq 0, \\ n-m \text{ odd}, \\ j=0}}^{\infty} 2^{-n-j} \sqrt{\binom{n+j}{j}} \sqrt{\binom{n+j}{m}} \, \mathrm{Re}\left\{u_{m,n}u_{j,n-m+j}^*\right\} \tag{E.8}$$

the *logarithmic weight* of a potential fluctuation. To solve for eigenstates, we need the Hamiltonian of the projected potential, $H_I = \sum_{j,l} |\psi_j\rangle U_{j,l} \langle\psi_l|$, where

$$U_{j,l} = \langle\psi_j|U|\psi_l\rangle = \begin{cases} 0 & j-l \text{ even} \\ \frac{1}{4\pi} \sum_{m=0}^{\infty} 2^{-m-j} \sqrt{\binom{m+j}{j}} \sqrt{\binom{m+j}{l}}\, u_{m,m+j-l} & j > l \end{cases} \tag{E.9}$$

The matrix U_{jl} is hermitian, $U_{jl} = U_{lj}^*$. Further, we need to handle the expression for the overlap integral, the top- and bottom level wavefunctions are related with each other by $\psi(\mathbf{r}) = \sum_j c_j \psi_j = \psi_t(\mathbf{r}) = \psi_b(-\mathbf{r})$, giving

$$\begin{aligned} \langle\psi_t|\partial_x U|\psi_b\rangle &= -\langle\partial_x\psi_t|U|\psi_b\rangle - \langle\psi_t|U|\partial_x\psi_b\rangle \\ &= -\sum_{j,m,n,l=0}^{\infty} \int c_j^* \, (\partial_x\psi_j^*)\psi_m^* u_{m,n} \psi_n \psi_l \, (-1)^l c_l \, d\mathbf{r} \\ &\quad -\sum_{j,m,n,l=0}^{\infty} \int c_j^* \, \psi_j^* \psi_m^* u_{m,n} \psi_n (\partial_x\psi_l) \, (-1)^l c_l \, d\mathbf{r}. \end{aligned} \tag{E.10}$$

We notice that we can rewrite the wavefunction $\psi_k(\mathbf{r}) = (2^{k+1}\pi k!)^{-1/2} z^k \exp[-z\bar{z}/4]$, where $z = x - iy$. The partial derivative then simply reads, $\partial_x = \partial_z + \partial_{\bar{z}}$, therefore

$$\begin{aligned} (\partial_x\psi_j^*)\psi_l &= \sqrt{\frac{j}{2}}\psi_{j-1}^*\psi_l - \frac{1}{2}\sqrt{\frac{j+1}{2}}\psi_{j+1}^*\psi_l - \frac{1}{2}\sqrt{\frac{l+1}{2}}\psi_j^*\psi_{l+1}, \\ \psi_j^*\partial_x\psi_l &= \sqrt{\frac{l}{2}}\psi_j^*\psi_{l-1} - \frac{1}{2}\sqrt{\frac{l+1}{2}}\psi_j^*\psi_{l+1} - \frac{1}{2}\sqrt{\frac{j+1}{2}}\psi_{j+1}^*\psi_l. \end{aligned}$$

Then (E.10) simply is

$$\langle \partial_x \psi_t | U | \psi_b \rangle =$$
$$\sum_{j,l=0}^{\infty} \left(\sqrt{\frac{j+1}{2}} c_{j+1}^* U_{j,l} - \frac{1}{2} \sqrt{\frac{j+1}{2}} c_j^* U_{j+1,l} - \frac{1}{2} c_j^* U_{j,l+1} \sqrt{\frac{l+1}{2}} \right) (-1)^l c_l,$$
$$\langle \psi_t | U | \partial_x \psi_b \rangle =$$
$$\sum_{j,l=0}^{\infty} c_j^* \left(-U_{j,l} \sqrt{\frac{l+1}{2}} c_{l+1} - \frac{1}{2} U_{j,l+1} \sqrt{\frac{l+1}{2}} c_l - \frac{1}{2} \sqrt{\frac{j+1}{2}} U_{j+1,l} c_l \right) (-1)^l.$$

Now, using the property that $\mathbf{c}$ is an eigenvector of $(U_{j,l})$

$$\sum_{j=0}^{\infty} c_j^* U_{j,l} = E\, c_l^*, \quad \sum_{l=0}^{\infty} U_{j,l} (-1)^l c_l = -E\, (-1)^j c_j,$$

we arrive at the following equations

$$\langle \partial_x \psi_t | U | \psi_b \rangle = \frac{E}{2} \sum_{j=0}^{\infty} (-1)^j \sqrt{\frac{j+1}{2}} \left(-2 c_{j+1}^* c_j - c_j^* c_{j+1} - c_{j+1}^* c_j \right),$$
$$\langle \psi_t | U | \partial_x \psi_b \rangle = \frac{E}{2} \sum_{j=0}^{\infty} (-1)^j \sqrt{\frac{j+1}{2}} \left(-2 c_{j+1} c_j^* - c_j c_{j+1}^* - c_{j+1} c_j^* \right).$$

In summary we find

$$\int \frac{\partial U}{\partial x} \psi_t^* \psi_b \, d\mathbf{r} = 2\sqrt{2} E \sum_{j=0}^{\infty} (-1)^j \sqrt{j+1}\, \mathrm{Re} \left\{ c_j c_{j+1}^* \right\}, \tag{E.11}$$

similarily

$$\int \frac{\partial U}{\partial y} \psi_t^* \psi_b \, d\mathbf{r} = 2\sqrt{2} E \sum_{j=0}^{\infty} (-1)^j \sqrt{j+1}\, \mathrm{Im} \left\{ c_j c_{j+1}^* \right\}.$$

E.1.1 Gradient formulas of the functional

We will solve for the potential $U(\mathbf{r})$ which minimizes (E.6), using the definition

$$W = \frac{\omega'^2}{4E^2} \int \frac{U^2}{2}\, d\mathbf{r}\,, \quad G = \frac{\omega'}{2E} \int \frac{\partial U}{\partial x} \psi_t^* \psi_b \, d\mathbf{r}\,, \quad \tilde{\mathcal{R}} = W - \ln G^2. \tag{E.12}$$

Given the interaction matrix U_{jl} we simply have to solve for the maximum eigenvalue $E_{\max}$ with corresponding eigenvector $\mathbf{c}$, where its coefficients determine $\psi_t = \sum_j c_j \psi_j$,

$$E = \langle \psi_t | U | \psi_t \rangle \quad \Leftrightarrow \quad (U_{jl})\,\mathbf{c} = E_{\max}\,\mathbf{c}, \quad E = E_{\max}.$$

For (E.6) being minimal, it has to be satisfied

$$\frac{\partial \tilde{\mathcal{R}}}{\partial u_{p,q}} = -\frac{2W}{E}\frac{\partial E}{\partial u_{p,q}} + \frac{\omega'^2}{4E^2}\frac{\partial}{\partial u_{p,q}} \int \frac{U^2}{2}\, d\mathbf{r} - \frac{\omega'}{G}\frac{\partial}{\partial u_{p,q}}\frac{1}{E}\int \frac{\partial U}{\partial x}\psi_t^*\psi_b \, d\mathbf{r} \;= 0, \tag{E.13}$$

where only $u_{p,q}$ for $p < q$ are truly independent, hence we can assume $p < q$ and $q - p$ odd, ($u_{p,q} = 0$ with even $q - p$). Therefore whenever we write $\partial/\partial u_{p,q}$ we actually mean $\partial/\partial u_{p,q} + \partial/\partial u_{p,q}^*$, thus

$$\frac{\partial E}{\partial u_{p,q}} = \sum_{j,l} c_j^* c_l \frac{\partial}{\partial u_{p,q}} U_{j,l} = \frac{1}{2\pi} \sum_{j=0}^{\infty} 2^{-q-j} \sqrt{\binom{q+j}{j}} \sqrt{\binom{q+j}{p}}\, \mathrm{Re}\left\{c_{q-p+j}^* c_j\right\} \tag{E.14}$$

and

$$\frac{\partial}{\partial u_{p,q}} \int \frac{U^2}{2}\, d\mathbf{r} = \frac{1}{2\pi} \sum_{j=0}^{\infty} 2^{-q-j} \sqrt{\binom{q+j}{j}} \sqrt{\binom{q+j}{p}}\, \mathrm{Re}\left\{u_{j,q-p+j}\right\}\,. \tag{E.15}$$

We still need the third term of (E.13), with the help of

$$\frac{\partial c_m^{(n)}}{\partial u_{p,q}} = \frac{1}{4\pi} \sum_k{}' \sum_{j=0}^{\infty} 2^{-q-j} \sqrt{\binom{q+j}{j}} \sqrt{\binom{q+j}{p}} \frac{c_{j+q-p}^{*(k)} c_j^{(n)} + c_j^{*(k)} c_{j+q-p}^{(n)}}{E^{(n)} - E^{(k)}} c_m^{(k)}, \tag{E.16}$$

here, $E^{(n)}$ is the eigenvalue with eigenfunction $\psi^{(n)} = \sum_j c_j^{(n)} \psi_j$. We used the notation $E^{(0)} = E_{\max}$ and $c_j^{(0)} = c_j$, (E.1.1). The sum $\sum'$ indicates that the summation index $k = n$ is excluded. Then we may write

$$\begin{aligned} \frac{\partial}{\partial u_{p,q}} \frac{1}{E} \int \frac{\partial U}{\partial x} \psi_t^* \psi_b \, d\mathbf{r} = \\ 2\sqrt{2} \sum_k{}' \frac{1}{E^{(0)} - E^{(k)}} \operatorname{Re} \left\{ \left(\sum_{n=0}^{\infty} (-1)^n \sqrt{n+1} (c_n^{(k)} c_{n+1}^{*(0)} + c_n^{*(0)} c_{n+1}^{(k)}) \right) \times \right. \\ \left. \left(\frac{1}{4\pi} \sum_{j=0}^{\infty} 2^{-q-j} \sqrt{\binom{q+j}{j}} \sqrt{\binom{q+j}{p}} \, c_{q-p+j}^{*(k)} c_j^{(0)} + c_j^{*(k)} c_{j+q-p}^{(0)} \right) \right\}. \end{aligned} \tag{E.17}$$

E.2 The conjugate gradient procedure

We have to minimize $\tilde{\mathcal{R}}$ in the high dimensional space $u_{m,n}$, where only $u_{m,n}$ for $m < n$ and $n - m$ odd are independent. The evaluation of the function $\tilde{\mathcal{R}}$ and its gradient $\partial \tilde{\mathcal{R}} / \partial u_{p.q}$ is achieved by:

1. Given the potential $U^{(s)}$ in coefficient form $u_{m,n}^{(s)}$ calculate the interaction matrix $U_{j,l}^{(s)}$ according to (E.9).

2. Diagonolize $(U_{j,l}^{(s)})$, calculate all eigenvalues and eigenvectors according to (E.1.1), the maximal eigenvalue is E_s and its corresponding eigenvector $\mathbf{c}_s$.

3. With given $\omega', U^{(s)}, E_s$ and $\mathbf{c}_s$ calculate $\tilde{\mathcal{R}}^{(s)}$ in (E.6) and its gradient $\partial \tilde{\mathcal{R}}^{(s)} / \partial u_{p.q}^{(s)}$

as in (E.13).

We solve for the optimal potential $U^{(\infty)}$ iteratively, using a conjugate gradient method (Polak-Ribiere, Numerical Recipes ch. 10.6):

1. First, choose some initial potential $U^{(0)}$ in terms of $u^{(0)}_{m,n}$ which reflects the proper symmetry. This can be done by writing the wavefunction

$$\psi(\mathbf{r}) = \frac{1}{2\pi}\exp[-(\mathbf{r}-\mathbf{r_0})^2/4 + i\mathbf{r}\wedge\mathbf{r_0}/2] = e^{-r_0^2/4}\sum_{j=0}^{\infty} c_j\psi_j, \quad c_j = \frac{(x_0+iy_0)^j}{2^{j/2}\sqrt{j!}}, \tag{E.18}$$

the coefficients $u^{(0)}_{m,n}$ for the initial setup potential $U^{(0)} = |\psi(\mathbf{r})|^2 - |\psi(-\mathbf{r})|^2$ are

$$u^{(0)}_{m,n} = \begin{cases} 0 & n-m \text{ even} \\ 2c^*_m c_n & \text{else} \end{cases}$$

Calculate the functional value $\tilde{\mathcal{R}}^{(0)}$ and its gradient at the point $u^{(0)}_{m,n}$ with the downhill direction $\mathbf{g}_0 = -\partial\tilde{\mathcal{R}}^{(0)}/\partial u^{(0)}_{p,q}$ and $\mathbf{h}_0 = \mathbf{g}_0$.

2. For given point $u^{(s)}_{m,n}$ and direction $\mathbf{h}_s$ find the local minimum of $\tilde{\mathcal{R}}$ along the direction $\mathbf{h}_s$, leading to a new point $u^{(s+1)}_{m,n} = u^{(s)}_{m,n} + \alpha\mathbf{h}_s$.

3. Obtain the new downhill gradient $\mathbf{g}_{s+1} = -\partial\tilde{\mathcal{R}}^{(s+1)}/\partial u^{(s+1)}_{p,q}$ and conjugate direction $\mathbf{h}_{s+1} = \mathbf{g}_{s+1} + \gamma_s\mathbf{h}_s$, where $\gamma_s = (\mathbf{g}_{s+1}-\mathbf{g}_s)\mathbf{g}^*_{s+1}/g_s^2$. Now start over with 2 until the minimum is reached with some accuracy.

E.3 The interative procedure for arbitrary precision

The solution obtained by the conjugate gradient method is supposedly very close to the exact solution to (E.5), our original functional. Indeed it is feasible to obtain a numerical representation of the optimal potential $U(\mathbf{r})$ with arbitrary precision. We simply have to apply

$$U(\mathbf{r}) = \lambda'(|\psi_t(\mathbf{r})|^2 - |\psi_b(\mathbf{r})|^2) + \frac{2}{\int \frac{\partial U}{\partial x}\psi_t^*\psi_b \, d\mathbf{r}} \frac{\delta}{\delta U(\mathbf{r})} \int \frac{\partial U}{\partial x}\psi_t^*\psi_b \, d\mathbf{r} \qquad \text{(E.19)}$$

iteratively. To do so, we need to represent (E.19) as an equation for the coefficients $u_{p,q}$. With the help of

$$\frac{\delta c_m^{(n)}}{\delta U(\mathbf{r})} = \frac{1}{2} {\sum_k}' \frac{\psi^{*(k)}(\mathbf{r})\psi^{(n)}(\mathbf{r}) - \psi^{*(k)}(-\mathbf{r})\psi^{(n)}(-\mathbf{r})}{E^{(n)} - E^{(k)}} c_m^{(k)},$$

for an antisymmetric potential $\frac{1}{2}(U(\mathbf{r}) - U(-\mathbf{r}))$ where $\psi^{(k)}(\mathbf{r}) = \sum_j c_j^{(k)}\psi_j$ are eigenfunctions with eigenvalue $E^{(k)}$ to the Hamiltonian $H_I = \sum_{j,k} |\psi_j\rangle U_{j,k}\langle\psi_k|$ it follows

$$\frac{\delta}{\delta U(\mathbf{r})} \int \frac{\partial U}{\partial x}\psi_t^*\psi_b \, d\mathbf{r}' = \sqrt{2} {\sum_k}' \mathrm{Re}\left\{ \frac{\psi^{*(k)}(\mathbf{r})\psi(\mathbf{r}) - \psi^{*(k)}(-\mathbf{r})\psi(-\mathbf{r})}{1 - E^{(k)}/E^{(0)}} \times \sum_{n=0}^{\infty} (-1)^n \sqrt{n+1}(c_n^{(k)} c_{n+1}^{*(0)} + c_n^{*(0)} c_{n+1}^{(k)}) \right\},$$

where $\omega' = 2E^{(0)}$ has been used. We find for $|q-p|$ odd

$$\begin{aligned} 2\lambda' c_p^* c_q &= \frac{\omega'}{2E} u_{p,q} - \frac{2\sqrt{2}}{G} {\sum_k}' \left\{ \frac{c_p^{*(k)} c_q \Phi_k + c_p c_q^{*(k)} \Phi_k^*}{1 - E^{(k)}/E} \right\} \\ \Phi_k &= \sum_{n=0}^{\infty} (-1)^n \sqrt{n+1} (c_n^{(k)} c_{n+1}^{*(0)} + c_n^{*(0)} c_{n+1}^{(k)}), \end{aligned} \tag{E.20}$$

where $c_j = c_j^{(0)}$ are the components of the eigenvector $\mathbf{c}$ which defines the eigenfunction $\psi(\mathbf{r}) = \sum_j c_j \psi_j$ with eigenvalue $E = E^{(0)}$. Provided we have λ', we will find the solution by iterating (E.19). To solve for λ' we can use

$$\omega' - \beta = \lambda' \int \left(|\psi(\mathbf{r})|^2 - |\psi(-\mathbf{r})|^2 \right)^2 \, d\mathbf{r},$$

with

$$\begin{aligned} \beta = \frac{2\sqrt{2}}{\pi G} {\sum_k}' \sum_{\substack{j>l\geq 0, \\ j-l \text{ odd}, \\ m=0}}^{\infty} 2^{-m-j} \sqrt{\binom{m+j}{j}} \sqrt{\binom{m+j}{l}} \\ \operatorname{Re} \left\{ \frac{c_j^* (c_m^{*(k)} c_{m+j-l} \Phi_k + c_m c_{m+j-l}^{*(k)} \Phi_k^*) c_l}{1 - E^{(k)}/E^{(0)}} \right\}. \end{aligned} \tag{E.21}$$

E.4 Direct variational method

Having defined x_0 as in (E.18) as half the separation distance of the wells in the setup potential $V^{(0)} \propto |\psi(\mathbf{r}))|^2 - |\psi(-\mathbf{r})|^2$, we find for the Euclidian action

$$\tilde{\mathcal{R}} = \underbrace{2(\omega/\gamma)^2 \left(1 + \exp(-x_0^2)\right)}_{W} + \underbrace{2x_0^2 - \ln x_0^2 - \ln \left(\frac{\omega}{v}\right)^2}_{-\ln G^2}, \quad \gamma = \sqrt{\frac{2}{\pi}} v. \tag{E.22}$$

We easily find the optimal half-way separation distanct x_0 as

$$x_0 = \sqrt{\ln\left(\frac{\omega}{\gamma}\right)^2}$$

and therefore

$$W = 2(\omega/\gamma)^2 + 2, \quad G^2 = \frac{1}{2\pi}\left(\frac{\omega}{\gamma}\right)^{-2} \ln\left(\frac{\omega}{\gamma}\right)^2, \tag{E.23}$$

where $\sigma \propto G^2 e^{-W}$ determines the asymptotic conductivity.

E.5 Numerical results

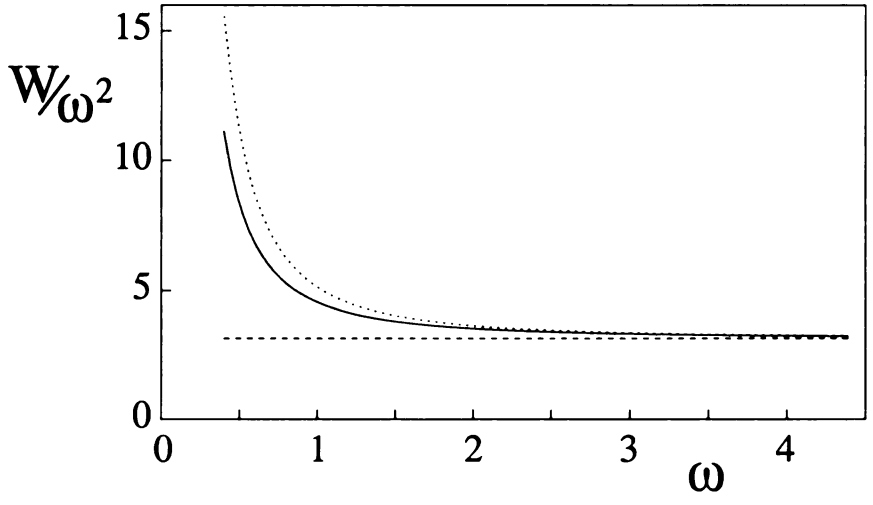

Figure E.1: Comparison between exact weight-function (solid line) with the one obtained from the direct variational approach (dotted line). Both of these curves approach the constant π, (dashed line).

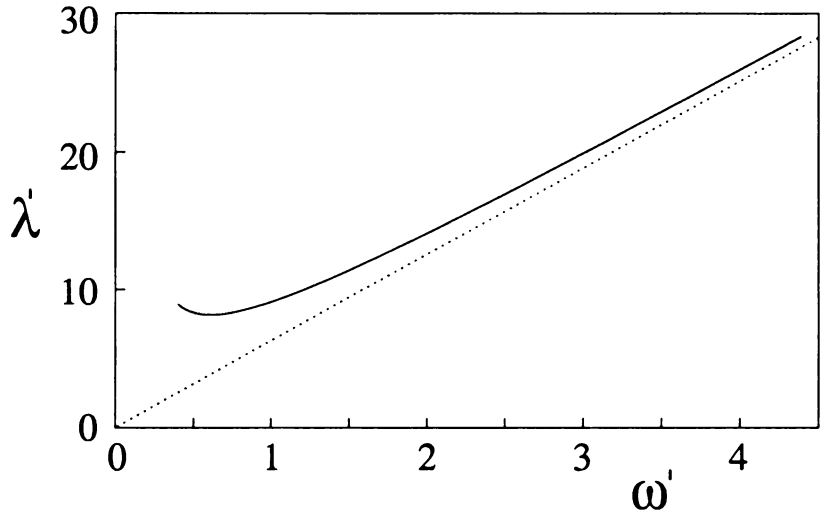

Figure E.2: Lagrange multiplier λ' plotted against frequencey ω'. It approaches in the weak overlap limit the straight line with slope 2π.

Appendix F

Polynomial reconstruction from moments

We seek an approximation scheme for finding a function $f(x)$ which has a known asymptotic behavior for large and small x described by the function $w(x)$, and given moments M_k. We interpolate this function as $f(x) = p(x)w(x)$, where $p(x)$ is a series. The coefficients in this series have to be restored from the moments, and the restoration has to be recursive. As explained in the text, this means that, if we approximate $p(x)$ by a polynomial function $p_n(x) = c_0 + c_1 x + \ldots + c_n x^n$ of degree n, the successive terms of the polynomial have to be found from the successive moments, as given by the equation

$$M_k = \int dx\ x^k p_n(x) w(x), \quad k = 0, 1, \ldots . \tag{F.1}$$

The weight function $w(x)$ in case of a Hermite reconstruction has the form $w(x) =$

$\exp(-x^2)$, whereas in the case of Laguerre reconstruction it is of the form $w(x) = x^\mu \exp(-x^2)$.

A consistent way to find the function $p_n(x)$ is to introduce an orthonormal set of polynomials $g_k(x)$ with respect to the weight function. That means

$$\int dx\ g_m(x) g_n(x) w(x) = \delta_{m,n}. \tag{F.2}$$

Now, $p_n(x)$ can be sought as an expansion in the functions (F.2),

$$p_n(x) = \sum_{k=0}^{n} g_k(x) d_k \tag{F.3}$$

with expansion coefficients d_k. The use of orthogonal polynomials allows one to solve for d_k successively, meaning that knowledge of higher moments doesn't change the already obtained expansion coefficients. This is because we use the property

$$\langle x^n; g_k \rangle = \int dx\ x^n g_k(x) w(x) \equiv 0 \text{ for } k > n. \tag{F.4}$$

Then one only has to solve a triangular matrix equation

$$\begin{pmatrix} \langle 1; g_0 \rangle & 0 & 0 & 0 \\ \langle x; g_0 \rangle & \langle x; g_1 \rangle & 0 & 0 \\ \vdots & & & \\ \langle x^n; g_0 \rangle & \langle x^n; g_1 \rangle & \cdots & \langle x^n; g_n \rangle \end{pmatrix} \begin{pmatrix} d_0 \\ d_1 \\ \vdots \\ d_n \end{pmatrix} = \begin{pmatrix} M_0 \\ M_1 \\ \vdots \\ M_n \end{pmatrix}. \tag{F.5}$$

The coefficients in the matrix are standard integrals in the both relevant cases of Hermite and Laguerre polynomials.

Appendix G

Outline for the classification program

It follows a simple documentation of the program procedure used in Sec 4.3 to numerically classify and count diagrams.

The container classes for generating diagrams of the order **SEQUENCE** and the exponential matrix **B** (4.15) and (4.16) also of that order are initialized.

```
Matrix         B(SEQUENCE);
Diagram diagram(SEQUENCE);
```

Here comes the main loop over all diagrams:

```
while (diagram.done()==False) {
  if ((diagram.is_simple_zero() == True) ||
      (diagram.is_parity_zero() == True)) {
    diagram.next(); // take the next diagram
```

```
  continue;        // and start all over
}
```

Now we probably have a non-zero diagram and can sum over the j-tupel (4.15). For each j-tupel we initialize the matrix $\mathbf{B}$ (4.16) and take care of all associated signs ± 1. Then one quickly obtains a unique key value for that contracted matrix, which only specifies where the zeros and ones are located (this procedure is very fast and allows to restore the structure of that matrix from its key value). Next, depending on whether the **DIAGRAM** is one that contracts the end-variables $q_1 = q_{2k+2}$ one counts those matrices (or better the keyvalue thereof) onto a different stack. Here we use an efficient binary tree to count the occurence of those contracted matrices.

```
// export the diagram into the DIAGRAM variable
diagram.get(DIAGRAM);
for(integer j=0; j<stopj; j++) {
  // initialize the matrix B which is then contracted
  B.initialize(j);     // the initialization and contraction
  B.contract(DIAGRAM); // procedure is explained in Sec (4.3)
  // determine the sign of the j-tupel
  sign = get_sign(j);  // sign has value +1 or -1
  // count the occurance of the contracted matrix
  if (DIAGRAM[1] == 1) {
    Tree1.update(B.key(), sign); // end variables are contracted
  } else {                       // put the rest onto a
```

```
      Tree2.update(B.key(), sign); // different stack
    }
  } // end for loop
diagram.next(); // take the next diagram
} // end while (diagram.done() == False) the main loop
```

Now, we have counted all diagrams and the number of contracted matrices is still large. The more, even different contracted matrices can give the same value after the integration in (4.15) is carried out. Before analytically integrating those large number of integrals (4.15), one for each stored matrix in the container structures `Tree1` and `Tree2`, one can numerically integrate them. The way to do that is shown in App. C.

```
// scan through all the accumulated data
while (Tree1.done() == False) {
  Tree1.get_contracted_matrix( &A, &multiplicity);
  value = numerically_integrate(A);
  // now sort according to the value classifier into different
  // bins, observe the multiplicty!
  ValueTree1.update(value, multiplicity);
  Tree1.next();
}
while (Tree2.done() == False) {
  Tree2.get_contracted_matrix( &A, &multiplicity);
  value = numerically_integrate(A);
```

```
    ValueTree2.update(value, multiplicity);
    Tree2.next();
  }
```

Finally, the data structures `ValueTree1` and `ValueTree2` contain only non-equivalent diagrams (represented as contracted matrices) according to the numerical classifier (4.17). The analytic integration then is done with *Mathematica* using a special integration tool [102].

Bibliography

Bibliography

[1] F. M. Peeters, *The Physics of the Two-Dimensional Electron Gas*, vol. 157 (Plenum Press, New York, 1987).

[2] M. E. Cage, R. F. Dziuba, and B. F. Field, IEEE Trans. Instrum. Meas. **IM-34**, 301 (1985).

[3] M. J. Lea, K. Djerfi, P. Fozooni, A. Kristensen, A. Santrich-Badal, A. Blackburn, M. I. Dykman, C. Fang-Yen, and P. J. Richardson, Surface Sci. **361 & 362**, 835 (1996).

[4] C. Fang-Yen, M. I. Dykman, and M. J. Lea, Phys. Rev. B **55**, 16272 (1997).

[5] F. Wegner, Z. Phys. B **25**, 279 (1983).

[6] S. Koch, R. J. Haug, K. von Klitzing, and K. Ploog, Phys. Rev. Lett. **67**, 883 (1991).

[7] E. Abrahams, S. V. Kravchenko, and M. P. Sarachik, cond-mat/0006055.

[8] B. Tanatar and C. M. Ceperley, Phys. Rev. B **39**, 5005 (1989).

[9] E. Y. Andrei, ed., *Two-dimensional electron systems on helium and other cryogenic substrates* (Kluwer, Bosten, 1997).

[10] P. Hansen, D. J. Levesque, and J. J. Weis, Phys. Rev. Lett. **43**, 979 (1979).

[11] R. K. Kalia, P. Vashishta, S. W. de Leeuw, and A. Rahman, Phys. Rev. B **23**, 4794 (1981).

[12] M. Dykman and L. Khazan, JETP **50**, 747 (1979).

[13] P. Adams and M. Paalanen, Phys. Rev. B **37**, 3805 (1988).

[14] R. W. van der Heijden, M. C. M. van de Sanden, J. G. Surewaard, A. T. A., M. de Waele, H. M. Gijsman, and F. M. Peeters, Europhys. Lett. **6**, 75 (1988).

[15] M. J. Lea, P. Fozooni, A. Kristensen, P. J. Richardson, K. Djerfi, M. I. Dykman, C. Fang-Yen, and A. Blackburn, Phys. Rev. B **55**, 16280 (1997).

[16] T. Ando, A. Fowler, and F. Stern, Rev. Mod. Phys. **54** (1982).

[17] B. Huckestein, Rev. Mod. Phys. **67**, 357 (1995).

[18] K. von Klitzing, G. Dorda, and M. Pepper, Phys. Rev. Lett. **45**, 494 (1980).

[19] National Institute of Standards and Technology: Fundamental Physical Constants.

[20] P. Anderson, Phys. Rev. **109**, 1492 (1958).

[21] R. B. Laughlin, Phys. Rev. B **23**, 5632 (1981).

[22] B. I. Halperin, Phys. Rev. B **25**, 2185 (1982).

[23] T. Ando and Y. Uemura, J. Phys. Soc. Japan **36**, 959 (1974).

[24] T. Ando, J. Phys. Soc. Japan **36**, 1521 (1974).

[25] T. Ando, J. Phys. Soc. Japan **37**, 622 (1974).

[26] T. Ando, J. Phys. Soc. Japan **37**, 1233 (1974).

[27] E. Brézin, D. J. Gross, and C. Itzykson, Nucl. Phys. B **235**, 24 (1984).

[28] L. B. Ioffe and A. I. Larkin, JETP **54**, 556 (1981).

[29] M. Böhm, K. Broderix, and H. Leschke, Z. Phys. B **104**, 111 (1997).

[30] A. Kristofferson and K. Olaussen, J. Phys. C **9**, 10801 (1997).

[31] R. Kubo, *Solid State Physics*, vol. 17 (Academic Press, New York, New York, 1965).

[32] W. Pook and M. Janßen, Z. Phys. B **82**, 295 (1991).

[33] M. Janßen, Int. J. Mod. Phys. B **8**, 943 (1994).

[34] F. Wegner, Z. Phys. B **25**, 327 (1976).

[35] F. Wegner, Z. Phys. B **25**, 207 (1979).

[36] E. Abrahams, P. W. Anderson, D. C. Licciardello, and T. V. Ramakrishnan, Phys. Rev. Lett. **42**, 673 (1979).

[37] H. Aoki and T. Ando, Solid State Commun. **38**, 1079 (1981).

[38] Y. Ono, J. Phys. Soc. Jpn. **51**, 2055 (1982).

[39] J. T. Chalker, J. Phys. C **20**, L493 (1987).

[40] A. M.M. Pruisken, Phys. Rev. B **32**, 2636 (1985).

[41] A. M.M. Pruisken, Nucl. Phys. **B235 [FS11]**, 277 (1984).

[42] H. Levine, S. B. Libby, and A. M.M. Pruisken, Phys. Rev. Lett. **51**, 1915 (1983).

[43] H. Levine, S. B. Libby, and A. M.M. Pruisken, Nuc. Phys. **B240**, 30 (1984), for a review, see A. M. M. Pruisken, in *Localization, Interaction and Transport Phenomena*, ed. by B. Kramer *et al.*, Springer Series in Solid-State Sciences, Vol. 61 (Springer, Berlin, 1985).

[44] B. Mieck, Europhys. Lett. **13**, 453 (1990).

[45] D. Stauffer, Phys. Rep. **54**, 2 (1979).

[46] G. V. Mil'nikov and I. M. Skolov, JETP Lett. **48**, 536 (1988).

[47] M. W. Cole and M. H. Cohen, Phys. Rev. Lett. **23**, 1238 (1969).

[48] A. J. Cole and W. F. Vinen, Physics Today **40**, 43 (1987).

[49] C. C. Grimes and G. Adams, Phys. Rev. Lett. **42**, 795 (1979).

[50] D. S. Fisher, B. I. Halperin, and P. M. Platzman, Phys. Rev. Lett. **42**, 798 (1979).

[51] G. Deville, J. Low Temp. Phys. **72**, 135 (1988).

[52] M. A. Stan and A. J. Dahm, Phys. Rev. B **40**, 8995 (1989).

[53] Y. Iye, J. Low Temp. Phys. **40**, 441 (1980).

[54] V. S. Edel'man, JETP **50**, 338 (1980).

[55] L. Wilen and R. Giannetta, Phys. Rev. Lett. **60**, 231 (1988).

[56] R. Mehrotra, C. J. Guo, Y. Z. Ruan, D. B. Mast, and A. J. Dahm, Phys. Rev. B **29**, 5239 (1984).

[57] V. A. Buntar', Y. Z. Kovdrya, V. N. Grigoriev, Y. P. Monarhka, and S. S. Sokolov, Sov. J. Low Temp. Phys. **13**, 451 (1987).

[58] V. A. Buntar', V. N. Grigoriev, O. I. Kirichek, Y. Z. Kovdrya, Y. P. Monarkha, and S. S. Sokolov, J. Low Temp. Phys. **79**, 323 (1990).

[59] R. W. van der Heijden, H. M. Gijsman, and F. M. Peeters, J. Phys. C **21**, L1165 (1988).

[60] A. O. Stone, P. Fozooni, M. J. Lea, and M. Abdul-Gader, J. Phys.: CM **1**, 2743 (1989).

[61] P. Scheuzger, J. Neuenschwander, and P. Wyder, Physica B **165 & 166**, 845 (1990).

[62] P. Scheuzger, J. Neuenschwander, and P. Wyder, Physica B **194 & 196**, 1231 (1994).

[63] P. J.M. Peters, P. Scheuzger, M. J. Lea, Y. P. Monarkha, P. K.H. Sommerfeld, and R. W. van der Heijden, Phys. Rev. B **50**, 11570 (1994).

[64] M. I. Dykman, M. J. Lea, P. Fozooni, and J. Frost, Phys. Rev. Lett. **70**, 3975 (1993).

[65] M. I. Dykman, M. J. Lea, P. Fozooni, and J. Frost, Physica B **197**, 340 (1994).

[66] M. J. Lea, P. Fozooni, P. J. Richardson, and A. Blackburn, Phys. Rev. Lett. **73**, 1142 (1994).

[67] S. Ito, K. Shirahama, and K. Kono, Czech. J. Phys. **46**, 339 (1996).

[68] J. Berthold, Phys. Rev. B **76**, 1902 (1976).

[69] M. Saitoh, J. Phys. Soc. Japan **42**, 201 (1977).

[70] L. Landau and E. Lifshitz, *Fluid Mechanics*, vol. 6 of *Course of Theoretical Physics* (Pergamon Press Ldt., Oxford, 1959).

[71] K. R. Atkins, Can. J. Phys. **31**, 1165 (1953).

[72] M. W. Cole, Phys. Rev. B **2**, 4239 (1970).

[73] Y. P. Monarkha, sov. J. Low Temp. Phys. **3**, 282 (1977).

[74] T. Kawaguchi, T. Ohtsuki, and M. Saitoh, Surface Sci. **263**, 671 (1992).

[75] V. Shikin and Y. P. Monarkha, J. Low. Temp. Phys. **16**, 193 (1974).

[76] M. I. Dykman, Sov. J. Low Temp. Phys. **6**, 268 (1980).

[77] V. I. Ryzhii, Sov. Phys. Semicond. **3**, 1432 (1969).

[78] M. I. Dykman and L. S. Khazan, JETP **50**, 747 (1979).

[79] N. A. Krall and A. W. Trivelpiece, *Principles of Plasma Physics* (McGraw-Hill, New York 1973).

[80] R. C. Gann, C. Chakravarti, and G. V. Chester, Phys. Rev. B **20**, 326 (1979).

[81] R. H. Morf, Phys. Rev. Lett. **43**, 931 (1979).

[82] R. H. Morf, Phys. Rev. B **20**, 4962 (1979).

[83] R. K. Kalia, P. Vashishta, S. W. de Leeuw, and A. Rahman, J. Phys. C **14**, L991 (1981).

[84] L. Cândido, J. P. Rino, and N. Studart, Phys. Rev. B **54**, 7046 (1996).

[85] L. Bonsall and A. A. Maradudin, Phys. Rev. B **15**, 1959 (1977).

[86] M. I. Dykman, J. Phys. C **15**, 7397 (1982).

[87] E. M. Baskin, L. N. Magarill, and V. E. M., JETP **48**, 365 (1978).

[88] R. Kubo, S. J. Miyake, and N. Hashitsume, Solid State Physics **17**, 269 (1965).

[89] W. Kohn, Phys. Rev. **123**, 1242 (1961).

[90] E. M. Conwell, *High Field Transport in Semiconductors* (Academic Press, New York 1967).

[91] K. Seeger, *Semiconductor Physics. An Introduction* (Springer, Berlin 1991), 5 ed.

[92] M. I. Dykman and M. A. Krivoglaz, *Soviet Physics Reviews* (Harwood, New York 1984).

[93] M. I. Dykman, C. Fang-Yen, and M. J. Lea, Phys. Rev. B **55**, 16249 (1997).

[94] A. M. Stoneham, *Theory of defects in solids: electronic structure of defects in insulators and semiconductors* (Clarendon Press, Oxford, 1975).

[95] M. I. Dykman, Phys. Stat. Sol. B **88**, 463 (1978).

[96] K. A. Benedict, Nucl. Phys. B **280**, 549 (1987).

[97] B. I. Halperin and M. Lax, Phys. Rev. **148**, 722 (1966).

[98] J. T. Chalker and P. D. Coddington, J. Phys. C **21**, 2665 (1988).

[99] J. T. Chalker and J. J. Daniell, Phys. Rev. Lett. **61**, 593 (1988).

[100] Z. Wang, M. P.A. Fisher, S. M. Girvin, and J. T. Chalker, Phys. Rev. B **61**, 8326 (2000).

[101] S. L. Sondhi, unpublished.

[102] http: www.mathsource.com/Content/Enhancements/ Calculus/0211-138.

[103] H. S. Wall, *Continued Fractions* (Van Nostrand, New York, 1948).

[104] O. Perron, *Die Lehre von Kettenbrüchen, Vol. I, III* (Teubner, Stuttgart, 1977).

[105] D. Lubinsky, H. N. Mhaskar, and E. B. Saff, Constr. Approx. **4**, 65 (1988).

[106] For a review see B.L. Altshuler and A.G. Aronov, in *Electron-Electron Interaction in Disordered Systems*, edited by A.L. Efros and M. Pollak (North-Holland, Amsterdam 1985).

[107] B. I. Shklovskii, JETP Lett. **36**, 51 (1982); B. I. Shklovskii and A. L. Efros, JETP **57**, 470 (1983). Qin Li and D. J. Thouless, Phys. Rev. B **40**, 9738 (1989); T. Martin and S. Feng, *ibid.* **44**, 9084 (1991); J. Haidu, M. E. Raikh, and T. V. Shahbazyan, *ibid.* **50**, 17625 (1994).

[108] F. Kuehnel, M. I. Dykman, and L. P. Pryadko, (unpublished) cond-mat/0001427 (2000).

[109] M. P.A. Fisher, D., G. Grinstein, and S. M. Girvin, Phys. Rev. Lett. **64**, 587 (1990).

[110] D. Polyakov and B. Shklovskii, Phys. Rev. Lett. **70**, 3796 (1993), *ibid.* **73**, 1150 (1994).

[111] M. J. Lea and M. I. Dykman, Physica B **251**, 628 (1998).

[112] E. Teske, Y. P. Monarkha, M. Seck, and P. Wyder, Phys. Rev. Lett. **82**, 2772 (1999).

[113] C. Kallin and B. I. Halperin, Phys. Rev. B **31**, 3635 (1985).

[114] M. Saitoh, Solid Stat comm. **52**, 63 (1987).

[115] J. R. Klauder and B. Skagerstam, eds., *Coherent States* (World Scientific, Singapore, 1985).

[116] J. von Neumann, *Mathematical Foundations of Quantum Mechanics* (Princeton University Press, Princeton NJ, 1955).